PALEOTECTONIC SETTING OF TAKLA GROUP VOLCANO-SEDIMENTARY ROCKS QUESNELLIA, NORTH CENTRAL BRITISH COLUMBIA

by

Kathleen Minehan

Department of Geological Sciences
McGill University
Montreal, Quebec

A thesis submitted in partial fulfilment
of the requirements for the degree of
Master of Science

September, 1989

ABSTRACT

Upper Triassic Takla Group rocks occur in Quesnellia and Stikinia, two allochthonous terranes of the Canadian Cordillera. The terranes are separated by the major, north-northwest trending, dextral transcurrent Findlay fault. The stratigraphy of the study area, east of the fault in Quesnellia, is comprised of interlayered volcaniclastic, volcanic, and sedimentary rocks. The strata have been intruded by abundant dykes, a felsic pluton, and satellite intrusions of an Alaskan-type ultramafite. Volcaniclastic rocks range from basic to felsic compositions and were deposited by several pyroclastic flows which originated subaerially and flowed into water. Igneous rocks are believed to have been comagmatic and differentiated by fractional crystallization. Major and trace element discrimination diagrams indicate an island arc tectonic setting. On the same basis, Takla Group rocks on the Stikinia side of the Findlay fault are distinguishable and more characteristic of oceanic island tectonic setting. It is recommended that the rocks of the study area be renamed Johanson Group.

SOMMAIRE

Les roches du groupe Takla, d'âge triasique supérieur, se retrouvent dans les deux allochtones Quesnellia et Stikinia qui font partie des Cordillères Canadiennes. Ces deux allochtones sont séparés par l'inportante faille transversale dextre Findlay orientée vers le nord-nordouest. L'étude en question se concentre sur la stratigraphie à l'est de cette faille qui consiste en roches volcaniclastiques, volcaniques, et sédimentaires interstratifiées. Un pluton felsique, de nombreux dykes, et une intrusion satellite de type ultramafique Alaska percent ces strates. Les roches volcaniclastiques ont une composition allant de felsique à mafique. Elles ont été déposees, au début, par plusieurs écoulements pyroclastiques subaériens pour ensuite se répondre dans l'eau. Les roches ignées sont probablement toutes comagmatiques mais se sont, par la suite, differenciées par cristallisation fractionnée. Des diagrammes de discrimination d'éléments principaux et de traces pointent vers un arc insulaire comme environnement tectonique de dépôt. Les roches du groupe Takla de part et d'autre de la faille se distiquent facilement par leur géochimie. Il est donc suggéré de donner le nouveau nom de groupe Johanson aux roches présentement étudiées.

ACKNOWLEDGEMENTS

It was Brendan Murphy who first introduced me to the possibility of studying geology deep in the Cordilleran Mountains. Since then I have received help and encouragement from so many people it is impossible to name them all here. Among them, Glenn Porrier, Roland Dechesne, Serge Perreault, Abdel Abdel-Raman, Anne Charland, Tom Skulski, and Nathalie Guillemette have helped considerably. Kim Bellefontaine, the other half of "Johanson Portable", assisted me in the field and shared with me the frustration and desperation of frigid temperatures, freeze dried food, and unrelenting precipitation.

As my advisor, Andrew Hynes allowed me the independence to forage my way towards the completion of this theses. For this, and for his skilled editorial judgement, I am grateful. I would also like to thank my husband Ed who provided much needed emotional support even though he had little idea what the hell I was doing over the past two years.

Personal funding came from a Natural Sciences and Engineering Research Council Postgraduate Scholarship. Fieldwork was supported by a Natural Sciences and Engineering Research Council grant to A. Hynes, and a grant from the British Columbia Geoscience Research Grant Program, Ministry of Energy, Mines and Petroleum Resources, to K. Minehan.

TABLE OF CONTENTS

LIST OF FIGURES

LIST OF TABLES

LIST OF PLATES

CHAPTER 1

INTRODUCTION

1.1 INTRODUCTION

The Canadian portion of the Cordilleran orogenic belt formed in response to the subduction of oceanic lithosphere at the continental margin, and the collision of two large, composite terranes, Terrane I and Terrane II (Monger, 1984). Upper Triassic Takla Group volcaniclastic, volcanic, and sedimentary rocks are located in north-central British Columbia within the allochthonous Terrane I.

Throughout north-central British Columbia large scale northwest-trending transcurrent faulting has been extensive. The faulting postdates the collision of the terranes and has disrupted original tectonic associations. Takla Group rocks occur in an area of Terrane I which is cut by the major Findlay-Ingenika-Pinchi transcurrent fault system. Takla rocks occur on both sides of the Findlay fault and no conclusive stratigraphic correlations have been made across the fault.

1.2 PURPOSE OF STUDY

Because Terrane I has been extensively cut by major transcurrent faults, unrelated assemblages of different origins and environments have been juxtaposed. Clearly a geologic setting which has been demonstrated in one location of the Intermontane Belt cannot confidently be assigned to adjacent units across major faults. In order to construct a detailed tectonic model for the Cordillera, it is necessary to determine the depositional environment of each rock unit and its relationship to associated units.

The objectives of this study are to determine the paleotectonic setting of eruption of Takla Group rocks in a well defined area of study, and to reevaluate their association with other rocks assigned to the Takla Group.

1.3 GEOLOGIC SETTING

The Cordilleran orogen can be divided into five geological belts; the Rocky Mountain Fold and Thrust Belt, The Omineca Crystalline Belt, the Intermontane Belt, the Coast Plutonic Belt, and the Insular Belt, each with a distinct history of development (Figure 1.1). The Intermontane Belt encompasses almost all rocks of Terrane I, and rocks of Terrane II occur largely within the Insular Belt. The Omineca

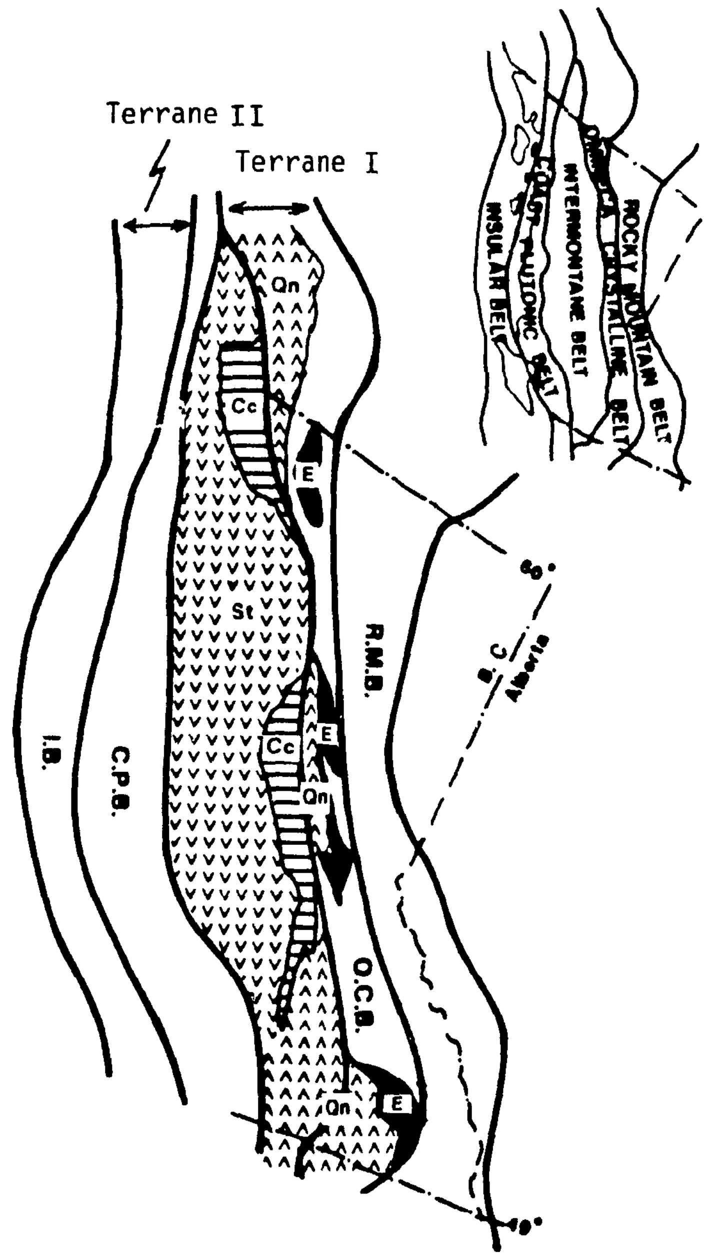

Figure 1.1 Distribution of the five geologic belts of the Canadian Cordillera (I.B.: Insular Belt, C.P.B.: Coast Plutonic Belt, O.C.B.: Omineca Crystalline Belt, R.M.B.: Rocky Mountain Fold and Thrust Belt), and the subterranes of Terrane I (St: Stikinia, Qn: Quesnellia, Cc: Cache Creek, E: Eastern). Modified after Monger, Price and Tempelman-Kluit (1982).

Crystalline Belt, which includes the remaining subterranes of Terrane I, and the Coast Plutonic Belt are the two main metamorphic and plutonic welts in which intense deformation, metamorphism, and granitic magmatism were concentrated during and following the collisions of the allochthonous terranes (Monger, Price and Tempelman-Kluit, 1982). The Rocky Mountain Fold and Thrust Belt represents an ancient continental margin clastic wedge which suffered shortening as the continent moved westward and met the resistance provided by the accreted terranes (Monger, 1984). It is currently accepted that both terranes I and II are composites of volcanic arcs, oceanic crust, and overlying deposits (Monger, 1984).

The subterranes which comprise composite Terrane I are, from east to west, Eastern or Slide Mountain, Quesnellia, Cache Creek, and Stikinia (Figure 1.1). Cache Creek and Slide Mountain terranes have both been interpreted as ocean floor complexes based on the occurrence of Alpine-Type ultramafics, basalt, chert, and argillite (Monger, Price, and Tempelman-Kluit, 1982). A significant feature of the Cache Creek Group is the occurrence of local blueschist indicating an associated subduction zone (Monger, Price, and Tempelman-Kluit, 1982). The dominance of volcaniclastic and volcanic rocks in Quesnellia and Stikinia, and their position next to ocean floor complexes, indicate that they may have formed in oceanic island or volcanic arc tectonic settings.

Rocks assigned to the Takla Group occur in both

Quesnellia and Stikinia. The two terranes are separated by the Findlay-Ingenika-Pinchi transcurrent fault system, which serves as the boundary between Quesnellia and terranes to the west. Offsets of geologic elements indicate post-Triassic dextral displacements of as much as 300 kilometres along the system (Gabrielse, 1985).

Stratigraphic and structural evidence presented by Monger et al. (1982) indicates that Quesnellia and Stikinia may have evolved as separate magmatic arcs, until they were amalgamated to form Terrane I by the subduction of the intervening ocean floor (partly preserved in the Cache Creek). Monger, Price, and Tempelman-Kluit (1982) propose that Quesnellia and Stikinia were amalgamated in Late Triassic - Early Jurassic time and collided with North America by Middle Jurassic time.

1.4 LOCATION AND PHYSIOGRAPHY OF STUDY AREA

A study area was chosen within Quesnellia, in an area bounded to the west by the Findlay fault and to the east by the Swannell fault and Proterozoic miogeoclinal rocks of the Ingenika Group (Figure 1.2).

During two seasons of field work approximately 75 square kilometres were studied on the westernmost lobe of the Ingenika ranges, just north of Johanson Lake in the northeast half of the McConnell Creek map sheet (94D). The field season

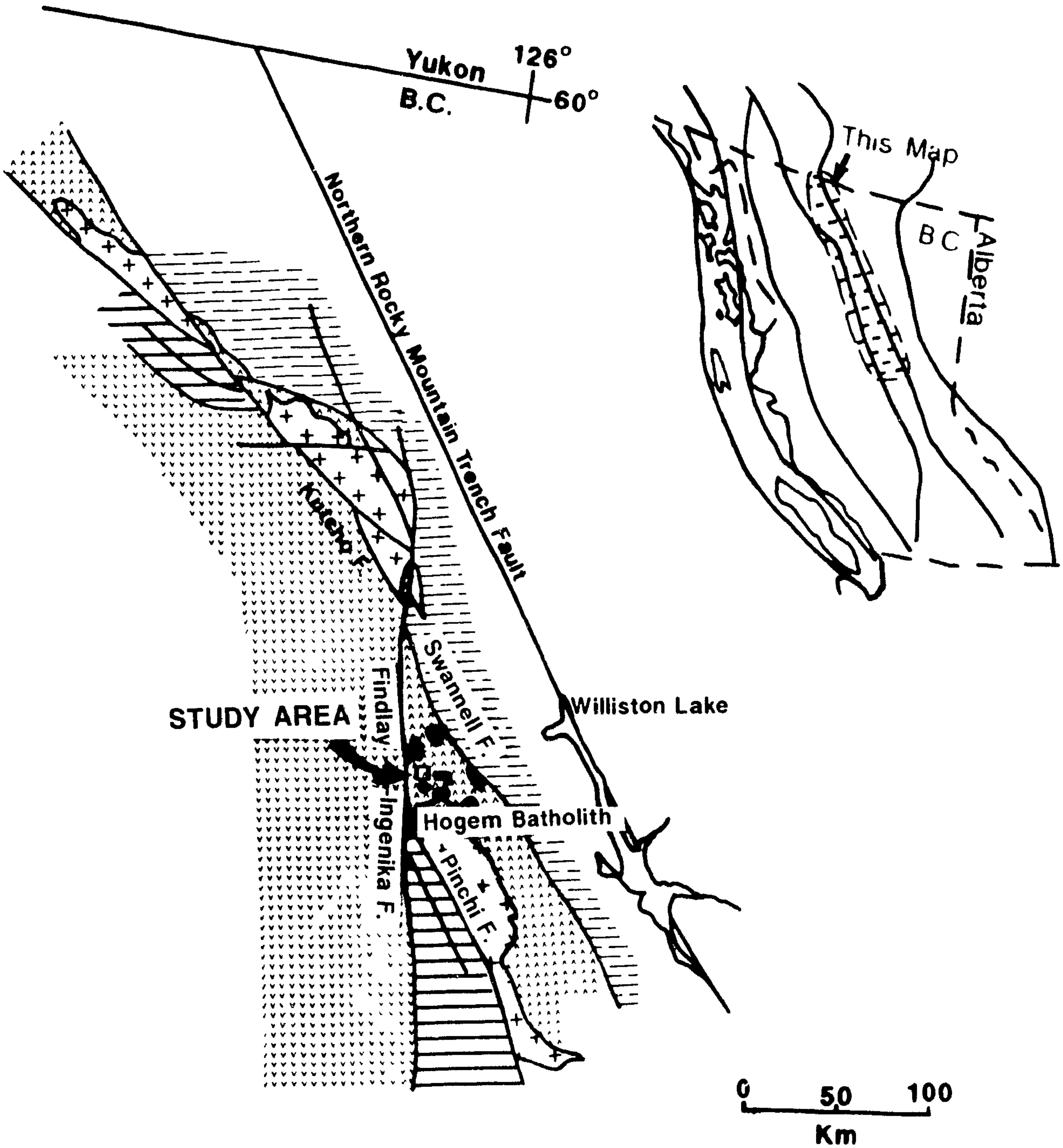

Figure 1.2 Location of study area. Upside down V: Quesnellia, V: Stikinia, solid horizontal line: Cache Creek, dashed horizontal line: Continental wedge rocks, cross: granitic batholiths, black bodies: Alaskan type ultramafics. Modified after Gabrielse (1985).

is short, lasting about three months between the first of June and the end of August, with snow or rain almost daily. The area is characterised by excellent exposure on prominent ridges which reach elevations of almost 2200 metres. Average relief from ridge crests to valley floors is approximately 300 metres.

Road access to the area is limited and helicopter transportation was necessary for all camp moves. A British Columbia Department of Mines and Petroleum Resources gravel road extends as far north as Johanson Lake, and in 1987 a private road was constructed along Moosevalley between Johanson Lake and the Sturdee air strip just north of Thutade Lake.

1.5 PREVIOUS WORK

Lord (1948) was the first to map volcanic and sedimentary strata within the study area and assign it to the Takla Group. In the McConnell Creek map area he divided the Takla Group into a Lower Division of Upper Triassic age and an Upper Division of Upper Triassic - Upper Jurassic age. Rocks of the study area were classified as Lower Division Takla, characterised by andesitic and basaltic tuffs, agglomerates, flows and tuffaceous argillites.

As part of the Takla Project undertaken by the Geological

Survey of Canada, several workers studied the McConnell Creek map-area to determine the plutonic, volcanic, sedimentary, and structural history of Late Triassic and Early Jurassic rocks. Irvine (1976) examined Alaskan-type ultramafic-gabbroic bodies which intrude Takla strata close to the study area; Monger (1976) studied the regional stratigraphy and environment of deposition; Woodsworth (1976) mapped and examined the Hogem batholith and associated granitic intrusives; and Richards (1976) re-mapped the area.

Monger and Church (1977) revised the stratigraphy proposed by Lord, and redefined the Takla Group as entirely Upper Triassic. Lord's Upper Division Takla was divided into Lower - Mid Jurassic Hazelton Group and Mid - Upper Jurassic Bowser Lake Group. The newly defined Takla was divided into three formations west of the Findlay fault, but remains undifferentiated east of the fault. Rocks of the study area are included in the newly defined and more restricted Takla Group. Monger (1977) described the stratigraphy and composition of Takla rocks in the McConnell Creek map area, on both sides of the Findlay fault.

1.6 GENERAL GEOLOGY AND AGE

Takla Group rocks within the study area are a diverse assemblage of volcaniclastic, volcanic and sedimentary rocks which were deposited subaqueously. Volcanic and volcaniclastic rocks are pyroxene-plagioclase porphyries of mafic composition and amphibole-plagioclase porphyries of intermediate to felsic composition. The strata have been extensively intruded by mafic to felsic porphyritic dykes and sills, a felsic pluton, and satellite intrusions of gabbro/diorite related to the local Alaskan-type ultramafite. The sequence is metamorphosed to lower greenschist grade, and cut by five major northwest-trending dextral transcurrent faults into six distinct fault blocks (Figure 1.3).

The age of the assemblage is Upper Triassic. Monger (1977) observed five fossil localities within the study area and identified Late Karnian or Early Norian Halobia (pelecypod) fragments in a sedimentary unit in the south-central map area.

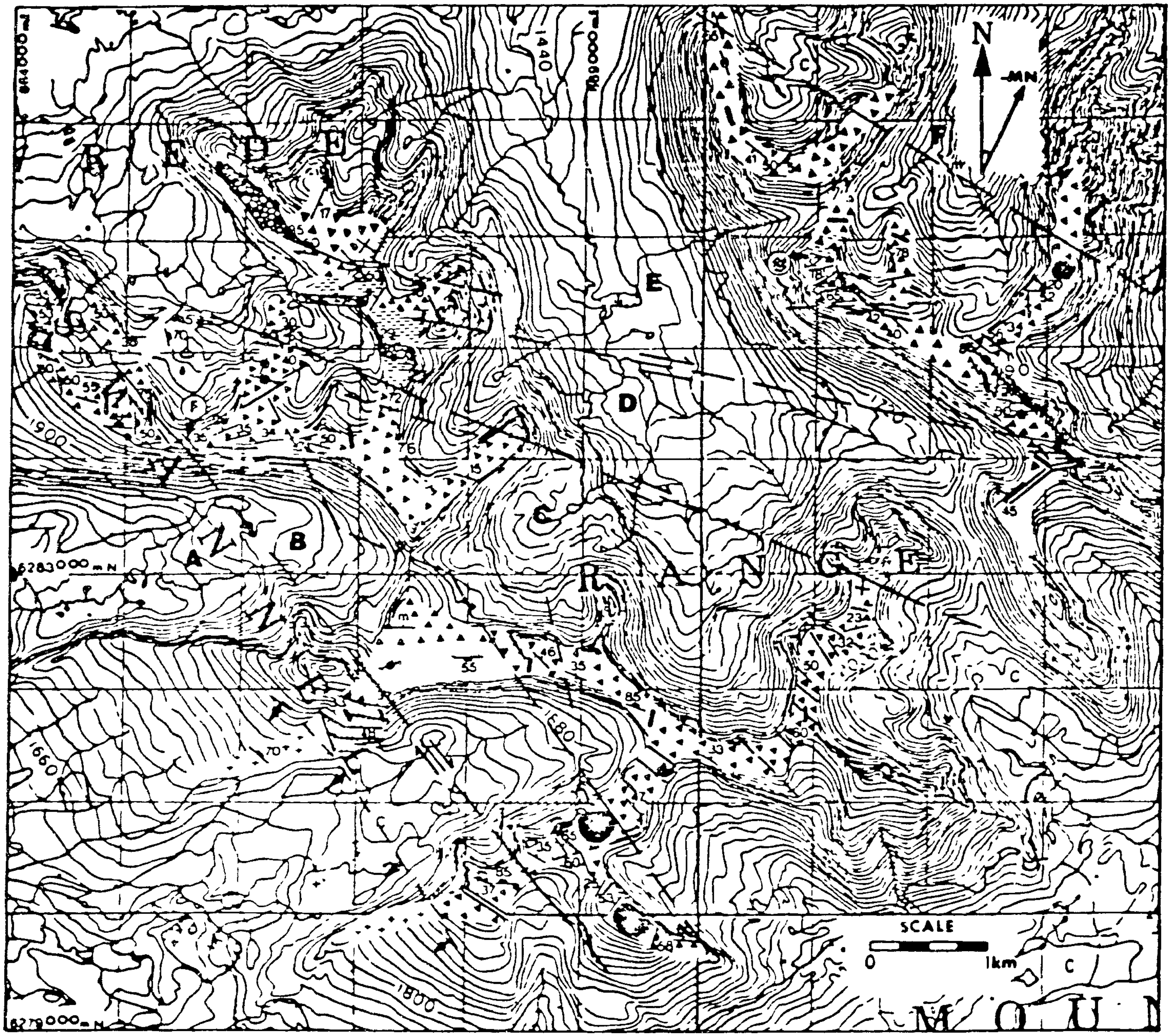

Figure 1.3 General Geology of the study area.

CHAPTER 2

ROCK DESCRIPTION

2.1 INTRODUCTION

Volcaniclastics are the dominant rock type in the study area, but post-deposition modification has made it impossible to confidently establish their origin, mode of transportation, or deposition as being wholly pyroclastic or epiclastic. For this reason the names that follow were assigned using a nongenetic classification scheme of Cas (1987) (Table 2.1).

Table 2.1 Classification of Volcaniclastics

Grainsize (diameter)	Rock Name
≤ 0.0625 mm	volcanogenic siltstone
0.0625 - 2 mm	volcanogenic sandstone
≥ 2 mm	volcanogenic breccia

2.2 STRATIGRAPHIC RELATIONSHIPS

The stratigraphic succession is divided among six distinct, northwest-trending fault blocks. The cumulative stratigraphic thickness, from all fault blocks, is approximately 7500 metres. Since no stratigraphic correlations have been established, it is possible there are lateral equivalents between blocks, and the cumulative thickness does not represent the actual stratigraphic thickness. The fault blocks are labelled A to E, from the southwestern to northeastern portion of the map area (Figures 1.3 and 2.1).

Volcanogenic breccia is the dominant volcaniclastic, and accounts for more than half of the stratigraphic column. The thickest units, up to 900 meters thick, occur in the bounding fault blocks A and E, while thinner units are more common toward the centre of the map area.

Approximately twenty percent of the stratigraphic succession is volcanogenic sandstone. The units attain thicknesses of up to 300 metres in the southwest portion of the map area, (fault block A), and become thinner and more abundant toward the centre of the map area, (fault block C). Volcanogenic sandstone occurs occasionally as thin units, in fault blocks D and E.

Volcanogenic siltstone is distributed among all fault blocks, making up approximately fifteen percent of the total succession. It is commonly associated with volcanogenic sandstone, and is also most common in the central map area.

All volcaniclastics are massive and resistant, forming the highest ridges. The effects of alteration and metamorphism are not apparent in most outcrops, except at major fault zones and in rare breccia fragments in which massive yellow-green epidote is abundant.

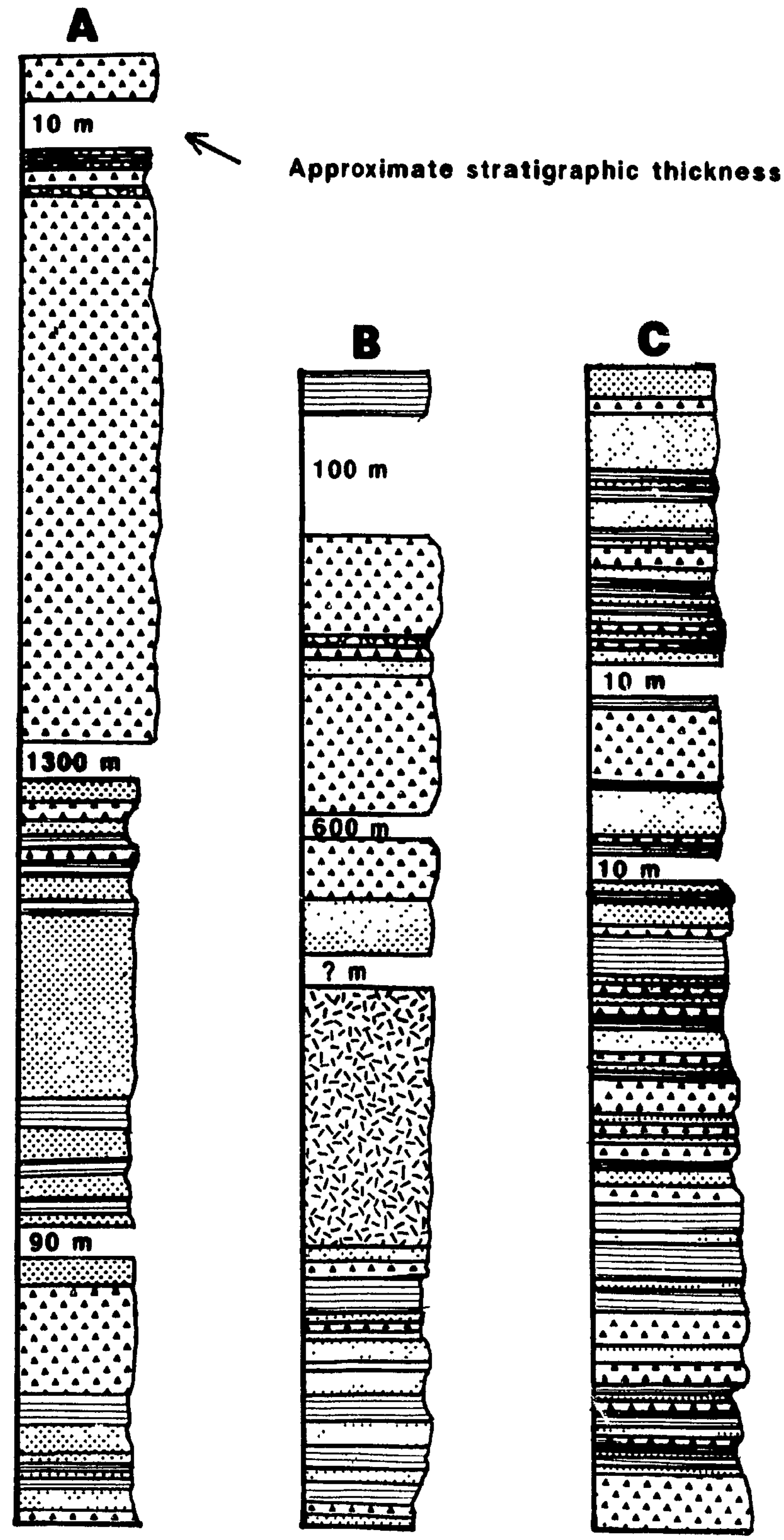

Figure 2.1 Stratigraphic columns of fault blocks A t
sandstone, horizontal lines: volcanogenic siltstone,
gabbro/diorite, irregular circles: flows.

ss missing

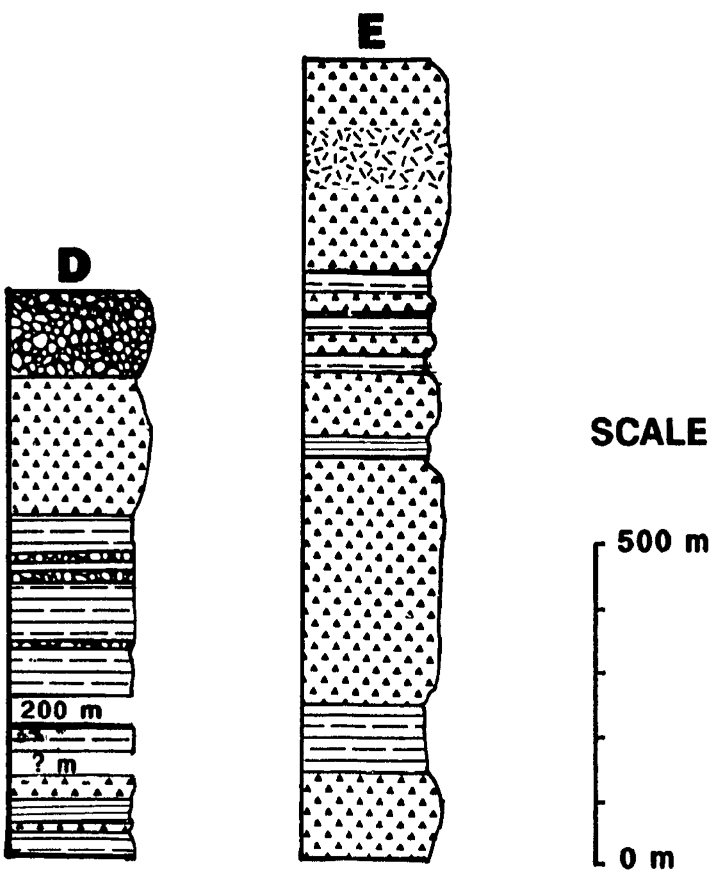

\ to E. Triangles: volcanogenic breccia, dots: volcanogenic
:, dashed horizontal lines: black siltstone, unoriented dashes:

An important stratigraphic relationship, which is common to all fault blocks, is the occurrence of fining upward units characterised by volcanogenic breccia passing upwards through volcanogenic sandstone to volcanogenic siltstone. The units are characterised by alternating beds of volcanogenic breccia, sandstone and siltstone, and display a gradual decrease in average grainsize towards the top. Individual beds of volcanogenic sandstone and siltstone, and massive units of breccia and sandstone, have sharp flat tops and bottoms, and commonly display internal normal and multiple grading. The grading is best developed in the bedded volcanogenic sandstone and siltstone.

Simple and compound lava flows make up less than five percent of the succession. They were identified in fault blocks A and D, and are concentrated in the northwest portion of the study area. The composite flow unit of block D contains abundant, large, purple-grey carbonate fragments and appears to have disrupted and incorporated a well bedded limestone unit. Simple flows show no apparent alteration, but the composite flow unit is epidote-rich.

Black siltstone occurs only in blocks D and E. Several units, approximately 100 metres thick, are found interlayered with thin lava flows in fault block D, and thinner units, typically 25 metres thick, are found interlayered with volcanogenic breccia in block E.

Due to the nature of exposure, along ridges which are cut by transcurrent faults and separated by valleys with abundant glacial till deposits, and the monotonously repeating stratigraphy, it is difficult to make stratigraphic correlations across the faults, recognize lateral facies changes, or to reconstruct the geometry and extent of volcanic and volcaniclastic units. However, some general observations can be made:

(1) Lava flows and coarse volcanogenic breccia are dominant in the northwestern portion of the study area, giving way to an increased amount of finer sediments to the southeast.

(2) Terrigenous siltstone is most abundant in the northern half of the map area.

Due to the absence of marker beds it is unknown if these relationships reflect geographic or temporal variations.

2.3 SEDIMENTARY STRUCTURES

Some sedimentary structures are preserved in volcanogenic sandstone, volcanogenic siltstone, and siltstone units. The most common are irregular or convolute beds and laminations as a result of dewatering (Plate 1). Large scale straight-crested ripple marks, characterized by a 20-centimetre wavelength and a 4-centimetre amplitude, were found in only one location in a volcanogenic sandstone unit. Smaller-scale ripple marks and cross-bedding were observed frequently in bedded black siltstone. Slump structures were occasionally observed in volcanogenic siltstone and sandstone, and were commonly associated with dewatering structures.

2.4 FIELD DESCRIPTION OF ROCKS

Volcanogenic breccia is dark green to greenish-grey in colour, compositionally heterogeneous, and comprised of cognate (juvenile magmatic), accessory (country rock that is ejected during eruption), and accidental (picked up locally by pyroclastic flows and surges) fragments, and crystals. Within an individual unit fragments display broad variations in texture and composition.

Cognate fragments are distinguished from accessory fragments based on their similarity to the groundmass. Cognate fragments and the groundmass are plagioclase, plagioclase-amphibole, or plagioclase-clinopyroxene porphyries. Pyroxene and amphibole phenocrysts are commonly euhedral, whereas plagioclase is anhedral or wispy. Phenocrysts range from a few millimetres to one centimetre in size. Accessory fragments include green-grey volcanogenic siltstone and sandstone and it is probable that there are also accessory fragments that cannot be distinguished from cognate fragments. Accidental fragments include purple-grey and buff coloured carbonate, rare black siltstone, and very rare red porphyritic igneous fragments.

In one fine-grained breccia unit altered pumice was observed. The round, cherty, pumice fragments are very pale green in colour and range from several millimetres in diameter at the bottom of the normally graded sequence, to 5 centimetres in diameter at the top of the sequence. Rare vesicular fragments (scoria) were also observed.

Crystals occurring in the groundmass are plagioclase, clinopyroxene and amphibole, and are usually unbroken. Commonly there are variations in concentration and morphology of crystals within an individual unit. Large euhedral clinopyroxene or amphibole may be dominant near the base of a unit, but these crystals may decrease in size and abundance toward the top of a unit, giving way to a higher concentration of larger plagioclase crystals.

The fragments are angular to sub-rounded, and average less than 10 centimetres in diameter, although some are as large as half a metre. Breccia units are massive and resistant, poorly sorted, and commonly display recessive calcareous patches. They vary in thickness from a few centimetres up to approximately 900 metres. Because of the classification scheme used, rocks here defined as volcanogenic breccia cover a large spectrum of crystal and fragment sizes (Plates 2, and 3).

Only four units of volcanogenic crystal breccia occur in the study area and all of them are closely associated in the northern portion of fault block B. They are approximately 1 metre thick and are characterised by a coarse centre, rich in large (5 millimetre) clinopyroxene crystals. Average thickness of the coarse grained centres is 50 centimetres while the fine grained margins are approximately 15 centimetres and 35 centimetres for the base and top respectively. Clinopyroxene is the only noticeable crystal phase, in a fine-grained matrix. There are no juvenile or lithic fragments aside from the pyroxene crystals.

Green-grey volcanogenic sandstone is composed predominantly of plagioclase, amphibole and clinopyroxene crystals, with minor small fragments which appear the same as those in the volcanogenic breccia. It may occur as graded, upward-facing beds averaging 10 centimetres in thickness, or as massive units attaining thicknesses of up to 300 metres. Bedded units commonly display pale green layers rich in plagioclase crystals and dark green layers rich in clinopyroxene or hornblende crystals (Plate 3). The finer, massive volcaniclastics are sometimes difficult to classify as igneous or sedimentary.

In one massive sandstone unit several accretionary lapilli were observed. They are cored by lithic fragments and coated with fine ash which may form concentric rings (Plate 4).

Volcanogenic siltstone (Plate 5) is green-grey in colour and exhibits wavy millimetre-scale alternating dark- and pale-green laminations, presumably reflecting alternating concentrations of clinopyroxene or amphibole, and plagioclase as in the volcanogenic sandstone. Bed thicknesses range from several millimetres to several centimetres.

Dark grey - black siltstone is the one sedimentary rock type that is clearly not a direct product of volcanic activity. It most commonly occurs as massive units which only rarely display thin rusty layers, but in some places is bedded, and individual beds may be internally laminated. Abundant fine-grained pyrite is distributed throughout the rock and bedding-parallel recessive calcareous zones are common (Plate 6). The unit is recessive relative to volcaniclastics and easily erodes to form deep cols in the ridges.

Dark green lava flows are difficult to recognise because of similarities to volcanogenic breccia in outcrop appearance, and their close association with breccia units. Flows average one to three metres in thickness and commonly pass upwards into brecciated flow tops. They are plagioclase - clinopyroxene or plagioclase - amphibole porphyries, with phenocrysts typically two to three millimetres in diameter. Chilled basal contacts and hyaloclastite textures were rarely observed.

The strata are cut by abundant intermediate to felsic dykes and sills which commonly change direction drastically over short distances. They are 1 to 3 metres thick and typically have no perceptible chilled margins. Dark green mafic and intermediate dykes and sills are plagioclase-clinopyroxene or plagioclase-amphibole porphyries, while more felsic buff-coloured dykes are plagioclase-amphibole-biotite porphyries. Phenocrysts of all compositions are typically 0.5 centimetre in diameter but may reach 2 centimetres. Crosscutting relationships between intermediate and felsic dykes are rare, but where they exist demonstrate that intermediate dykes are generally younger than felsic ones.

Massive dark green gabbro/diorite outcrops in several locations. It is plagioclase and amphibole porphyritic, and grain size increases from fine to medium away from inferred original contacts, which are faulted in several cases. Although intrusive relationships are not apparent, there is no evidence for flow origin. It is assumed these bodies are satellite intrusions of Upper Triassic or Lower Jurassic Alaskan-type ultramafic-gabbroic bodies which are locally abundant. All but one of the Alaskan-type intrusives intrudes Takla rocks, and they are thought to be genetically related to Takla magma (Irvine, 1976).

The Jensen Peak Pluton of mid-Cretaceous age or older (Richards, 1976) intrudes the strata in the southernmost part of the map area. It is of tonalitic composition, coarse-grained, and porphyritic with plagioclase, amphibole, and biotite. Although the contact zone is epidote-rich and highly fractured as a result of local movements, intrusive relationships are evident.

2.5 PETROGRAPHY

Thin section examination was conducted primarily on dykes, flows, gabbro/diorite bodies, tonalite intrusives, and volcanogenic breccia. Virtually all of the samples are porphyritic, with plagioclase, clinopyroxene, and amphibole as the main phenocryst phases (Plates 7 through 9).

Mafic to intermediate dykes, volcanic flows, and mafic volcanogenic breccia fragments are all porphyritic with plagioclase and pyroxene and very similar in appearance. At intermediate compositions pyroxene is replaced by amphibole. Intermediate dykes are very similar to the gabbro/diorite intrusives and intermediate breccia fragments, all of which are porphyritic with plagioclase and amphibole. Biotite appears as a phenocryst only in the most evolved dyke samples and tonalite.

Plagioclase is ubiquitous throughout the suite, comprising up to fifty percent of some rocks. Pyroxene or amphibole commonly account for forty percent of the rock volume. Sphene, altered magnetite, and sulphides occur as microphenocrysts. Porphyritic texture is the most common, but glomeroporphyritic, seriate, equigranular, and granitic textures also occur in some dyke samples.

The matrix of all samples is fine-grained and comprised predominantly of plagioclase microlites which commonly display a trachytic texture (Figure 9). Minor quartz and potassium feldspar may also occur. The matrix is commonly completely replaced by metamorphic assemblages. Epidote, calcite and leucoxene are the most abundant metamorphic phases.

Lava flows, volcanogenic breccia, and volcanogenic sandstone are commonly characterised by a locally glassy matrix or glassy fragments. In rare volcanogenic sandstone units glassy fragments may comprise up to eighty percent of the rock volume. The glassy patches in the matrix, and glassy fragments, are pale brown to colourless in plane polarized light and nearly isotropic under crossed Nicols. They are rarely amorphous but more commonly exhibit a streaky lamination, and may be recrystallized to microcrystalline, fibrous aggregates. Glass shards and devitrification spherulites were rarely observed.

Plagioclase phenocrysts are euhedral, commonly twinned with albite, pericline and minor Carlsbad twins, and commonly concentrically zoned. Colourless to pale brown clinopyroxene occurs only in basaltic compositions and is commonly characterised by euhedral eight-sided cross-sections with or without simple and lamellar twins. Some mafic dyke samples contain crystals with pronounced concentric zoning. Green-brown and blue-green amphibole occur as euhedral six-sided cross-sections or subhedral prisms with poorly developed terminations. Paired and lamellar twins are common. Amphiboles may display a brown dusty alteration along mineral lineations, and brown hornblende commonly shows a peripheral zone of green hornblende.

Clinopyroxene and hornblende rarely coexist, although hornblende and biotite commonly do. Biotite is observed forming reaction rims and overgrowths on hornblende. Neither olivine nor orthopyroxene was observed. Magnetite, which has been altered to limonite and sphene, occurs sporadically throughout the suite. Pyrite and chalcopyrite comprise less than five percent of most rocks but are more abundant in volcanogenic breccia units near major fault zones.

Intrusives and flows commonly exhibit irregular patches having a different texture or even a different composition from the rest of the rock. The fragments in volcanogenic breccia are usually easily identified by differences in composition and texture, and sharp fragment boundaries (Plate 8).

2.6 DEFORMATION

Faulting is the dominant style of deformation in the study area. Five major vertical to steeply dipping, northwest-trending, transcurrent faults divide the area into six distinct fault blocks (Plate 11). Rotation of bedding was observed associated with three of the transcurrent faults and demonstrates a dextral sense of movement (see Figure A.1). Several smaller scale faults were observed or inferred throughout the map area. These are vertical to steeply-dipping. Their sense of movement is unknown, and they display no consistent orientation. Small-scale reverse faults were observed in the southeastern end of fault block E. They are closely spaced (several metres) and offsets of dykes indicate displacements of tens of metres.

Small-scale kink folds were observed rarely in volcanogenic sandstone and siltstone units closely associated with major faults (Plate 10). In the south-central portion of the map area large-scale recumbent folds with varied sense of vergence were observed on a cliff face (Plate 12). Detailed observation was not possible due to their location. They occur in a thick unit of volcanogenic sandstone bounded by volcanogenic breccia.

2.7 METAMORPHISM

The predominant metamorphic minerals are calcite, epidote, actinolite, and leucoxene, with minor chlorite, and muscovite. Based on this metamorphic assemblage the sequence is assigned to the lower greenschist facies. The appearance of biotite and elimination of calcite, which marks the entrance into the upper greenschist facies, is not observed. There is no obvious increase in metamorphic grade towards the Hogem Batholith to the south of the map area (Figure 1.2), or to the Jensen Peak and other related plutons (Woodsworth, 1976), indicating regional rather than contact metamorphism.

Clinopyroxene and hornblende are commonly completely replaced by actinolite, and may also display cores of epidote, chlorite, and minor calcite. Plagioclase may suffer only minor replacement by epidote or leucoxene, or may be completely replaced and recognised only by a ghost of its crystal shape. The cores are usually the most altered part of zoned plagioclase crystals. Aggregates of calcite, epidote intergrown with chlorite, or quartz, also occur.

Plate 1 Convolute beds and laminations as a result of dewatering.

Plate 2 Coarse-grained volcanogenic breccia.

Plate 3 Fine-grained volcanogenic breccia bounding a thin bed of volcanogenic siltstone.

Plate 4 Accretionary lapilli in a volcanogenic sandstone unit. Note hammer head for scale.

Plate 1

Plate 2

Plate 3

Plate 4

Plate 5 Volcanogenic siltstone unit displaying wavy laminations.

Plate 6 Black siltstone unit.

Plate 5


Plate 6

Plate 7 Thin section of plagioclase-amphibole porphyry. Section shows plagioclase phenocrysts and microphenocrysts in a fine-grained matrix composed largely of epidote.

Plate 8 Thin section of volcanogenic breccia. Section shows large fragment to the left of centre which contains plagioclase and euhedral pyroxene.

Plate 9 Thin section of volcanogenic breccia displaying amphibole phenocrysts and a trachytic texture in the matrix.

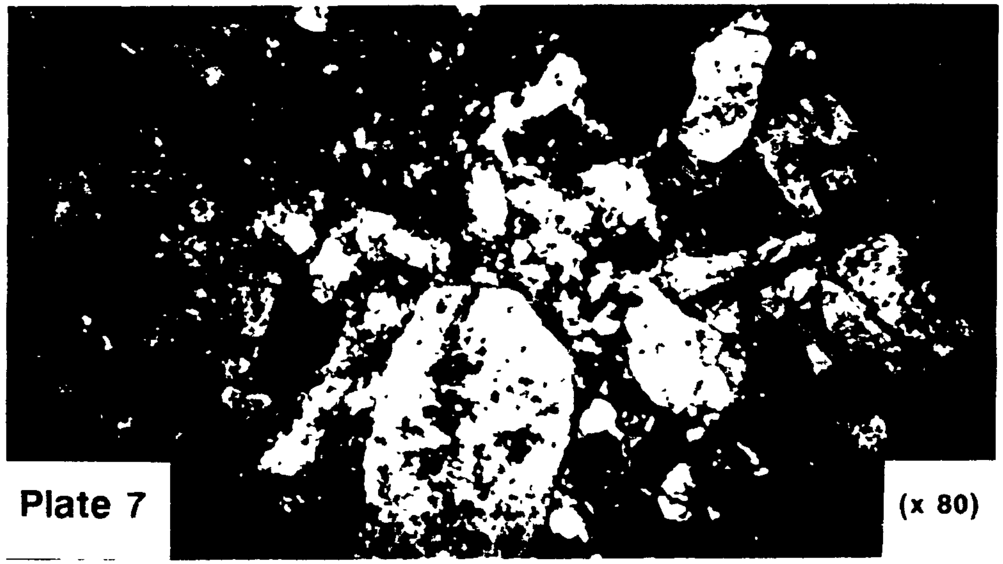

Plate 7 (x 80)

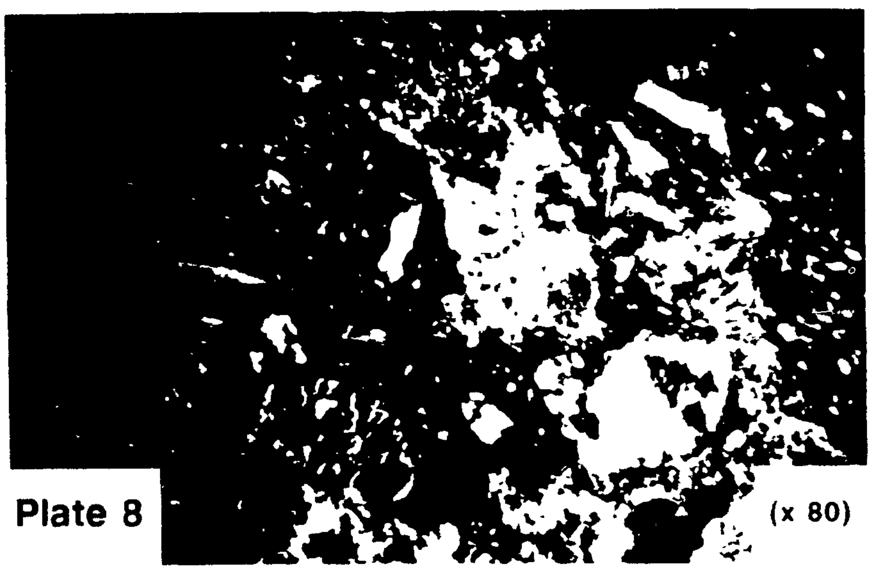

Plate 8 (x 80)

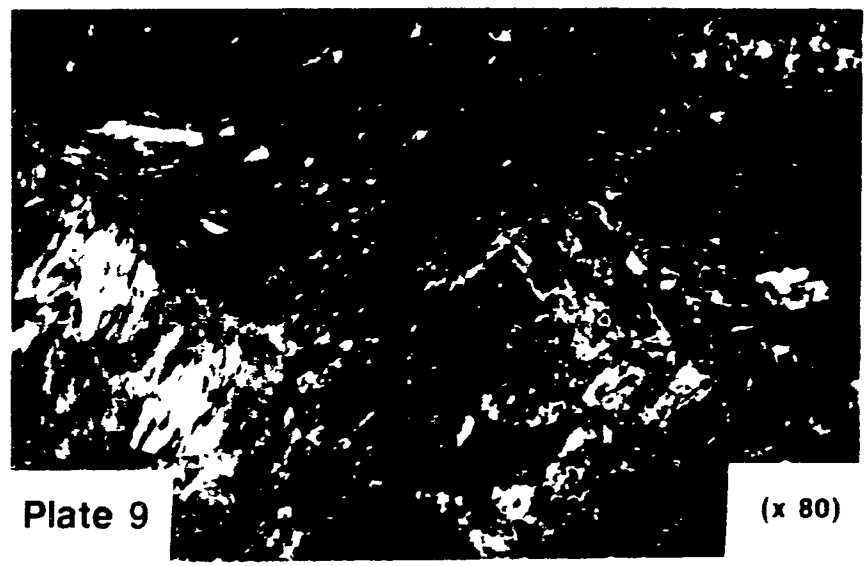

Plate 9 (x 80)

Plate 10 Small-scale "s" fold typical of folds associated with major faults.

Plate 11 Major transcurrent fault which juxtaposes a sequence of rusty black siltstone against a green volcaniclastic sequence.

Plate 12 Large-scale folds with varied sense of vergence in the southeast portion of the map area. Note person in lower right for scale.

Plate 10

Plate 11

Plate 12

CHAPTER 3

MODE OF FORMATION OF THE VOLCANO-SEDIMENTARY SUCCESSION

3.1 INTRODUCTION

The origin, depositional processes, and environment of deposition of the volcaniclastic sequence can provide data with which to evaluate the paleotectonic environment. There are different patterns and conditions of volcanism associated with different tectonic settings (Cas and Wright, 1987). To constrain the tectonic environment of the Takla volcano-sedimentary succession, significant facies associations and distinctive characteristics of the different rock types are evaluated.

3.2 MODE OF FRAGMENTATION

To determine the origin of the volcaniclastics it is necessary to determine their mode of fragmentation. The fragments in volcaniclastic rocks can be produced both by primary volcanic processes contemporaneous with eruption and by secondary surface processes (Table 3.1, after Cas and Wright, 1987). The relative proportions of pyroclastic, autoclastic, and epiclastic fragments, and the type of pyroclastic eruption can often be determined from the types, abundances, and morphologies of fragments. Magmatic explosions which result from the exsolution of volatiles should produce abundant vesicular fragments, pumice and glass shards. In phreatic or phreatomagmatic explosions vesicular fragments and pumice are not as common, the fragments are usually more blocky, and some quench fragmentation should be observed. Autoclastic processes should produce splintery and blocky glassy fragments with sharp edges and corners, or slabs of plastically deformed lava. Obviously epiclastic fragmentation would not produce any of these textures.

Table 3.1 Modes of Formation of Volcaniclastic Deposits

Magmatic explosions Phreatic or steam explosions Phreatomagmatic explosions	Pyroclastic Processes	Primary Volcanic Processes
Quench- and Chill-shatter fragmentation Flow fragmentation	Autoclastic Processes	
Epiclastic fragmentation		Secondary Surface Processes

The presence of pumice, glassy fragments, glassy zones in the groundmass of flows, volcanogenic breccia, and volcanogenic sandstone, and occasional vesicular fragments indicate that the majority of fragments were produced pyroclastically during several magmatic explosions. The presence of accretionary lapilli indicate that at least some of the explosions were subaerial. Although the evidence suggests fragmentation by pyroclastic eruptions produced by the exsolution of volatiles, phreatic or phreatomagmatic explosions may also have occurred. Accretionary lapilli are most frequently the result of phreatic or phreatomagmatic eruptions in which fine ash accretes on water droplets in steam rich columns (Cas and Wright, 1987).

3.3 MODE OF DEPOSITION

It is evident from dewatering structures, excellently graded beds, oscillation ripple marks, abundant carbonate fragments, reverse grading of pumice, and the close association with sedimentary siltstone, that the volcaniclastic sequence was ultimately deposited subaqueously. Whether deposits are the result of subaerial pyroclastic flows which flowed into water, primary subaerial deposit which were epiclastically remobilized, or subaqueous eruptions, is difficult to determine. The principles which govern the deposition of epiclastic rocks are very similar to those that control the deposition of pyroclastic rocks, making the two processes difficult, perhaps impossible, to distinguish in ancient deposits.

The volcaniclastic sequence in the study area is homogeneous over its entire thickness. Such a thick package of rock deposited by epiclastic processes would probably contain a wider range of volcanogenic and sedimentary deposits. Consequently the volcaniclastics are believed to have been deposited directly by pyroclastic processes.

There are three types of pyroclastic deposit, which are classified according to their mode of transportation and deposition (Cas and Wright, 1987). They are: pyroclastic fall deposits, pyroclastic flow deposits, and pyroclastic surge deposits (Figure 3.1). Pyroclastic fall deposits are formed as fine tephra settles out of expanding eruption columns. They are generally well sorted, show mantle bedding (cover irregular surfaces in an equal thickness of ash), and sometimes internal stratification or lamination. Pyroclastic flow deposits are hot, gravity controlled flows of pyroclastic debris which moves as a high-particle-concentration gas-solid dispersion. They contain large, generally non-vesicular cognate lithic blocks which can exceed 5 metres in diameter, and are usually massive, poorly sorted, and found filling topographic depressions. Pyroclastic surge deposits travel as turbulent, low-particle-concentration gas-solid dispersions. They are, to some degree, topographically controlled, but usually have sufficient energy to mount some topographic highs. They commonly exhibit low-angle cross stratification, dune forms, pinch and swell structures, and chute and pool structures. It is common for an individual

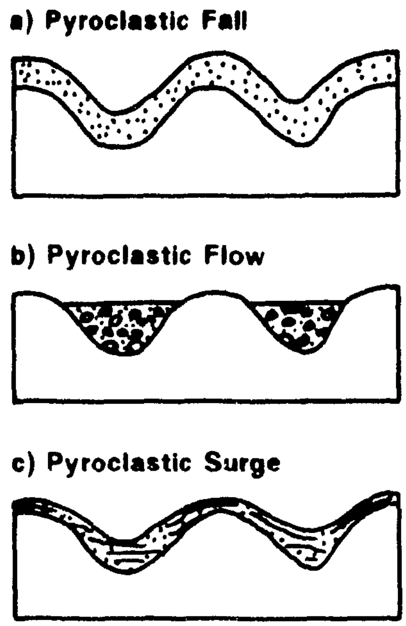

Figure 3.1 Geometric relationships of pyroclastic fall, flow, and surge deposits overlying the same topography. After Cas and Wright, 1987.

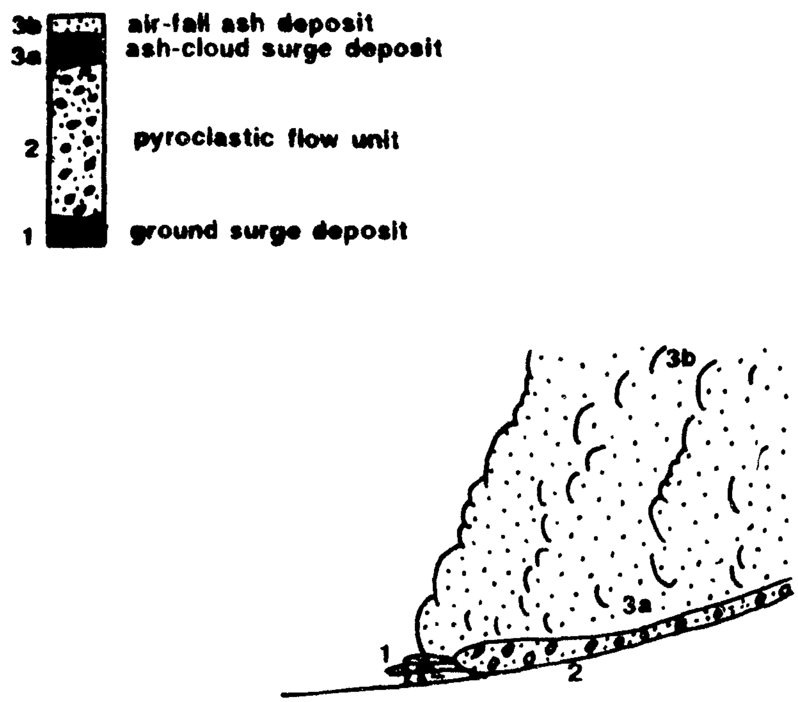

Figure 3.2 Schematic diagram showing the structure and idealised deposits of one pyroclastic flow. After Cas and Wright, 1987.

eruption to produce all three types of pyroclastic deposit,and an ideal pyroclastic "flow" unit produces associated pyroclastic surge and fall deposits (Figure 3.2).

To determine the type of pyroclastic process (fall, flow or surge) which is primarily responsible for the deposition of the sequence, volcanogenic breccia, which occupies the greatest thickness of the sequence, was examined. Considering the grain size of these units, it is unlikely that they were deposited by pyroclastic fall, and the absence of any of the features typical of pyroclastic surges indicates that the volcanogenic breccias are most likely pyroclastic flow deposits. Because the volcanogenic sandstone and volcanogenic siltstone units are so closely associated with the volcanogenic breccia in fining-upward units, they are probably pyroclastic flow deposits. Sand- and silt-size fragments may have settled out of turbulent clouds of ash commonly associated with pyroclastic flows (Figure 3.2).

3.4 PROPOSED MODE OF FORMATION

The proposed mode of eruption and deposition of Takla Group rocks in the study area involves several pyroclastic eruptions brought on by the exsolution of volatiles. Each eruption may have generated one or more pyroclastic flows with associated overriding turbulent ash clouds. The flows entered a body of water, and having sufficient momentum to continue subaqueously, flowed in similar fashion to turbidites (Figure 3.3). The main body of the pyroclastic flow may have deposited the volcanogenic breccia and massive volcanogenic sandstone, while the overriding turbulent cloud of ash deposited the well-bedded and graded volcanogenic sandstone and siltstone. Assuming that the rocks in each of the fault blocks are of the same age, the predominance of coarse volcaniclastics in the northern half of the study area may indicate a northerly source for the pyroclastic flows.

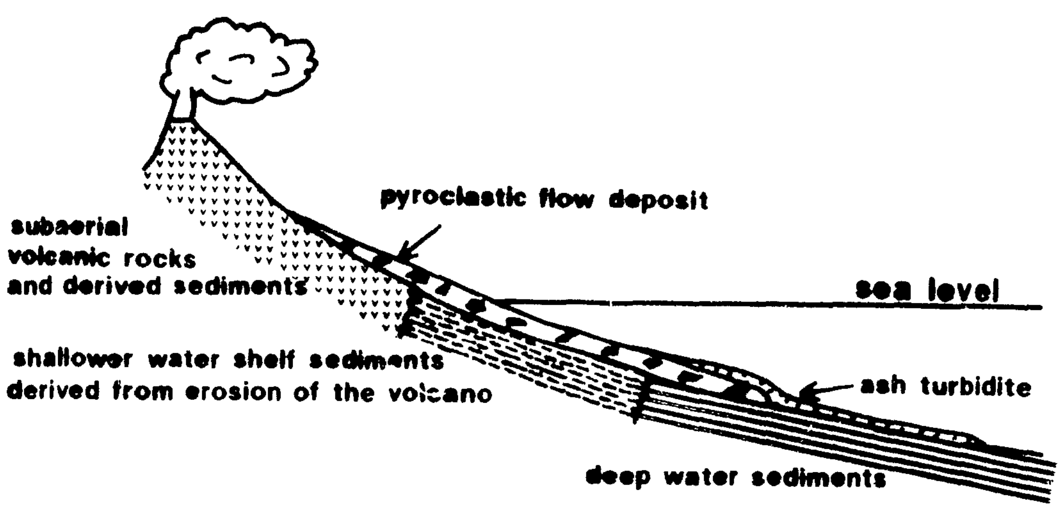

Figure 3.3 Schematic diagram showing the passage of a subaerial pyroclastic flow into a body of water. After Cas and Wright, 1987.

CHAPTER 4

GEOCHEMISTRY

4.1 SAMPLE SELECTION

Based on hand sample and thin-section study, a group of least altered samples representing the compositional range of the suite was chosen for whole rock analysis. There was some difficulty in determining which samples might yield potential original liquid compositions and which ones might not. Although the volcaniclastics are believed to have been deposited directly by pyroclastic processes, they are suspect and may not be reliable geochemical samples. The abundant dykes and sills clearly represent the igneous activity of the study area over space and time and are therefore the preferred rocktype for geochemical analysis. Other demonstrably igneous samples including gabbroic intrusives, tonalite intrusives, lava flows, and some breccia fragments, were sampled to asses genetic relationships to the dykes and sills. Lava flows, intrusives, and breccia fragments chosen for analysis do not display any cumulate textures, but phenocrysts of plagioclase and clinopyroxene are commonly zoned. Selected breccia fragments do not contain fragments themselves. Breccia whole rock and matrix samples were analyzed to assess the degree of syndepositional alteration or contamination of the breccia units.

To avoid analyzing samples which may have undergone appreciable secondary alteration, the samples selected displayed no obvious calcareous, or epidote-rich zones, and no tectonic fabric. Thirty-seven samples were selected and are divided between twenty dykes and sills, three flows, two gabbroic intrusives, one tonalite intrusive, six breccia fragments, two breccia matrix, and two breccia whole rock (Table A.1). Sample locations are presented in Figure A.1.

4.2 ANALYTICAL METHODOLOGY

Major and trace element abundances were determined at Geochemical Laboratories, McGill University using a PW 1400 X-ray Fluorescence (XRF) spectrometer. The samples were prepared for analysis by first removing the weathered rind with a diamond rock saw and sanding fresh surfaces to remove any contamination left by the saw blade. They were then crushed to less than 5 millimetre pieces in a TM Jaw Crusher and ground to a fine powder in a Surface Hardened SAE 1018 Iron Grinding Barrel. To minimise contamination, the samples were prepared in gradational order with respect to composition, the jaw crusher was cleaned with a brush and air hose, and the grinding barrel cleaned with an air hose and primed between samples. Loss on Ignition (LOI) was determined by heating the sample powders to 1000°C for one hour.

The detection limit for major elements is 0.01 wt%; for Cr_2O_3 it is 15 ppm, and for the rest of the trace elements 10 ppm. Analytical precision is ± 1 % absolute for major elements and ± 5 % absolute for trace elements (Ahmedali, 1983). Total iron was recalculated as Fe_2O_3.

Ferrous and ferric iron concentrations were determined by ammonium metavanadate titration on five rock powders of various compositions (see Table A.1). The detection limit was 0.01 wt% and the analytical error ± 1 % absolute.

4.3 ANALYTICAL RESULTS

Major and trace element concentrations are presented in Table A.2. The concentrations of Pb, Th, and U were below or very close to the detection limits and are not susceptible to further study.

Zirconium was chosen as an index of differentiation because of its incompatibility (Pearce, 1982), and major and trace element versus zirconium plots are presented in Figure 4.1. Most major elements show well defined trends. The gradual increase in silica, phosphorous and alkalis, and decrease in calcium, magnesium, manganese, and total iron with increased differentiation indicates that the suite may be comagmatic and differentiated by a continuous process. This possibility is more fully examined in Chapter 6, using trace element data. Ferric and ferrous oxide concentrations and ratios are presented in Table 4.1. Appropriate concentrations of ferric and ferrous iron are assigned to source magma compositions and product magma compositions in least squares mixing calculations in Chapter 6.

Table 4.1 Ferric and Ferrous Iron Concentrations

Analysis	Sample Number	FeO(wt%)	Fe_2O_3(wt%)	Fe_2O_3/FeO
1	24	7.05	2.78	0.394
2	23	8.08	2.72	0.337
3	20	3.43	0.57	0.166
4	21	2.12	0.61	0.288
5	19	4.58	0.86	0.189

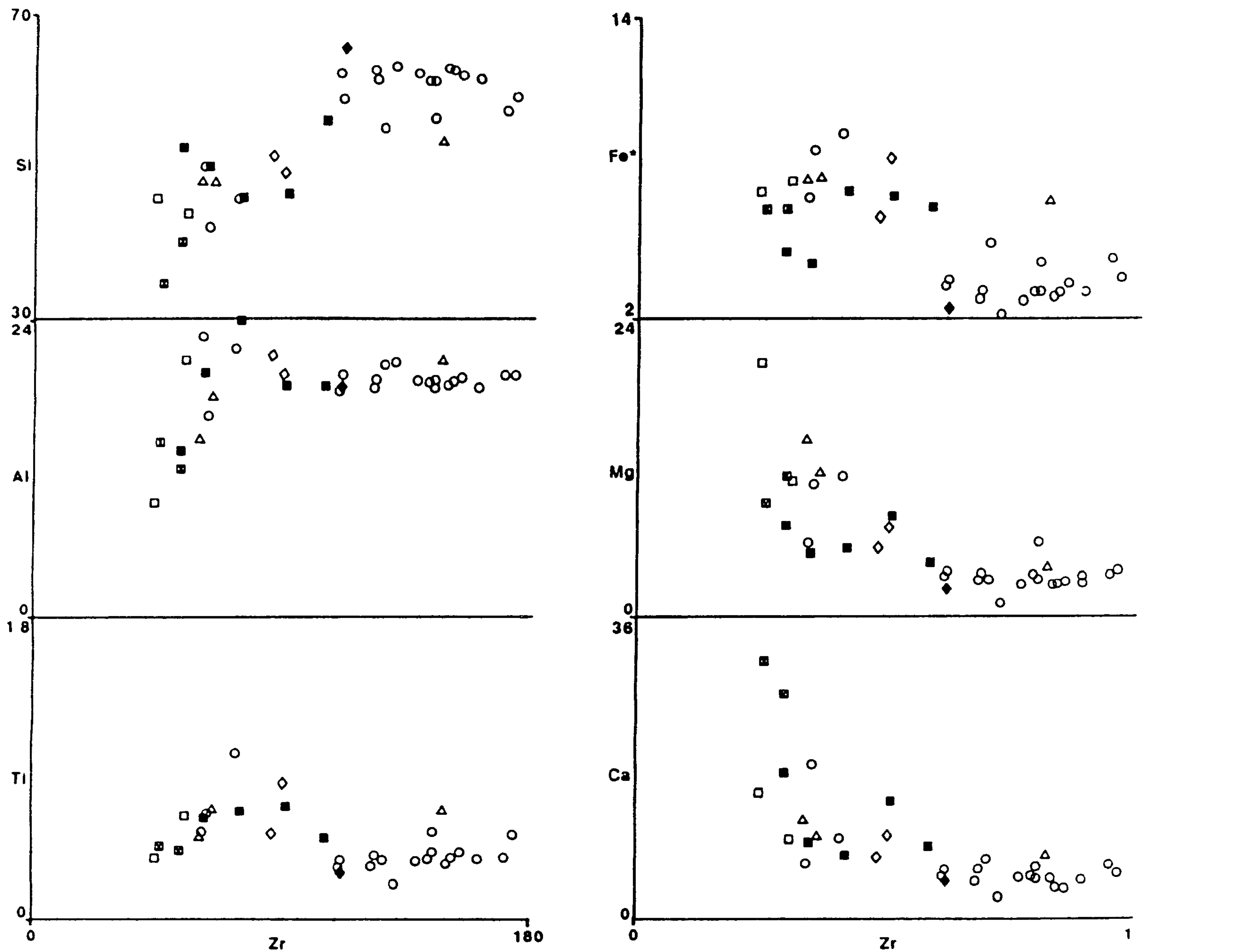

Figure 4.1 Major and trace element concentrations (cation percent and ppm respectively) against Zr (index of fractionation). For symbols see Table A.1.

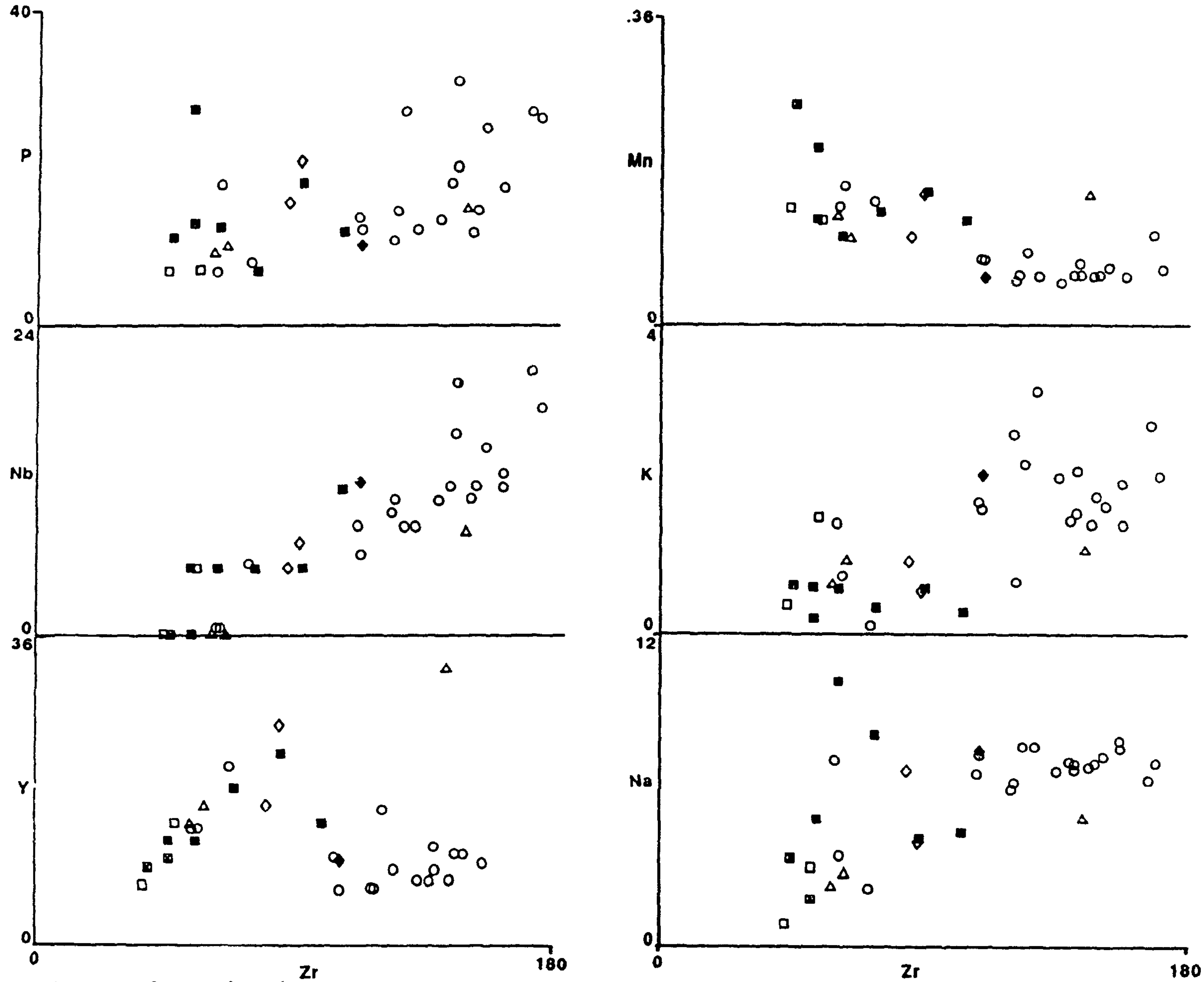

Figure 4.1 continued.

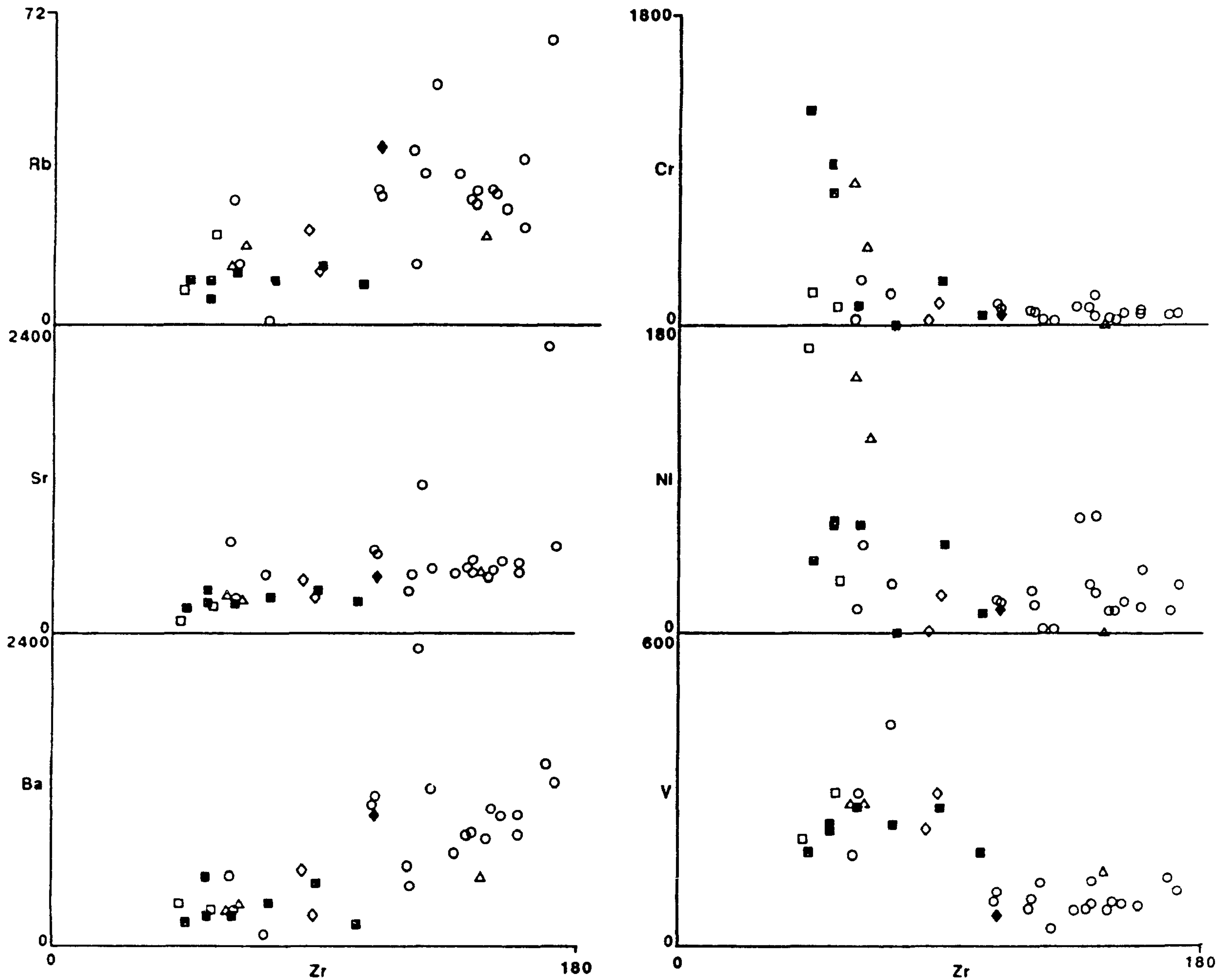

Figure 4.1 continued.

4.4 ALTERATION

The volatile content, estimated from the loss on ignition (LOI), is an indication of the degree of alteration. The most altered samples are volcanogenic breccia matrix. They are characterised by LOI's of 17.73 and 11.70 weight percent relative to the average of 3.21 weight percent (Table A.2). When classified on an alkalies versus silica classification plot (Figure 4.5), one volcanogenic breccia matrix sample is lower in SiO_2 than a picrite and is unlikely to be a liquid composition. These two matrix samples have been eliminated from further study.

4.5 ROCK CLASSIFICATION

The rocks were first classified according to the major series; alkaline, tholeiitic, or calcalkaline, using major element chemistry. Trace element data will also be used to discriminate between these series in chapter six, on petrogenesis.

To distinguish alkaline and subalkaline volcanics, a weight percent plot of (Na_2O + K_2O) against SiO_2 was used (Figure 4.2). All the data fell either on the dividing line between alkaline and subalkaline or in the subalkaline field. For distinction between tholeiitic and calcalkaline suites a

FeO^*/MgO versus SiO_2 plot (Figure 4.3) and an AFM diagram (Figure 4.4) were used. In figure 4.3 a dividing slope is used to separate the two suites. The Takla suite defines a lower slope than the dividing slope, indicating low iron enrichment with fractionation, typical of calcalkaline rocks. This finding is supported by the AFM diagram (Figure 4.4).

For classification of rock types, all samples were plotted on a total alkali versus silica classification diagram of LeBas et al. (1986), and show a broad compositional range from picro-basalt to dacite (Figure 4.5).

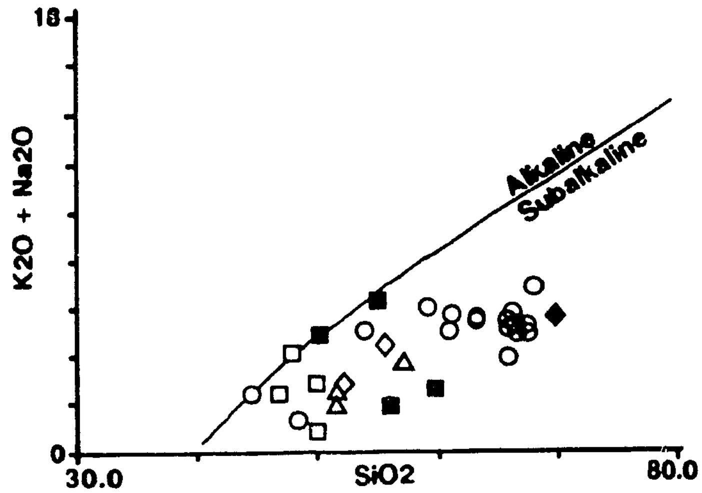

Figure 4.2 Alkaline versus subalkaline plot after Irvine and Baragar (1971). Values in weight percent.

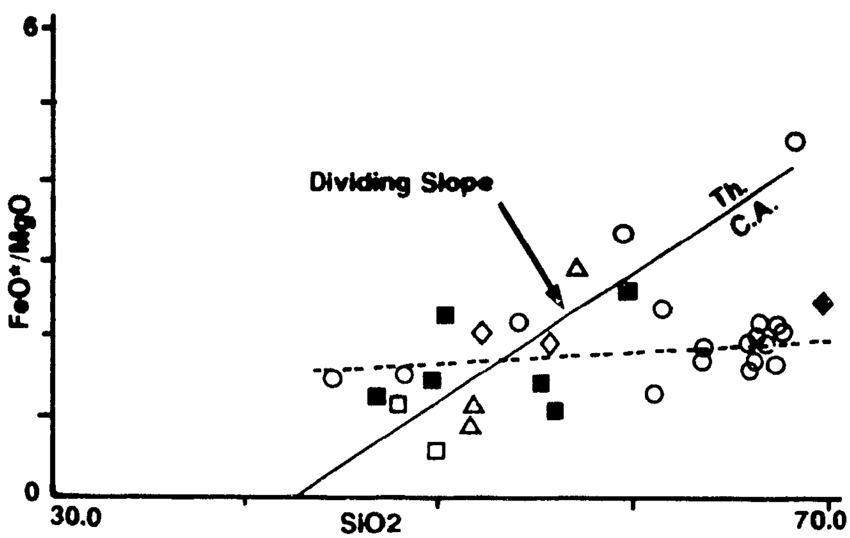

Figure 4.3 Tholeiitic versus calc-alkaline plot. Modified after Miyashiro, 1974. Values in weight percent.

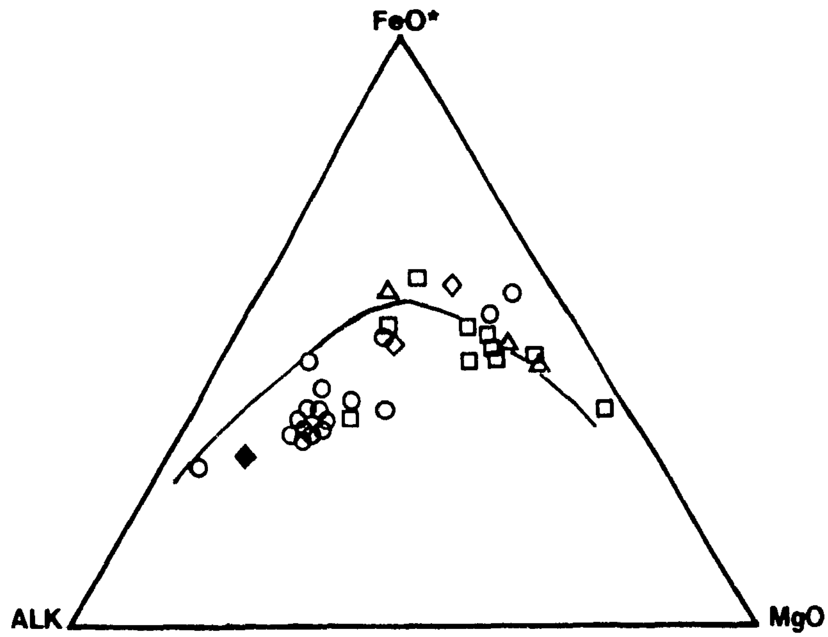

Figure 4.4 AFM plot after Irvine and Baragar (1971). Dividing line separates tholeiitic above, and calc-alkaline below. Values in weight percent.

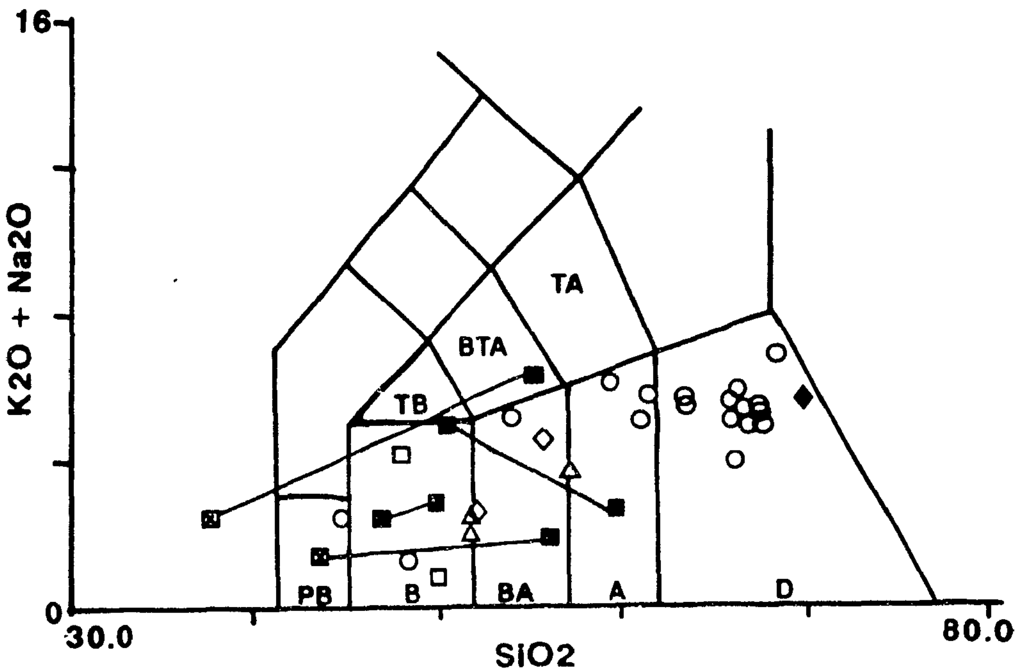

Figure 4.5 Total alkalies versus silica (weight percent) classification plot of LeBas et. al. (1986). PB = picro-basalt, B = basalt, BA = basaltic andesite, A = andesite, D = dacite, TB = trachy-basalt , BTA = basaltic trachy-andesite, TA = trachy-andesite. Tie lines connect samples from the same volcanogenic breccia.

CHAPTER 5

PALEOTECTONIC ENVIRONMENT

5.1 INTRODUCTION

To determine the paleotectonic environment in which Takla rocks were erupted, major and trace element concentrations were used in tectonic discrimination diagrams. Discriminant plots are based on the principle that elemental compositions of igneous rocks should reflect tectonic conditions at the time of their emplacement (Barker, 1983). Therefore geochemical features of known, present day tectonic environments can be used to identify the tectonic setting of ancient successions by comparison. Classification on a geochemical basis is especially useful when studying tectonically isolated terranes for which original geographic relationships to adjacent terranes are unavailable.

5.2 WHOLE ROCK DISCRIMINANT PLOTS

For application of whole rock element concentrations to discriminant plots, the samples were separated into basic, intermediate, and felsic.

Basic samples, meeting the criterion: $12 < (CaO + MgO) >$

20 wt % were used in two trace element plots of Pearce and Cann (1973, Figure 5.1 and 5.2 this thesis), and one of Pearce (1982, Figure 5.3 this thesis). In Figure 5.1, Ti, Zr, and Y are used to discriminate between low potassium tholeiites, ocean floor basalts, calcalkali basalts, and within-plate basalts. All analyses fall in field B which encompasses all magma types except within-plate basalts. In Figure 5.2, which discriminates on the bases of Ti, Zr, and Sr, there is a better separation of fields and the same samples plot in the fields of low potassium tholeiites and calcalkali basalts, indicating a volcanic arc tectonic setting. In Figure 5.3 Cr and Y are used to discriminate between volcanic arc basalt, within-plate basalt, and mid-ocean ridge basalt. Again all analyses fall in the volcanic arc field.

Intermediate samples, falling between 51 and 60 wt% SiO_2, are plotted on an Al_2O_3-FeO^*-MgO diagram of Pearce, Gorman, and Birkett (1977, Figure 5.4 this thesis). The samples show a broad distribution about the orogenic (volcanic arc) field. Although the samples show a wide scatter, this is similar to the scatter that was observed for orogenic rocks when the plot was developed (Pearce, Gorman, and Birkett, 1977).

The most felsic samples, with greater than 55 weight percent SiO_2, are used in a Rb versus Y + Nb discriminant diagram of Pearce, Harris, and Tindle (1984, Figure 5.5 this thesis). Again all samples fall in the field of volcanic arcs.

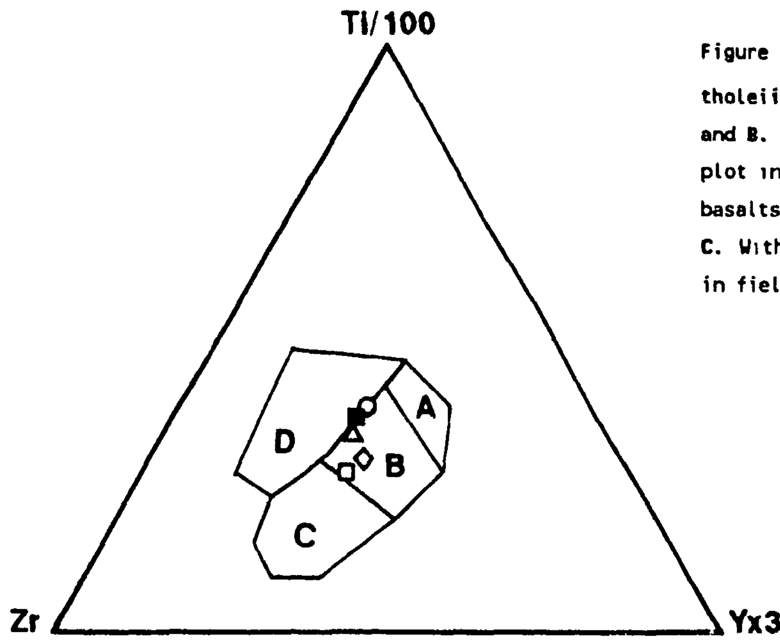

Figure 5.1 Low potassium tholeiites plot is fields A and B. Ocean floor basalts plot in field B. Calc-alkali basalts plot in fields B and C. Within plate basalts plot in field D.

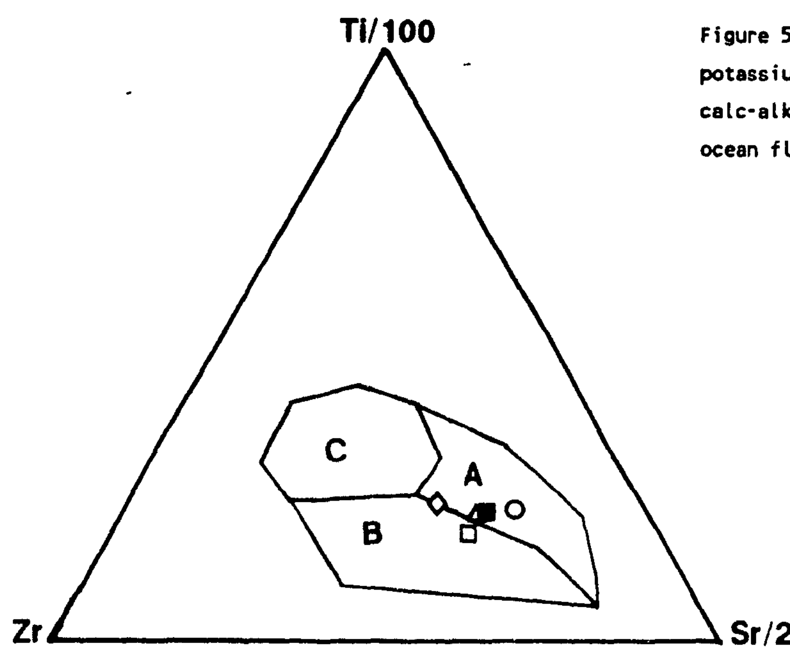

Figure 5.2 Field A : low potassium tholeiite. Field B: calc-alkali basalts. Field C: ocean floor basalts.

Figures 5.1 and 5.2 Tectonic discrimination plots for basaltic compositions. After Pearce and Cann, 1973.

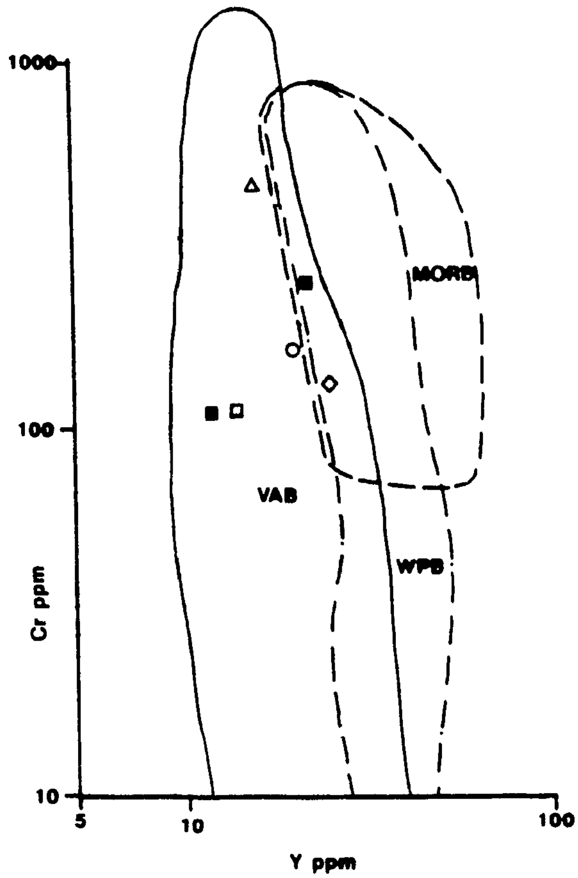

Figure 5.3 Discrimination plot for basaltic compositions. After Pearce 1982. **VAB** : volcanic arc basalt, **WPB** : within plate basalt, **MORB**: mid-ocean ridge basalt.

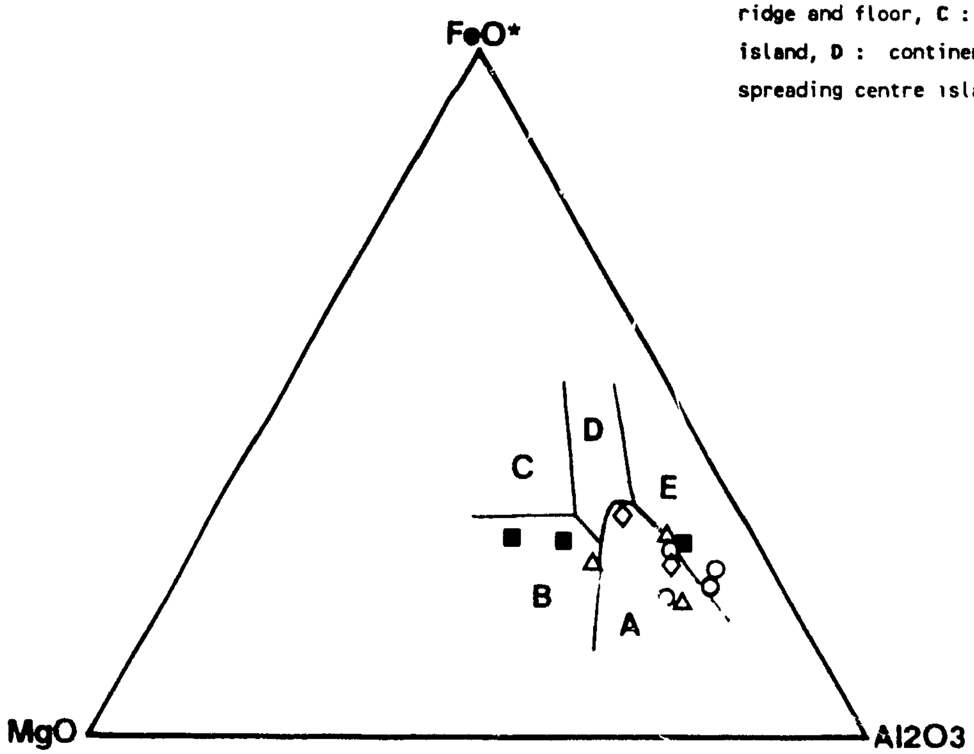

Figure 5.4 Discriminant plot applicable to subalkaline rocks characterised by 51 - 56 wt% SiO_2. Modified after Pearce, Gorman, and Birkett, 1977. Field **A** : orogenic, **B** : ocean ridge and floor, **C** : oceanic island, **D** : continental, **E**: spreading centre island.

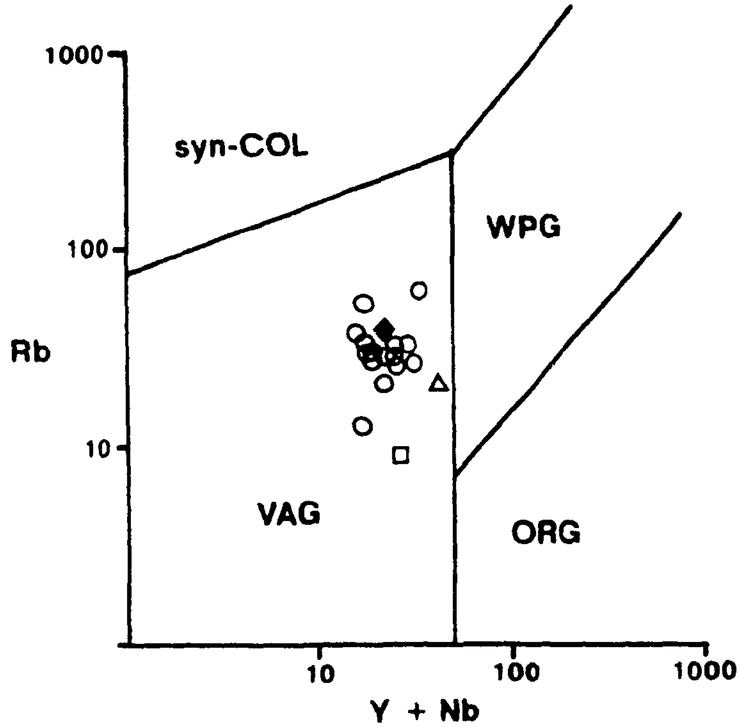

Figure 5.5 Tectonic discrimination plot for granitic compositions (wt% SiO_2 > 55). After Pearce, Harris, and Tindle, 1984. **VAG** : volcanic arc granite, **ORG** : ocean ridge granite, **WPG** : within plate granite, **syn-COL** : syn-collisional granite.

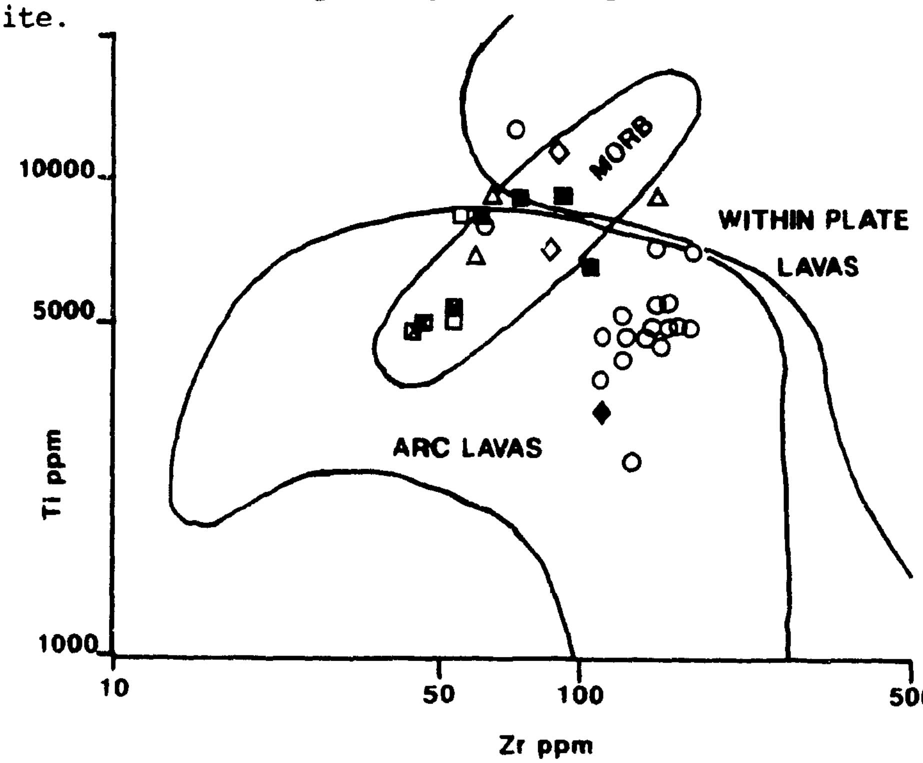

Figure 5.6 Tectonic discrimination plot suitable for igneous rocks of all compositions. After Pearce (1982).

An additional whole rock discriminant plot of Ti versus Zr which is suitable for all rock compositions is presented in Figure 5.6. All but six of the samples fall in the volcanic arc field.

5.3 CLINOPYROXENE DISCRIMINANT PLOTS

There are significant compositional variations in clinopyroxene from different tectonic settings which make clinopyroxene compositions useful for determining the tectonic settings of eruption of the host magmas. Discrimination is possible because differences in the bulk chemistry of the host magma affect the partitioning of cations into the pyroxene lattice (Nisbet and Pearce, 1977). These discriminants have the advantage over those using bulk chemistry that they are probably unaffected by secondary processes. Concentrically zoned and unzoned clinopyroxene were analyzed. In zoned crystals, several analyses were taken from core to rim.

TiO_2, MnO, and Na_2O were found to provide the best separation between magma types and are used in the ternary plot of Figure 5.7. The clinopyroxene compositions plot predominantly in field 3, which encompasses all magma types, and therefore are not discriminated. A better separation of magma types is achieved using a discriminant function diagram which makes use of all major element abundances to find the

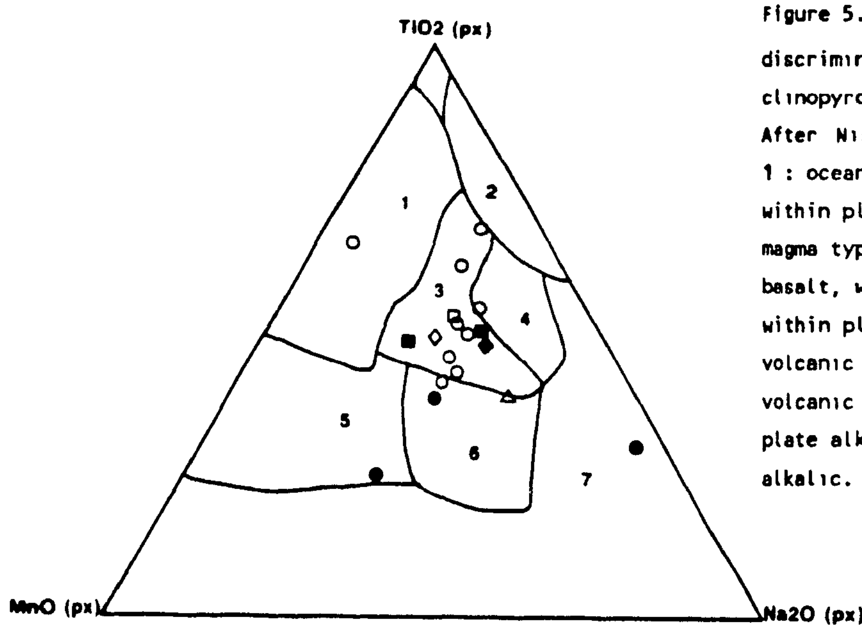

Figure 5.7 Tectonic discrimination diagram using clinopyroxene compositions. After Nisbet and Pearce (1977). 1 : ocean floor basalt, 2 : within plate alkalic, 3 : all magma types, 4 : volcanic arc basalt, within plate tholeiite, within plate alkalic, 5 : volcanic arc basalt, 6 : volcanic arc basalt, within plate alkalic, 7 . within plate alkalic.

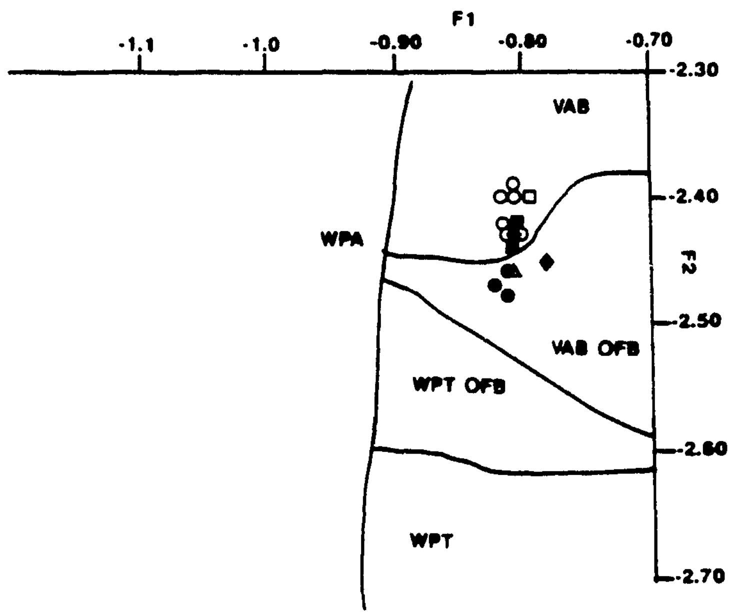

Figure 5.8 Discriminant function plot of clinopyroxene compositions. After Nisbet and Pearce (1977). VAB : volcanic arc basalt, OFB : ocean floor basalt, WPT : within plate tholeiite, WPA : within plate alkalic. Similar symbols represent analyses of different zones of the same crystal.

best separation between fields (Figure 5.7). The discriminant functions are:

$$F1 = -0.012 \times SiO_2 - 0.0307 \times TiO_2 + 0.0026 \times Al_2O_3 - 0.0012 \times FeO^* - 0.0626 \times MnO + 0.0087 \times MgO - 0.0128 \times CaO - 0.0419 \times Na_2O,$$

$$F2 = -0.0469 \times SiO_2 - 0.0818 \times TiO_2 + 0.0212 \times Al_2O_3 - 0.0041 \times FeO^* - 0.1435 \times MnO + 0.0029 \times MgO - 0.0085 \times CaO - 0.0160 \times Na_2O.$$

All analyses fall in the volcanic arc basalt, and volcanic arc basalt plus ocean floor basalt field.

5.4 TRACE ELEMENT PATTERNS

Takla Group trace element patterns (spider diagrams) of basaltic compositions relative to Mid Ocean Ridge Basalt (MORB), and intermediate and felsic compositions relative to Ocean Ridge Granite (ORG), are presented in Figure 5.9. The trace element pattern of the average basaltic composition displays a typical volcanic arc pattern. There are high concentrations of low ionic potential elements (Sr, K, Rb, and Ba) and low concentrations of high ionic potential elements relative to MORB. The absolute abundances of these trace elements indicate that they belong to the calcalkaline rather than the tholeiitic suite. Typically, calcalkaline basalts show higher concentrations of the trace elements used in Figure 5.9A, and especially the low ionic potential elements, in comparison to tholeiites (Pearce, 1982).

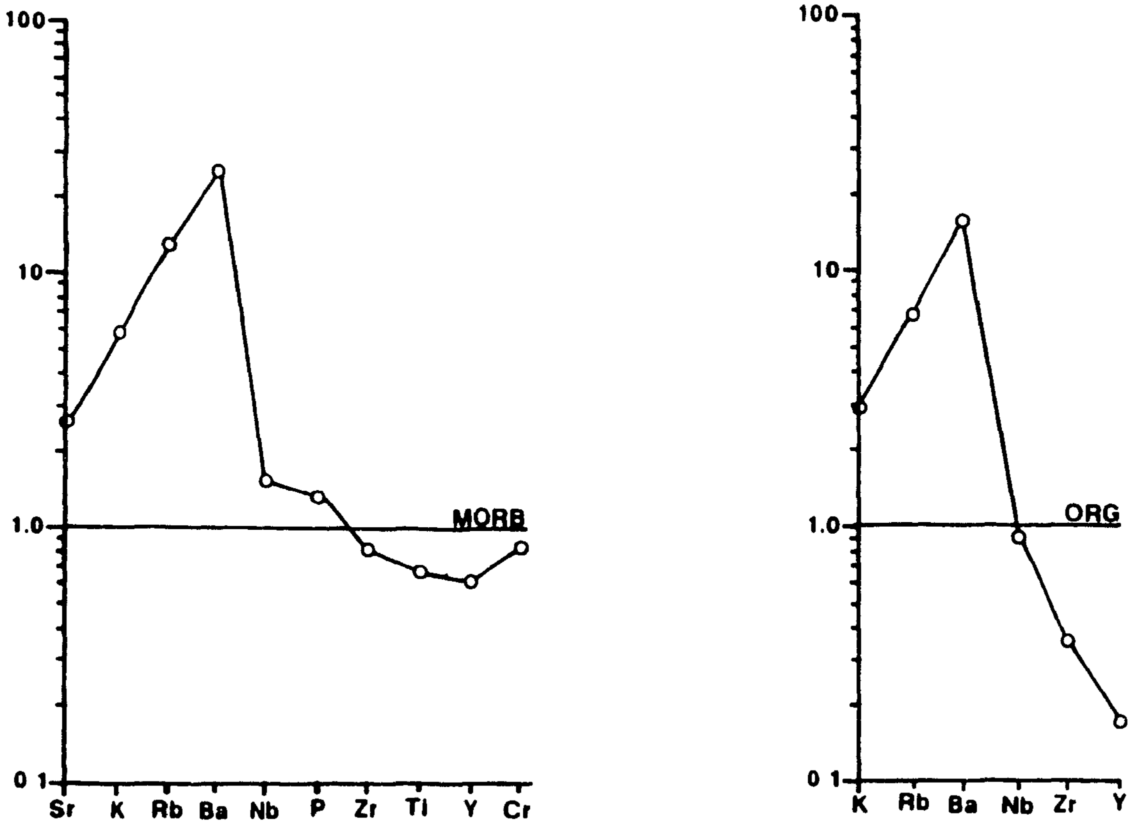

Figure 5.9A and B Trace element plots (spider diagrams) of the average basaltic composition normalised to mid-ocean ridge basalt (MORB) (Figure A), and average intermediate to felsic compositions normalised to ocean ridge granite (ORG) (Figure B).
Normalizing values ;
MORB : Sr = 120 ppm, K_2O = 0.15 %, Rb = 2.0 ppm, Ba = 20 ppm, Nb = 3.5 ppm, P_2O_5 = 0.12 %, Zr = 90 ppm, TiO_2 = 1.5 per cent, Y = 30 ppm, Cr = 250 ppm, after Pearce (1982).
ORG : K_2O = 0.40 %, Rb = 4.0 ppm, Ba = 50 %, Nb = 10 ppm, Zr = 340 ppm, Y = 70 ppm, after Pearce, Harris, and Tindle, (1984).

Intermediate and felsic patterns of volcanic arcs typically resemble basaltic patterns. They similarly have high concentrations of low ionic potential elements and low concentrations of high ionic potential, especially Y, relative to mid ocean ridge. Figure 5.9B shows the trace element pattern for the average of all intermediate and felsic compositions. The samples show enrichment in K, Rb, and Ba relative to Nb, Zr, and Y, and a low abundance of Y relative to ORG.

5.5 ISLAND ARC OR SUBDUCTION-RELATED ACTIVE CONTINENTAL MARGIN ?

The previous three sections have indicated that the volcanic succession of the study area was probably formed in a volcanic arc tectonic setting. However, these plots fail to distinguish between island arcs and subduction-related active continental margins.

For this distinction Takla analyses of granitic composition (> 55 wt% SiO_2) were used in a Rb/Sr versus K/Rb plot of Clarke and Beddoe-Stephens (1987), which discriminates between M-type and I-type granites. M-type granites are those which are derived from a parental magma which in turn is derived directly from the mantle or the subducted ocean crust beneath island arcs, and I-type granites are formed in Andino-type marginal continental arcs from a similar parental magma which underplates the continental crust and is then remelted (Pitcher, 1982). All analyses plot in the Alpine field (M-type granite) indicating an island arc tectonic setting rather than an active continental margin (Figure 5.10).

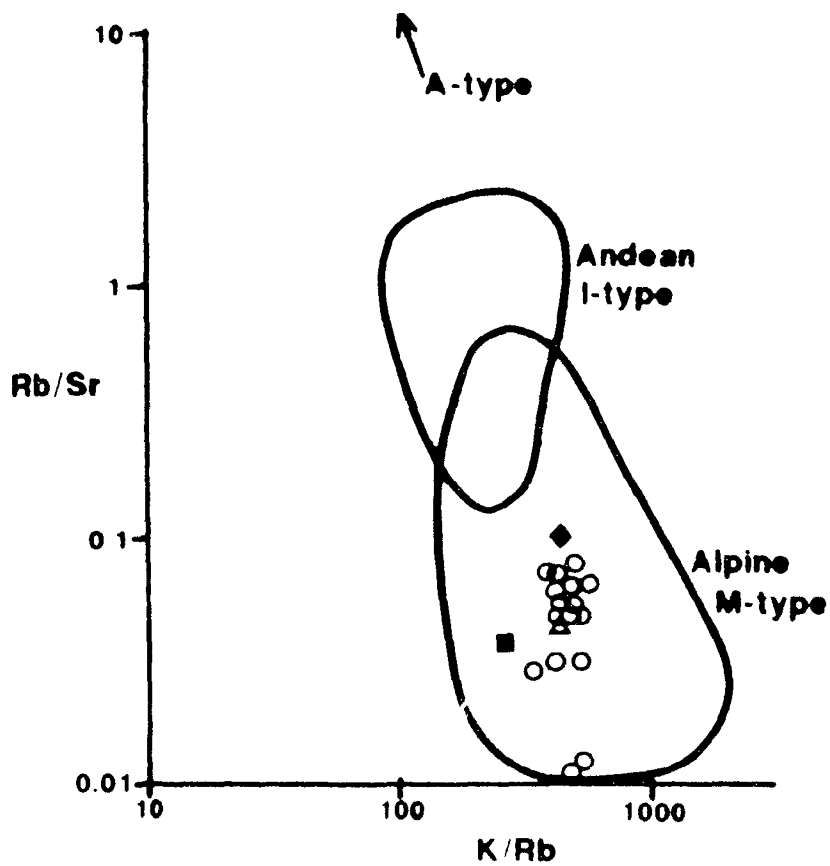

Figure 5.10 Tectonic discrimination diagram for granitic compositions. After Clarke and Beddoe-Stephens (1987).

Further evidence for an island arc environment is found by determining the crustal thickness beneath the volcanic arc. The crustal thickness of island arcs is typically 12 - 33 kilometres thick, while Andino-type marginal continental arcs are characterized by crustal thicknesses between 30 and 65 kilometres (Plank and Langmuir, 1988). Plank and Langmuir (1988) found that Na_2O and CaO at 6% MgO ($Na_{6.0}$ and $Ca_{6.0}$) correlate strongly with the thickness of the associated crust and developed a figure relating the two by a straight line (Figure 5.12). The crustal thickness is believed to determine the height of the mantle column available for melting, and therefore the proportions of $Na_{6.0}$ and $Ca_{6.0}$ in the parental magma. The thicker the crust above the mantle wedge, the shorter the mantle column available for melting. The shorter column results in a lower degree of melting and therefore in a higher $Na_{6.0}$ and a lower $Ca_{6.0}$. Samples characterised by between 3 and 10 wt% MgO are plotted against CaO and NaO to determine the amount of CaO and NaO at 6 wt % MgO. The intercept of 6 wt% MgO with the best fitting line is then used to determine the crustal thickness. The value of 6 wt% MgO is used to minimise the effects of crystal fractionation (Plank and Langmuir, 1988).

This procedure was applied to Takla samples and the results are shown in Figure 5.11 and 5.12. The values of $Na_{6.0}$ and $Ca_{6.0}$ indicate crustal thicknesses of approximately 26 kilometres and less than 10 kilometres respectively. Although a discrepancy exists between the two values, probably due to mobility of Ca as indicated by the presence of calcite in some samples, the results clearly indicate a crustal thickness typical of island arc environments rather than subduction-related active continental margin settings.

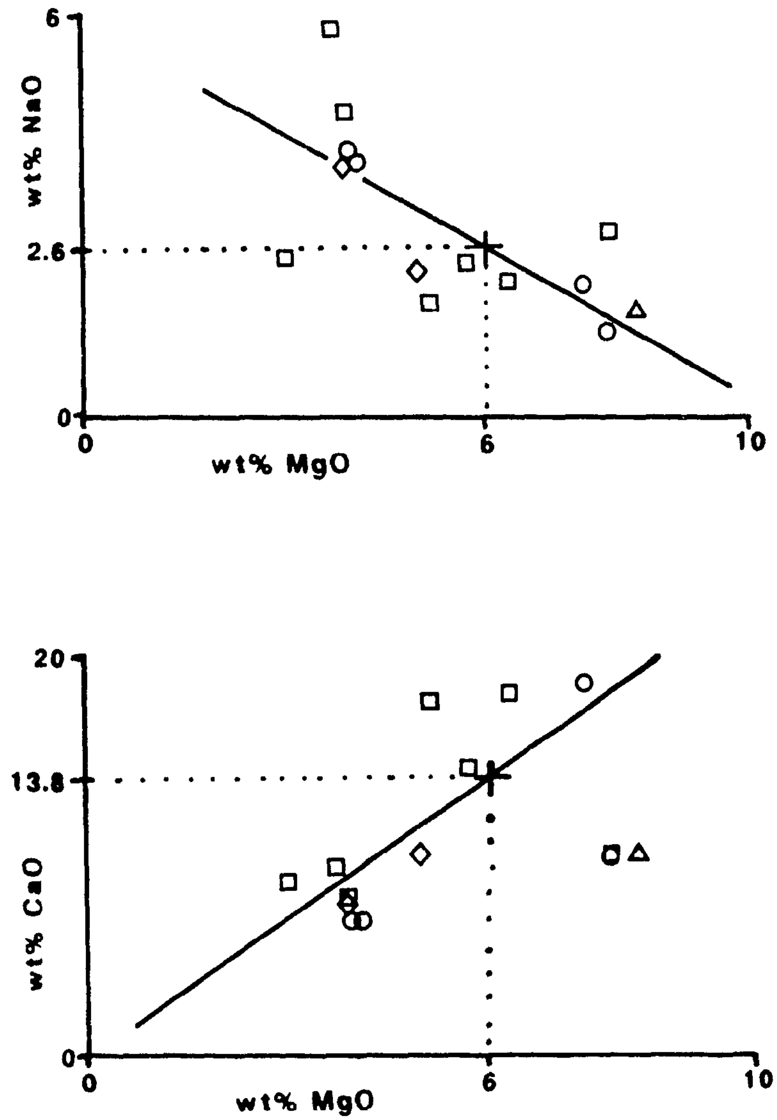

Figure 5.11 Na_2O and CaO versus MgO (wt%) for determination of crustal thickness in Figure 5.13. After Plank and Langmuir (1988). Average slope calculated by least squares best fit.

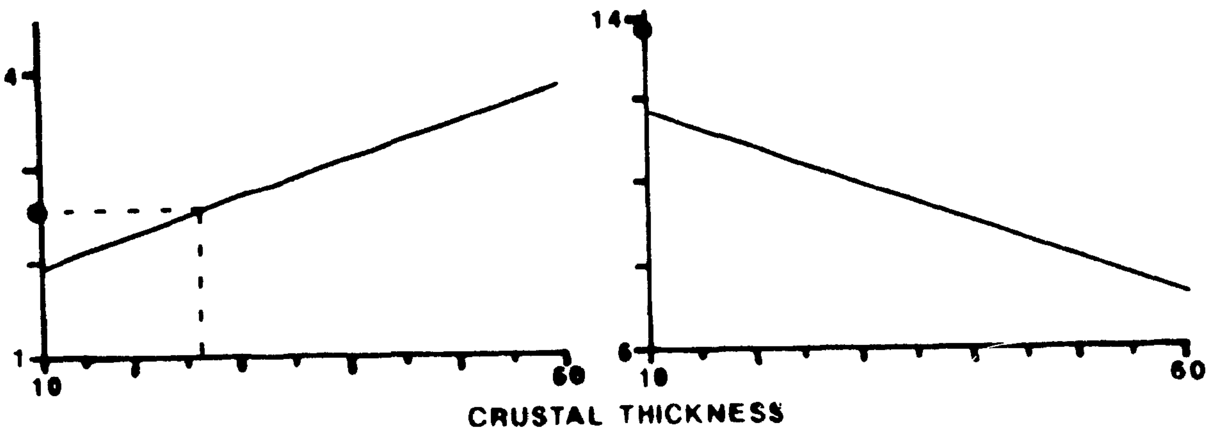

Figure 5.12 Na_2O and CaO at 6 wt% MgO ($Na_{6.0}$ and $Ca_{6.0}$) versus crustal thickness. After Plank and Langmuir (1988).

5.6 TECTONIC ASSOCIATIONS

Rocks assigned to the Takla Group occur in both Quesnellia and Stikinia. Because the two Takla groups are found in different and distinct terranes, it is questionable whether they are genetically related. Many authors have interpreted the Late Triassic to earliest Jurassic igneous rocks of Quesnellia and Stikinia to constitute a single magmatic belt (e.g. Mortimer, 1986). However, Mortimer (1986) presented structural and stratigraphic evidence indicating long-range ties between Cache Creek and adjacent terranes in Late Triassic time, and completely separate evolutionary histories of Quesnellia and Stikinia until they were juxtaposed in Middle Jurassic time.

Takla rocks west of the Findlay fault, in Stikinia, have been divided into the Dewar, Savage Mountain, and Moosevale formations (Monger, 1977) (Figure 5.13).

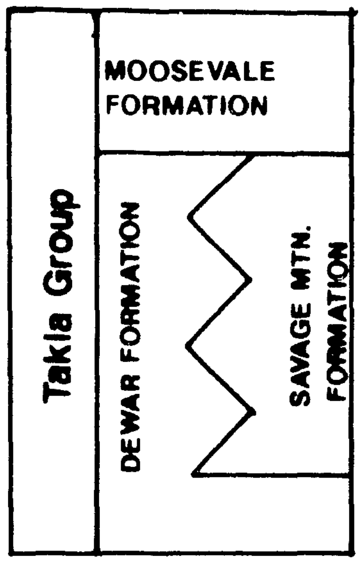

Figure 5.13 Formations of the Takla Group in Stikinia. After Monger (1977).

The Dewar Formation is comprised of grey-black argillite, fine to medium-grained grey-green sandstone and siltstone, and massive volcanogenic breccia with fragments of augite porphyry and augite-feldspar porphyry. The Savage Mountain Formation consists of basic flows and abundant pyroclastic rocks which are augite or augite-feldspar porphyries. The outcrop appearance and composition of the rocks in this formation closely resemble those of the Takla Group east of the Findlay fault, but they do not contain amphibole phenocrysts, and are metamorphosed to prehnite-pumpellyite grade. The lower portion of the Moosevale Formation is similar to the Savage Mountain Formation but contains up to ten percent of red clasts of fine-grained feldspar porphyry. In the upper portion the breccia is locally reddish and interbedded with grey sandstone and red mudstone.

The group evolves from basic to intermediate compositions, and from submarine environments, in the Dewar, Savage Mountain, and lower Moosevale formations, to subaerial environments in the upper Moosevale Formation. Monger (1977) determined that the submarine deposits were the result of submarine sliding and turbidity currents.

To reassess the relationship between the two Takla Groups, major element whole rock chemistry of Takla Group samples west of the Findlay fault (from Monger 1977, Table A.4 this thesis) were placed in several discrimination diagrams for comparison with Takla rocks of the study area.
First, a total alkalis versus silica plot is used to discriminate between alkaline and subalkaline suites (Figure 5.14). All samples of the Moosevale Formation fall in the alkaline field, while those of the Savage Mountain Formation straddle the dividing line. One analysis of the Dewar Formation fell in the cluster of Savage Mountain points within the alkaline field. The three formations are easily

distinguished from Takla rocks of the study area, which all fall in the subalkaline field (Figure 4.2).

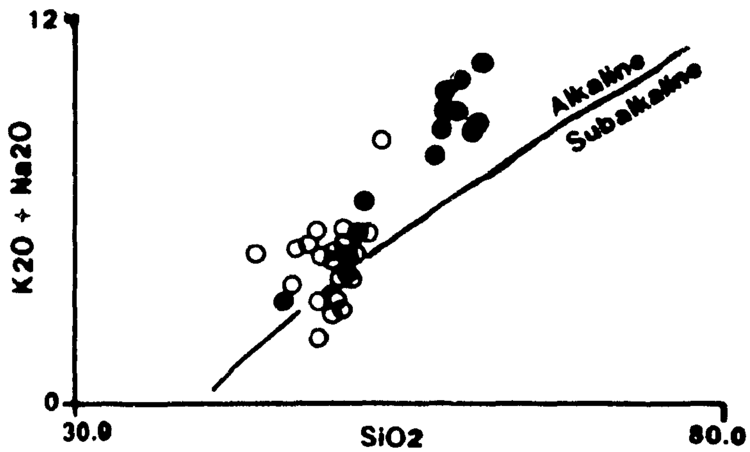

Figure 5.14 Alkaline versus subalkaline plot, After Irvine and Baragar (1971).

Because only major element chemistry was available for Takla rocks of Stikinia, only one tectonic discrimination diagram which was applied to rocks of the study area was useful. Samples of intermediate composition were placed on a FeO^{*}-MgO-Al_2O_3 plot to distinguish between five tectonic environments (Figure 5.15). An obvious difference is observed between samples from Stikinia, which fall in the field of oceanic islands, and rocks of the study area which cluster around the orogenic field. The few Stikinia samples which do fall in the orogenic field differ from rocks of the study area in that they are all alkaline using the discriminant of Figure 5.14.

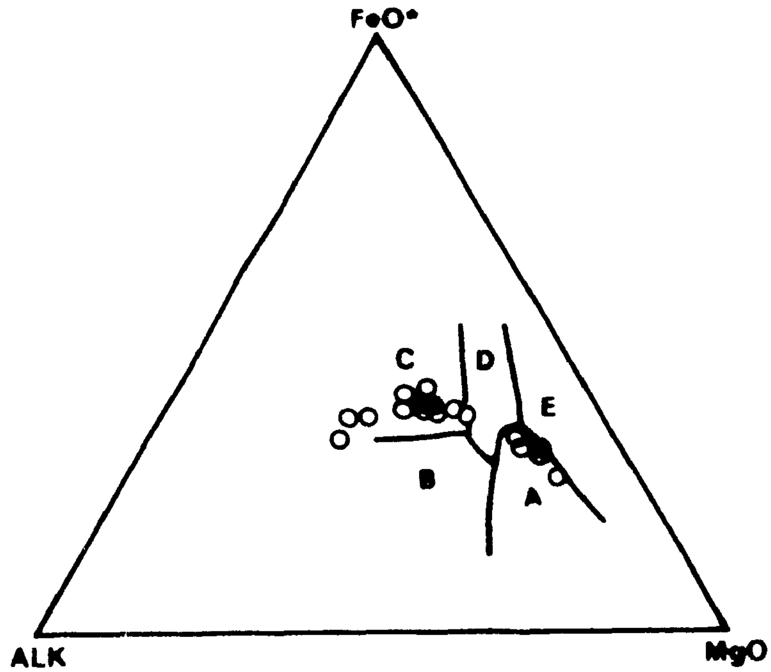

Figure 5.15 Discriminant plot for intermediate compositions. After Pearce, Gorman and Birkett (1977).

Although the two Takla successions are spatially and temporally related, they are easily distinguished on these discrimination plots, indicating that they are not genetically related. It has been previously suggested that the two groups are unrelated, having evolved as separate arcs, and that the "Takla Group" of Stikinia should be included in the more closely associated Upper Triassic Stuhini Group (Philippo Ferri, personal communication, February, 1989).

CHAPTER 6

PETROGENESIS

6.1 INTRODUCTION

Several petrogenetic models have been proposed to explain the occurrence of the basalt-andesite-dacite-rhyolite volcanic suite, of the tholeiitic or calcalkaline series, in island arc settings. A common feature of most models is the release of water via dehydration or melting reactions in the subducted oceanic crust. The release of water may instigate hydrous melting of peridotite above the Benioff zone to produce olivine-tholeiite or quartz-tholeiite parental liquids which, through fractionation of olivine, pyroxene, plagioclase, and magnetite, may yield basaltic andesite, andesite, and dacite of the tholeiite series (Green, 1980). Alternatively, partial melting of subducted oceanic crust of eclogite mineralogy may produce a silicic, light ion lithophile (LIL) enriched magma which may react with the overlying mantle wedge and mantle-derived hydrous tholeiitic magma. The contaminated magma may then fractionate hornblende, pyroxene, magnetite, and calcic-plagioclase on its way to the surface to produce the calcalkaline series (Green, 1980). Commonly, rocks of the tholeiitic suite occur in the early stages of arc development, and rocks of the calcalkaline series occur in more mature arcs.

Petrological and geochemical evidence suggests that low pressure hydrous fractional crystallization is the dominant process responsible for the evolution of the primary magma to intermediate and felsic compositions (Foden, 1983 in Wilson and Davidson, 1984), but magma mixing and crustal contamination may also be important (Grove, Gerlach, and Sando, 1982).

Smooth trends revealed in plots of major and trace elements versus Zr (Figure 6.1), and Mg# versus Zr (Figure 6.1) are often interpreted as evidence of cogenesis via crystal fractionation. Mixing of the least evolved magmas with the most evolved magmas cannot be employed to explain the compositional variation of the suite since mixing of these two magmas would produce linear trends on element-element variation diagrams rather then the non-linear trends observed in Figure 4.1. The lack of isotope data precludes any examination of crustal contamination.

All of the Takla samples are characterized by chromium and nickel contents, and Mg#'s, below what is expected of parental magmas from a peridotitic mantle source (Table 6.1), and on a sail diagram (Figure 6.2), do not fall within the field of liquids which could have co-existed with the upper mantle. These features, and the porphyritic nature of Takla samples, indicate that all of the rocks experienced some fractionation before they reached the surface.

Table 6.1		
	Takla	Peridotite Mantle
$\frac{Mg}{Mg + Fe^{2+}}$ (Mg#)	18 - 61	70-74 (Wilson and Davidson, 1984)
Cr ppm	<15 - 1220	3000 (Green, 1980)
Ni ppm	<10 - 166	2000 (Green, 1980)

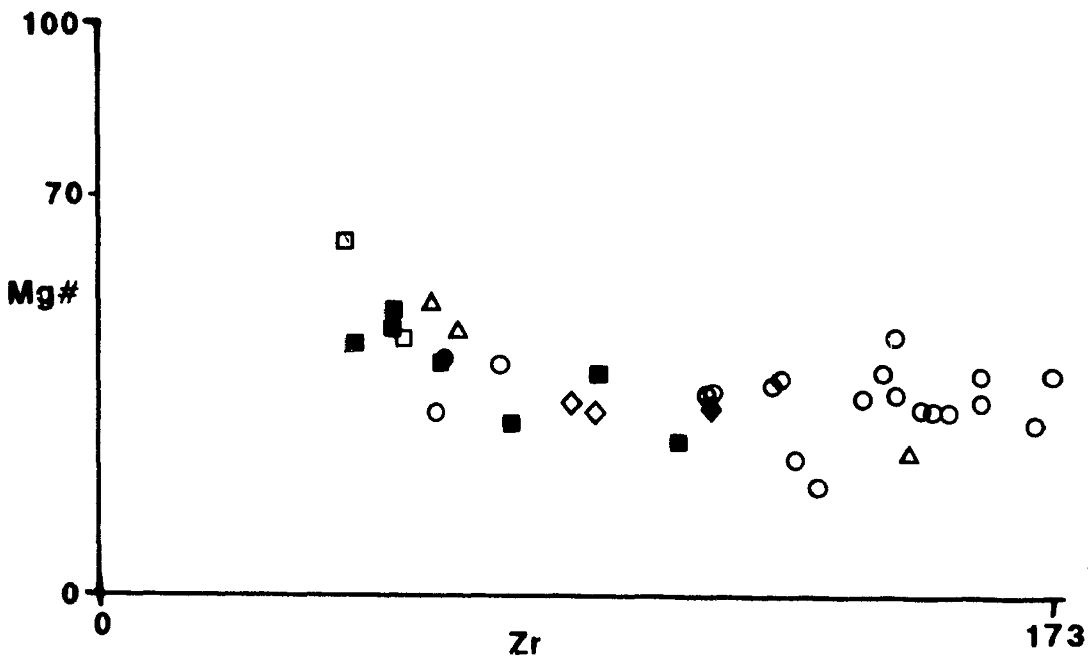

Figure 6.1 Mg # [100(Mg/Mg + Fe^{2+})] versus Zr (ppm).

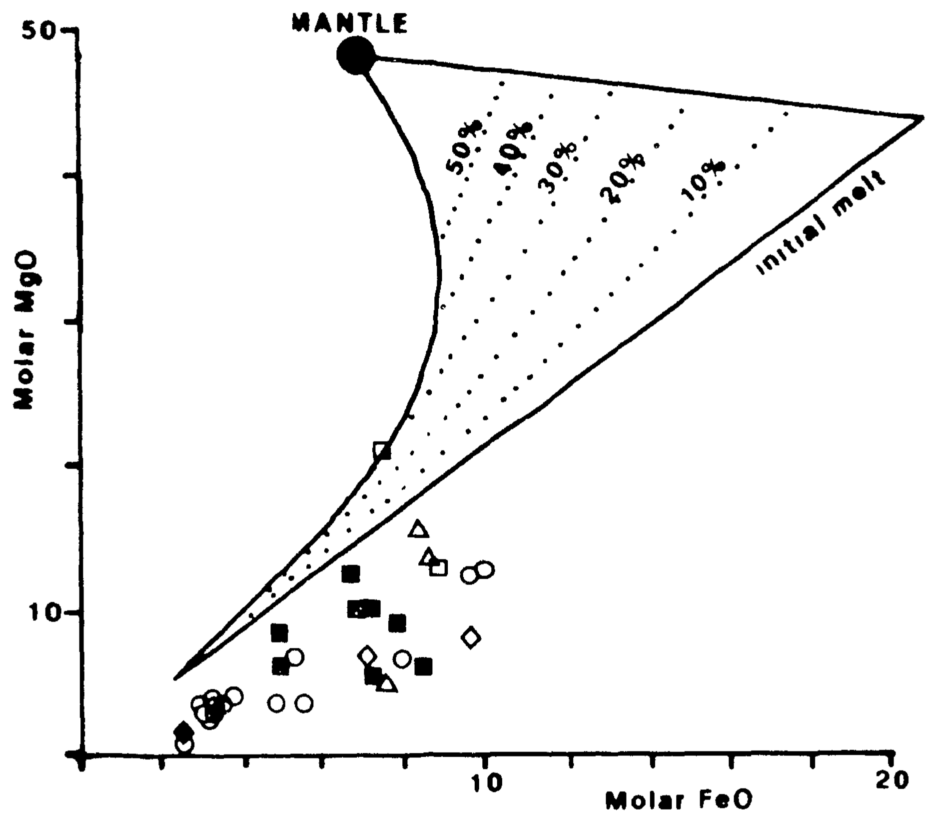

Figure 6.2 Composition of Takla Rocks in a molar MgO versus FeO* (sail Diagram). The contoured field encloses all compositions capable of co-existing with an upper mantle composition. The dashed lines indicate the percent of partial melting of the mantle. After Francis et al. (1981).

Petrographic observations of phenocryst phases and associations, trace element characteristics of whole rock samples, and a least squares crystal mixing program, are used to develop a model for the petrogenetic evolution of the Takla volcanic succession.

6.2 PETROGRAPHIC OBSERVATIONS

It is a logical first step to assume that crystal fractionation of the dominant phenocryst phases was responsible for the compositional variation of the suite. Petrographic evidence indicates that the important crystallizing phases are pyroxene and plagioclase at basaltic compositions, amphibole and plagioclase at intermediate and felsic compositions, and amphibole, biotite, and plagioclase in the most felsic compositions. Magnetite occurs rarely throughout the suite, but may have been partially responsible for the lack of an iron enrichment trend.

6.3 TRACE ELEMENT CHARACTERISTICS

As a magma evolves from basic to felsic compositions by fractional crystallisation, variations in Ti, Zr, Y, and Nb concentrations can be interpreted in terms of the nature and proportions of crystallising phases, and can also indicate the tectonic setting in which the magma is generated (Pearce and Norry, 1979). Because these are high field strength elements they are not usually affected by metasomatic alteration and are particularly useful for studying metamorphosed and weathered rocks. Three plots, of Y versus Zr, TiO_2 versus Zr, and Nb versus Zr, with their associated modelled fractionation vectors, are presented in Figure 6.3. Fractionation vectors were calculated by Pearce and Norry (1979) using mineral liquid distribution coefficients for the appropriate mineral, or mineral assemblages, at basic, intermediate, and felsic compositions.

On a Y-Zr diagram (Figure 6.3) the samples of basic composition exhibit a trend compatible with fractionation of a combination of olivine, plagioclase, and clinopyroxene, with the possible addition of magnetite and orthopyroxene. The sudden change in slope at intermediate compositions, reflecting a decrease in Y with increasing Zr, may be explained by the appearance of amphibole as a crystallising phase. The decrease in both Y and Zr at silicic compositions may be due to a larger proportion of amphibole, and possibly, the addition of biotite.

The presence of amphibole as a fractionating phase is significant in terms of distinguishing between the tholeiitic and calcalkaline suites. Petrographic observations and least squares crystal mixing calculations have shown that tholeiitic magmas typically fractionate olivine, clinopyroxene, and plagioclase throughout the sequence, while in calcalkaline lavas amphibole is often a crystallizing phase at intermediate and acid compositions (Pearce and Norry, 1979).

On a TiO_2 versus Zr plot (Figure 6.3) the samples show a trend similar to that on the Y versus Zr plot. At basic compositions the positive slope is again due to the

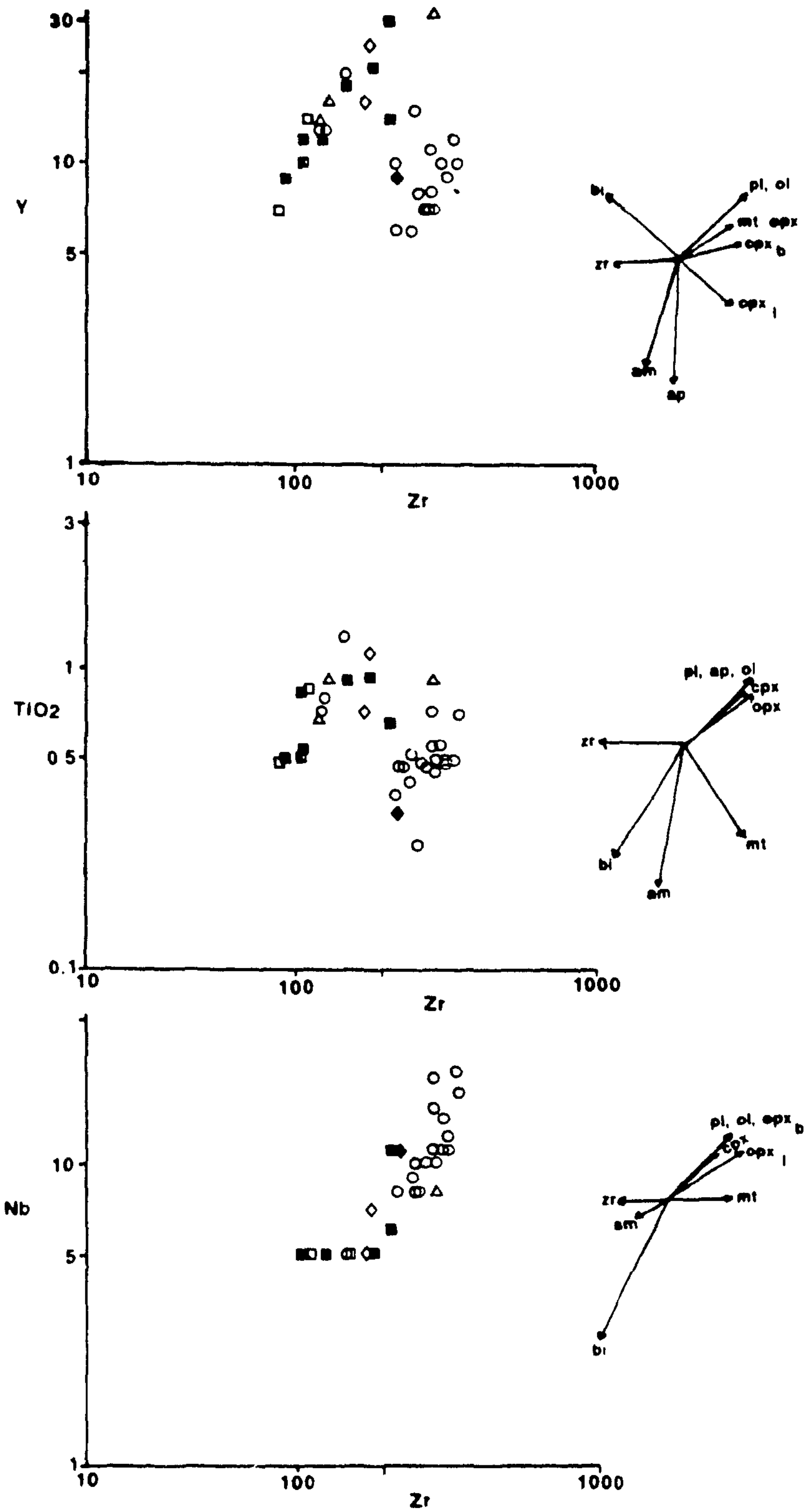

Figure 6.3 Fractionation trends of Takla rocks and associated fractionation vectors of major phases. After Pearce and Norry, 1979. Y, Nb, Zr in ppm, TiO_2 in weight percent.

crystallisation of olivine, clinopyroxene, and plagioclase. The subsequent decrease in Ti is attributed to the presence of magnetite or amphibole as a crystallizing phase. Amphibole, plus or minus biotite, becomes more important at more felsic compositions as Ti and Zr begin to decrease.

In the Nb versus Zr plot (Figure 6.3) the addition of amphibole as a crystallizing phase would cause the fractionation trend to move back on itself, making it difficult to identify. When compared with the two previous figures, this diagram displays an overlap of intermediate and felsic compositions compatible with the introduction of amphibole as a crystallizing phase at intermediate compositions.

6.4 Least Squares Mixing Calculations

Least squares mixing calculations can be used to estimate the proportions of various fractionating phases necessary to explain the differences between the bulk compositions of the parent and daughter magmas in a closed fractionating system, provided the compositions of the fractionating materials do not change significantly during evolution from parent to daughter (Le Maitre, 1979). By mixing major element oxide concentrations of the daughter magmas with major element oxide concentrations of the fractionating phases, a best estimate is made of the relative proportions and amounts of fractionating phases necessary to satisfy the composition of the parental magma. An equation which may represent the relationship between source, or parental magma, and product, or daughter magma, for the Takla suite is:

Parental Magma = Daughter Magma + Fractionating Phases

Basalt = Dacite + Pyroxene + Amphibole + Biotite + Plagioclase + Magnetite + Sphene

It is also possible to assign different weightings to specific oxides. Lower weightings can be assigned to the more unreliable elements (the alkalis) so that their effect on the calculated proportions is less than that of the more reliable elements. The factor represents the proportion of each mineral phase in the calculation.

To emulate the two-stage crystallization process evident in petrographic observations and trace element fractionation trends, calculations were performed in two steps. First, the parental magma composition is approximated by mixing a magma of intermediate composition with pyroxene, plagioclase and magnetite. In the second step, the intermediate magma composition is approximated by mixing the daughter magma with amphibole, biotite, plagioclase, magnetite and sphene.

For selection of appropriate parental and daughter magmatic compositions the least and most evolved samples (based on Zr plots) which were characterised by low LOI's, appeared unaltered in thin section, and displayed good igneous textures were chosen. For both parent and daughter magmas the average of three whole rock samples was used (Table 6.2). An intermediate composition was chosen by averaging samples 22 and 23 which lie at the first inflection point, corresponding to the appearance of amphibole, in Figure 6.3. For their oxide concentrations see Table A.2. Ferric-ferrous iron ratios were assigned to parental, intermediate, and daughter magmas by adopting the values of compositionally similar samples.

Table 6.2 Samples Chosen For Magma Compositions

	Sample Number	Description	Fe_2O_3/FeO
Parental Magma	13	basaltic-andesite dyke	
	25	basaltic flow	.394
	27	basaltic breccia fragment	(sample 24)
Intermediate Magma	22	gabbro/diorite	.337
	23	gabbro/diorite	(sample 23)
Daughter Magma	17	dacite dyke	
	3	dacite dyke	.189
	19	dacite dyke	(sample 19)

To obtain oxide concentrations of fractionating phases, an electron microprobe was used to analyze all major and some minor phases. For analytical methodology and results see Appendix B. For least squares crystal fractionation modelling an average of all plagioclase analyses was used. The average plagioclase composition is approximately 34% An. An average of all clinopyroxene, and an average of all amphibole, excluding actinolite and actinolitic hornblende, were used.

Results of least squares mixing calculations are presented in Table 6.3. Equal weightings were assigned to all oxides, and results reveal acceptable proportions of crystallizing phases, and small differences in oxide concentrations between parent and result for most elements.

Table 6.3 Results of Least Squares Mixing Calculations

MAFIC COMPOSITIONS

	SiO2	TiO2	Al2O3	FeO	Fe2O3	MnO	MgO	CaO	Na2O	K2O	Factor
Weighting	1.00	1.00	1.00	1.00	1.00	1.00	1.00	1.00	1.00	1.00	
Daughter	53.92	0.94	18.43	7.23	2.27	0.16	4.52	8.92	2.98	0.63	87.61
Pyroxene	52.23	0.31	2.77	5.81	0.00	0.15	16.39	22.15	0.19	0.00	3.87
Plagioclase	60.17	0.02	24.85	0.22	0.00	0.01	0.00	6.92	7.58	0.24	5.45
Magnetite	0.15	10.00	1.00	35.00	53.85	0.00	0.00	0.00	0.00	0.00	0.88
Parent	52.09	0.79	18.66	6.64	2.62	0.17	6.11	8.93	3.32	0.67	
Result	52.55	0.93	17.63	6.88	2.46	0.15	4.60	9.06	3.03	0.57	
Difference	0.46	0.14	-1.03	0.25	-0.16	-0.02	-1.51	0.13	-0.29	-0.10	

INTERMEDIATE TO FELSIC COMPOSITIONS

	SiO2	TiO2	Al2O3	FeO	Fe2O3	MnO	MgO	CaO	Na2O	K2O	Factor
Weighting	1.00	1.00	1.00	1.00	1.00	1.00	1.00	1.00	1.00	1.00	
Daughter	63.91	0.57	17.34	3.86	0.72	0.10	2.28	5.47	3.90	1.86	22.99
Amphibole	44.90	1.48	12.59	13.44	0.00	0.31	13.31	11.81	1.86	0.28	33.63
Plagioclase	60.17	0.02	24.85	0.22	0.00	0.01	0.00	6.92	7.58	0.24	38.60
Biotite	39.16	2.16	20.16	15.99	0.00	0.21	11.21	0.08	0.11	10.92	0.47
Magnetite	0.15	10.00	1.00	35.00	53.85	0.00	0.00	0.00	0.00	0.00	3.95
Sphene	41.10	19.98	3.83	6.24	0.00	0.23	6.15	22.16	0.20	0.10	1.87
Parent	53.92	0.94	18.43	7.23	2.27	0.16	4.52	8.92	2.98	0.63	
Result	53.98	1.42	18.02	7.07	2.30	0.14	5.17	8.32	4.46	0.67	
Difference	0.06	0.48	-0.41	-0.16	0.03	-0.02	0.65	-0.60	1.48	0.04	

This crystal fractionation model can be tested using the Rayleigh fractional crystallization equation (Allegre and Minster, 1978): $C_{li} = C_{o,li} f^{(Di - 1)}$,

where $Di = D_i X$.

X = weight fraction of crystallizing mineral.

D^i = partition coefficient of element i between mineral and liquid.

f = weight proportion of residual magma.

$C_{o,li}$ = concentration of element i in the parental magma.

C_{li} = concentration of element i in the daughter magma.

Bulk mineral-liquid partition coefficients were calculated using published mineral-liquid partition coefficients (Table 6.5) and the weight fraction of crystallizing mineral determined in least squares calculations. The actual element abundances are compared to the calculated values in Table 6.6 and Figure 6.5.

Trace element modelling calculations indicate a close correspondence between calculated and observed values for most elements. The few disparities may be due to a number of factors, the most obvious of which is crystal fractionation in an open magmatic system. Other possible factors include a poor choice of magma compositions used in least squares calculations, an undetected phase that was not included in least squares modelling, or inappropriate partition coefficients.

Table 6.4 Mineral-Liquid and Bulk Partition Coefficients							
Zr, Y, Nb from Pearce and Norry (1979) Rb, Sr, Ba from Cox, Bell, and Pankhurst (1979)							
Element	D^l_{plag}		D^l_{pyx}	D^l_{amph}	D^l_{bio}	D^l_{mt}	
	M-I	I-F	M-I	I-F	I-F	M-I	I-F
Zr	0.01	0.03	0.1	1.4	1.2	0.1	0.2
Y	0.03	0.06	0.5	2.5	1.2	0.2	0.5
Nb	0.01	0.025	0.1	1.3	1.8	0.4	1.0
Rb	0.07	0.04	0.001	0.01	2.0	0.01	0.01
Sr	2.2	4.4	0.07	0.02	-	0.01	0.01
Ba	0.2	0.3	0.001	0.04	10.0	0.01	0.01

	Di	
	M-I	I-F
Zr	.0054	.49
Y	.023	.89
Nb	.0081	.49
Rb	.0040	.028
Sr	.12	-
Ba	.011	.17

M: mafic compositions
I: intermediate compositions
F: felsic compositions

Table 6.5 Rayleigh Fractionation Model Values (in ppm) ± measurement error in ppm

	Zr	Y	Nb	Rb		Ba
Parental Magma	65±5.7	15±1.3	2±.25	17±1.6	428±40.2	3[illegible]±31.9
Calculated Intermediate Magma	73±5.7	17±1.3	2±.25	19±1.6	472±40.2	3[illegible]±31.9
Intermediate Magma	88±6.2	20±1.5	6±.43	17±1.2	334±24.1	391±30.1
Calculated Daughter Magma	188±6.2	24±1.5	13±.43	72±1.2	-	1341±30.1
Daughter Magma	168±14.5	10±0.9	16±1.4	45±4.1	-	1181±103.3

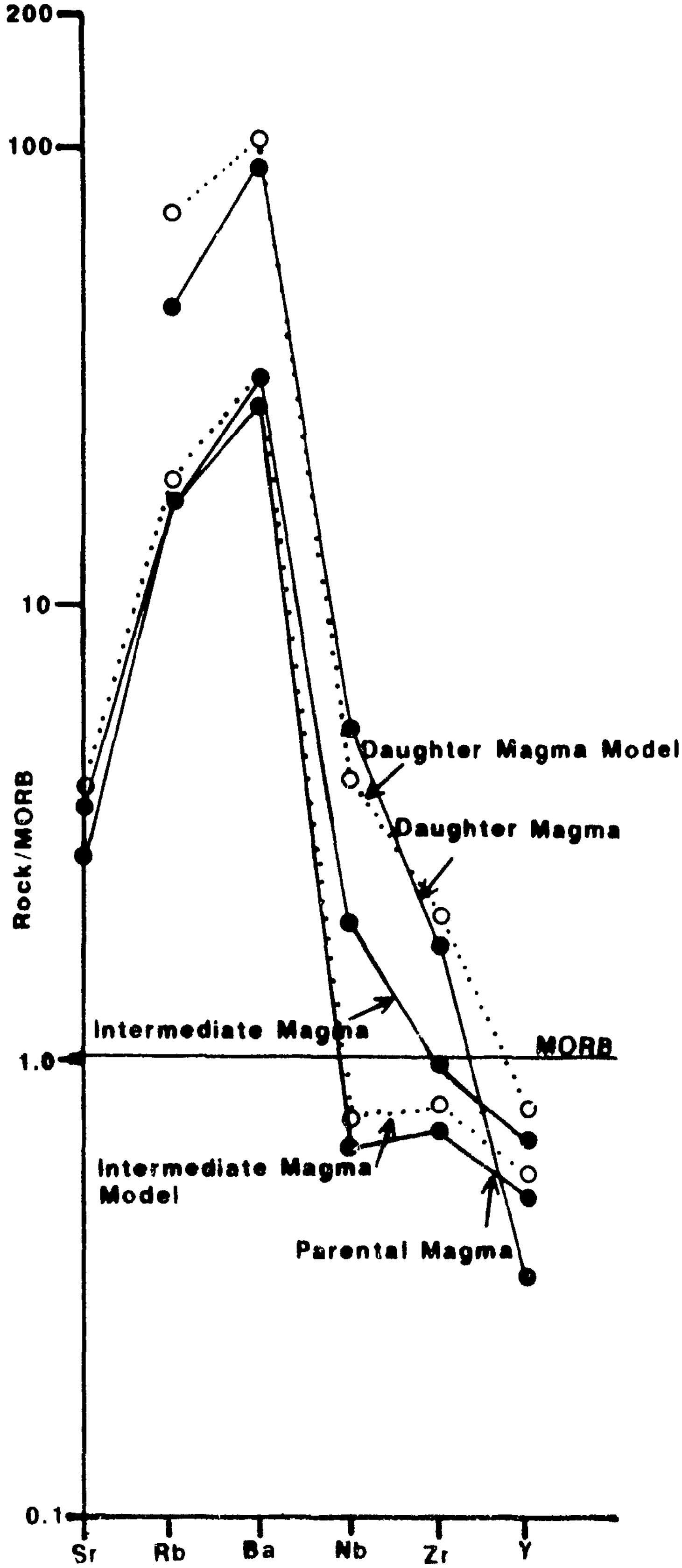

Figure 6.5 Rayleigh Fractionation Model. Normalization factors are the same as for Figure 5.9.

CHAPTER 7

CONCLUSIONS

7.1 CONCLUSIONS

The results of this study indicate that Takla Group volcaniclastic rocks of Quesnellia were pyroclastically erupted and deposited in an island arc tectonic setting.

The suite is characterized by a broad range in compositions from basalt through dacite and may well have evolved through low pressure crystal fractionation of the major phenocryst phases observed in the rocks. A comparison of Takla Group rocks of Stikinia and Takla Group rocks of Quesnellia suggests no genetic relationship between the two.

Lines of evidence in support of an island arc tectonic setting for Takla rocks in Quesnellia include;

1) The abundance of pyroclastic rocks.
2) Their compositional range from basalt to dacite.
3) Their calcalkaline signature.
4) Major and trace element tectonic discrimination plots, all of which indicate a volcanic arc environment.
5) Crustal thicknesses in the range of typical island arcs as opposed to Andino-type arcs.

Petrographic observations, trace element characteristics, and least squares mixing calculations indicate that the suite may have evolved from a basaltic parental magma to a dacitic daughter magma primarily through the fractionation of plagioclase, pyroxene, amphibole, biotite, magnetite, and sphene. The dominant fractionating phases were plagioclase and clinopyroxene at basic compositions, plagioclase and hornblende at intermediate compositions, and plagioclase, hornblende, and biotite at felsic compositions.

Several comparisons were made between the Takla groups of Quesnellia and Stikinia. The two are similar in their physical appearance but significant geochemical differences were identified. Takla rocks of Stikinia are predominantly alkaline, the rest being tholeiitic, while those in Quesnellia are calcalkaline. Paleotectonic classifications suggests that the rocks of Stikinia were formed in an oceanic island setting while those of Quesnellia were formed in an island arc environment. It is recommended that the group name "Takla" be restricted to Stikinia where it was first described near Takla Lake, and that the "Takla Group" rocks of Quesnellia be renamed Johanson Group.

7.2 RECOMMENDATIONS FOR FUTURE WORK

It is recommended that a more detailed geochemical study be done on distinct rock packages throughout the Cordillera. Only after each package is studied individually to determine its paleotectonic setting can associations between packages be assimilated into a detailed tectonic model for the formation of the Cordillera. More geochemical data of the "Takla Group" of Stikinia would be particularly useful for a more detailed comparison with Takla rocks of Quesnellia and more closely related groups within Stikinia. It has been largely accepted that the majority of volcaniclastic assemblages within Terrane 1 were formed in island arc tectonic settings (Mortimer, 1986) but, the preliminary examination in this study suggests the Takla rocks of Stikinia may have formed in an oceanic island environment.

APPENDIX A

Table A.1

No.	Sample	Desription	Symbol	Analysis Performed
1	K17E	dyke	○	major and trace XRF
2	K17I	dyke	○	major and trace XRF
3	K7I	dyke	○	major and trace XRF
4	K5H	dyke	○	major and trace XRF
5	K2	dyke	○	major and trace XRF
6	K19H	dyke	○	major and trace XRF
7	K22F	dyke	○	major and trace XRF
8	K28B	dyke	○	major and trace XRF
9	K28G	dyke	○	major and trace XRF
10	KM53	dyke	○	major and trace XRF
11	KM115	dyke	○	major and trace XRF
12	KM73	dyke	○	major and trace XRF
13	KM61	dyke	○	major and trace XRF
14	KM72	dyke	○	major and trace XRF
15	KM109	dyke	○	major and trace XRF
16	KM63	dyke	○	major and trace XRF
17	KM41	dyke	○	major and trace XRF
18	KM3	dyke	○	major and trace XRF
19	KM114	dyke	○	major and trace XRF, FeO
20	KM120	dyke	○	major and trace XRF, FeO
21	K6	tonalite	◆	major and trace XRF, FeO
22	KM156	gabbro/diorite	◇	major and trace XRF
23	K27B	gabbro/diorite	◇	major and trace XRF, FeO
24	KM35	flow	△	major and trace XRF, FeO
25	KM37	flow	△	major and trace XRF
26	K7C	dyke/flow	△	major and trace XRF
27	K16Ja	breccia fragment	■	major and trace XRF
28	K16Jb	breccia fragment	■	major and trace XRF
29	K16Jc	breccia fragment	■	trace XRF
30	K22Da	breccia matrix	▣	major and trace XRF
31	K22Db	breccia fragment	■	major and trace XRF
32	KM36a	breccia fragment	■	major and trace XRF
33	KM36b	breccia matrix	▣	major and trace XRF
34	KM38	breccia fragment	■	major and trace XRF
35	KM38b	breccia fragment	■	major XRF
36	KM23	wholerock breccia	□	major and trace XRF
37	KM10d	wholerock breccia	□	major and trace XRF

FeO : Iron Titrations

Table A.2 X-Ray Fluorescence Results (in order of increasing SiO_2 content) n.a. : not analysed

Sample	30	33	15	35	37	18	34	36	27	25	24	23	13	31	22	32	26	11	28	9
Weight%																				
SiO2	37.38	42.99	44.43	46.71	47.82	48.08	49.56	49.80	50.30	51.54	51.65	52.06	53.94	55.14	55.53	55.94	57.03	59.21	59.46	60.92
TiO2	0.61	0.58	0.87	0.93	0.70	1.38	0.96	0.51	0.93	0.70	0.93	1.15	0.74	0.88	0.73	0.58	0.93	0.49	0.68	0.74
Al2O3	12.82	10.91	14.38	16.24	18.98	19.17	16.91	8.64	22.21	13.14	16.09	17.56	20.45	18.36	19.21	12.09	18.59	18.22	16.70	16.74
Fe2O3	2.01	1.99	2.71	2.06	2.37	2.92	2.16	2.25	2.25	2.38	2.39	2.61	2.13	1.35	1.91	1.46	2.09	1.56	2.00	1.29
Cr2O3	0.00	0.00	0.00	0.00	0.00	0.00	0.00	0 00	0.00	0.00	0.00	0.00	0.00	0.00	0.00	0.00	0.00	0.00	0.00	0.00
MgO	6.62	8.16	7.56	6.42	7.98	7.96	5.80	14.80	3.96	10.30	8.40	5.08	4.02	3.78	3.94	5.23	2.90	1.92	3.08	4.17
FeO	6.40	6.36	8.64	6.58	7.57	9.31	6.88	7.17	7.18	7.59	7.63	8.34	6.78	4.31	6.08	4.67	6.66	4.99	6.39	4.12
MnO	0.33	0.26	0.21	0.22	0.16	0.18	0.20	0.18	0.17	0.16	0.13	0.19	0.17	0.14	0.13	0.16	0.19	0.11	0.15	0.09
NiO	0.00	0.00	0.00	0.00	0.00	0.00	0.00	0.00	0.00	0.00	0.00	0.00	0.00	0.00	0.00	0.00	0.00	0.00	0.00	0.00
CaO	31.28	27.05	18.52	18.17	10.08	9.65	14.53	15.79	7.99	12.17	10.24	10.09	6.54	9.55	7.71	17.66	7.77	7.06	8.74	6.45
Na2O	1.88	1.04	1.87	2.00	2.77	1.21	2.31	0.46	4.61	1.34	1.59	2.19	3.98	5.81	3.76	1.68	2.73	4.28	2.39	3.79
K2O	0.51	0.49	0.58	0.39	1.28	0.04	0.47	0.31	0.29	0.55	0.80	0.46	1.18	0.51	0.80	0.17	0.93	1.81	0.24	1.29
P2O5	0.15	0.17	0.23	0.27	0.10	0.10	0.24	0.09	0.09	0.12	0.13	0.26	0.08	0.17	0.20	0.35	0.19	0.35	0.15	0.40
LOI	17.73	11.70	7.50	5.85	4.53	5.58	2.42	4.04	2.56	1.78	2.07	1.20	1.98	4.36	1.84	5.92	0.80	4.41	2.65	1.97
Total	100.00	100.00	100.00	100.00	100.00	100.00	100.00	100.00	100.00	100.00	100.00	100.00	100.00	100.00	100.00	100.00	100.00	100.00	100.00	100.00
ppm																				
Rb	10.0	10.0	13.0	n.a.	21.0	0.0	13.0	8.0	10.0	13.0	19.0	12.0	28.0	12.0	22.0	6.0	21.0	34.0	9.0	27.0
Sr	206.0	243.0	235.0	n.a.	215.0	431.0	341.0	98.0	295.0	303.0	274.0	271.0	685.0	273.0	398.0	335.0	488.0	1135.0	249.0	571.0
Ba	177.0	228.0	229.0	403.0	251.0	74.0	478.0	312.0	297.0	258.0	302.0	222.0	503.0	210.0	560.0	504.0	527.0	2254.0	151.0	825.0
Y	9.0	10.0	13.0	n.a.	14.0	20.0	22.0	7.0	18.0	14.0	16.0	25.0	13.0	12.0	16.0	12.0	32.0	15.0	14.0	11.0
Zr	46.0	53.0	63.0	n.a.	55.0	73.0	91.0	44.0	75.0	60.0	65.0	90.0	61.0	62.0	86.0	53.0	147.0	126.0	105.0	144.0
V	183.0	231.0	286.0	243.0	296.0	423.0	267.0	208.0	231.0	273.0	276.0	295.0	168.0	269.0	222.0	220.0	150.0	120.0	180.0	124.0
Nb	0.0	5.0	0.0	n.a.	5.0	5.0	5.0	0.0	5.0	0.0	0.0	7.0	0.0	5.0	5.0	0.0	8.0	8.0	11.0	19.0
Cr	186.0	759.0	237.0	289.0	111.0	165.0	251.0	220.0	0.0	819.0	459.0	132.0	21.0	110.0	27.0	923.0	0.0	31.0	58.0	150.0
Ni	42.0	66.0	50.0	34.0	31.0	26.0	52.0	166.0	0.0	150.0	114.0	22.0	12.0	63.0	0.0	63.0	0.0	0.0	12.0	67.0
Rb/Sr	0.049	0.041	0.055	0.000	0.098	0.000	0.038	0.082	0.034	0.043	0.069	0.044	0.041	0.044	0.055	0.018	0.043	0.030	0.036	0.047
Zr/Y	5.11	5.30	4.85	0.00	3.93	3.65	4.14	6.29	4.17	4.29	4.06	3.60	4.69	5.17	5.38	4.42	4.59	8.40	7.50	13.09
Nb/Zr	0.000	0.094	0.000	0.000	0.091	0.068	0.055	0.000	0.067	0.000	0.000	0.078	0.000	0.081	0.058	0.000	0.054	0.063	0.105	0.132

Table A.2 X-Ray Fluorescence Results (Cont.)

Sample	19	3	7	2	4	8	6	17	14	20	1	12	16	5	10	21
weight %																
SiO2	61.37	63.35	63.41	65.81	65.90	66.03	66.15	66.24	66.41	66.69	66.70	67.24	67.35	67.55	68.19	69.75
TiO2	0.50	0.71	0.49	0.57	0.50	0.53	0.50	0.50	0.57	0.39	0.48	0.44	0.50	0.45	0.27	0.33
Al2O3	17.51	17.55	17.65	16.98	16.98	17.15	16.84	16.77	17.44	16.24	17.11	16.66	16.99	16.73	18.55	16.34
Fe2O3	1.34	1.08	1.08	0.93	0.92	0.94	0.91	0.92	1.02	1.00	0.82	0.84	0.93	0.86	0.66	0.66
Cr2O3	0.00	0.00	0.00	0.00	0.00	0.00	0.00	0.00	0.00	0.00	0.00	0.00	0.00	0.00	0.00	0.00
MgO	2.32	2.61	2.39	2.01	2.33	2.31	2.23	1.88	1.96	2.15	1.72	2.00	1.79	1.71	0.59	1.12
FeO	4.28	3.43	3.43	2.96	2.95	3.01	2.92	2.93	3.26	3.18	2.62	2.67	2.96	2.75	2.09	2.10
MnO	0.13	0.08	0.09	0.07	0.07	0.07	0.07	0.07	0.08	0.09	0.06	0.06	0.07	0.07	0.07	0.06
NiO	0.00	0.00	0.00	0.00	0.00	0.00	0.00	0.00	0.00	0.00	0.00	0.00	0.00	0.00	0.00	0.00
CaO	6.45	5.24	5.86	4.84	5.02	5.84	4.63	4.65	3.55	5.06	4.93	4.52	3.93	4.75	2.53	3.86
Na2O	3.50	3.92	4.09	3.82	3.88	3.40	4.35	4.23	4.02	3.64	3.72	3.30	3.85	3.80	4.29	4.01
K2O	2.24	1.70	1.35	1.73	1.22	0.53	1.16	1.59	1.36	1.37	1.66	2.14	1.45	1.17	2.61	1.65
P2O5	0.35	0.34	0.16	0.26	0.23	0.18	0.23	0.22	0.32	0.18	0.17	0.14	0.18	0.15	0.15	0.12
LOI	1.51	1.12	3.52	2.26	0.95	1.49	2.43	1.62	2.21	2.60	1.54	4.69	1.94	0.61	1.45	0.75
Total	100.00	100.00	100.00	100.00	100.00	100.00	100.00	100.00	100.00	100.00	100.00	100.00	100.00	100.00	100.00	100.00
ppm																
Rb	64.0	34.0	29.0	30.0	28.0	13.0	22.0	37.0	26.0	30.0	34.0	39.0	29.0	30.0	54.0	39.0
Sr	2248.0	675.0	604.0	479.0	499.0	444.0	473.0	543.0	560.0	642.0	450.0	313.0	485.0	430.0	483.0	393.0
Ba	1360.0	1217.0	1114.0	851.0	810.0	444.0	809.0	967.0	962.0	1041.0	674.0	577.0	1006.0	781.0	1168.0	907.0
Y	12.0	10.0	6.0	8.0	7.0	6.0	9.0	9.0	10.0	10.0	7.0	6.0	10.0	7.0	8.0	9.0
Zr	170.0	173.0	111.0	144.0	142.0	123.0	160.0	160.0	154.0	110.0	138.0	122.0	151.0	149.0	130.0	111.0
V	125.0	103.0	101.0	78.0	68.0	84.0	78.0	76.0	78.0	81.0	65.0	69.0	82.0	65.0	28.0	45.0
Nb	20.0	17.0	6.0	15.0	11.0	10.0	12.0	11.0	14.0	8.0	10.0	9.0	11.0	10.0	8.0	11.0
Cr	48.0	51.0	77.0	38.0	95.0	63.0	75.0	49.0	51.0	89.0	92.0	63.0	16.0	29.0	0.0	39.0
Ni	11.0	27.0	14.0	21.0	26.0	15.0	35.0	14.0	16.0	18.0	66.0	23.0	12.0	11.0	0.0	11.0
Rb/Sr	0.028	0.050	0.048	0.063	0.056	0.029	0.047	0.068	0.047	0.046	0.076	0.125	0.060	0.070	0.112	0.099
Zr/Y	14.17	17.30	18.50	18.00	20.29	20.50	17.78	17.78	15.40	11.00	19.71	20.33	15.10	21.29	16.25	12.33
Nb/Zr	0.118	0.098	0.054	0.104	0.077	0.081	0.075	0.069	0.093	0.071	0.072	0.074	0.073	0.067	0.062	0.099

TABLE A.3 MAJOR ELEMENT CHEMISTRY OF TAKLA GROUP ROCKS IN STIKINIA

MOOSEVALE FORMATION

SAMPLE	1	2	3	4	5	6	7	8	9	10	11	12
SiO2	56.38	48.61	45.80	60.48	58.93	59.97	60.40	57.58	58.16	57.03	59.40	51.72
TiO2	0.88	0.71	0.76	0.60	0.57	0.61	0.63	0.73	0.69	0.95	0.60	1.25
Al2O3	16.40	17.47	16.01	18.45	18.70	18.47	18.60	18.00	13.25	18.40	19.90	18.32
Fe2O3	2.42	2.27	6.00	2.90	4.10	2.60	5.30	5.80	3.42	6.51	2.90	5.87
MgO	3.23	1.65	8.11	1.35	1.41	2.90	1.49	2.47	2.63	1.74	3.00	4.90
FeO	4.56	5.98	2.78	1.80	0.60	2.30	0.80	0.40	1.50	0.30	0.90	3.70
MnO	0.18	0.18	0.16	0.14	0.13	0.21	0.16	0.17	0.13	0.17	0.10	0.18
CaO	4.83	12.20	16.90	5.09	4.34	4.11	1.34	5.31	5.31	6.61	3.00	7.54
Na2O	7.85	3.68	2.33	8.10	7.50	7.70	7.70	6.70	6.63	5.59	6 40	3.90
K2O	0.22	1.15	0.78	0.37	1.28	0.53	2.45	2.09	2.78	1.89	3.50	2.14
P2O5	0.27	0.23	0.18	0.27	0.27	0.25	0.31	0.25	0.33	0.44	0.30	0.28
TOTAL	97.22	94.13	99.81	99.55	99.83	99.65	99.18	99.50	99.83	99.63	100.00	99.80

SAVAGE MOUNTAIN FORMATON

SAMPLE	1	2	3	4	5	6	7	8	9	10	11	12
SiO2	52.51	51.91	50.96	49.90	49.48	48.11	47.16	50.21	46.15	49.56	48.30	50 70
TiO2	0.94	0.99	0.71	0.80	0.70	0.64	1.01	0.83	0.74	0.67	0.80	0.90
Al2O3	17.45	20.00	11.67	13.00	10.83	10.29	14.15	12.22	12.24	9.29	11.50	13.30
Fe2O3	2.49	4.30	6.80	9.70	7.97	6.57	2.56	2.42	2.30	3.50	5.20	4.30
MgO	3.82	4.03	9.41	8.20	11.96	15.13	8.16	7.87	10.88	12 46	10.20	8.00
FeO	6.08	3.50	4.87	2.70	4.19	5.43	10.33	10.29	10.74	7.56	7.50	7.10
MnO	0.14	0.15	0.16	0.10	0.18	0.19	0.21	0.20	0.22	0.19	0.20	0.20
CaO	6.84	9.49	10.56	10.30	11.25	11.17	10.40	10.36	10.53	13.79	13.20	11 60
Na2O	4.45	3.70	2.60	2.90	1.20	0.90	3.12	3.66	2.33	1.50	1.60	2 20
K2O	3.22	1.16	1.58	1.60	1.60	0.87	1.32	1.28	2.00	0.92	1.20	1.40
P2O5	0.47	0.42	0.28	0.20	0.22	0.20	0.32	0.24	0.24	0.21	0.20	0.30
TOTAL	98.41	99.65	99.60	99.40	99.58	99.50	98.74	99.58	98.37	99.65	99.90	100.00

SAMPLE	13	14	15	16	17	18	19	20	21	22	23	24
SiO2	48.17	49.90	49.24	49.39	49.84	48.60	49.64	50.61	50.66	50.81	46.70	49 67
TiO2	1.02	0.81	1.04	1.07	0.75	1.00	1.14	0.83	0.85	1.25	0.95	0.72
Al2O3	18.40	12.90	14.73	15.22	11.34	16.60	18.71	12.68	20.12	18.26	14.12	10.88
Fe2O3	2.59	6.20	9.78	6.50	5.20	6.70	1.50	5.93	2.68	3.77	9.00	9.91
MgO	6.73	8.55	7.59	7.10	9.03	7.40	5.18	8.56	4.76	5.10	10.31	15 30
FeO	7.41	6.50	3.20	5.40	7.20	4.20	8.06	6.03	6.71	6.53	3.65	1 94
MnO	0.24	0.22	0.23	0.23	0.21	0.20	0.22	0.21	0.17	0.18	0.28	0.20
CaO	9.68	10.47	9.72	10.28	12.05	10.90	10.65	11.24	9.70	9.22	11.39	8.62
Na2O	3.88	2.10	3.10	2.10	1.90	2.70	3.10	1.50	2.99	3.77	11.94	1.51
K2O	0.98	1.88	0.95	2.06	1.64	1.50	1.28	1.91	1.12	0.61	1.39	1 03
P2O5	0.25	0.27	0.24	0.32	0.21	0.20	0 24	0.21	0.16	0.24	1.14	0 22
TOTAL	99.35	99.80	99.82	99.67	99.37	100.00	99.72	99.71	99.92	99.74	110.87	100.00

TABLE A.3 continued SAVAGE MOUNTAIN FORMATION

SAMPLE	25	26
SiO2	44.99	41.30
TiO2	0.86	0.77
Al2O3	12.78	10.73
Fe2O3	2.43	2.32
MgO	12.76	6.11
FeO	11.07	9.42
MnO	0.26	0.24
CaO	10.93	18.94
Na2O	1.69	2.56
K2O	1.14	1.51
P2O5	0.27	0.24
TOTAL	99.18	94.14

DEWAR FORMATION

SAMPLE	1
SiO2	45.24
TiO2	0.86
Al2O3	16.11
Fe2O3	2.43
MgO	9.19
FeO	7.14
MnO	0.20
CaO	15.26
Na2O	2.09
K2O	0.94
P2O5	0.24
TOTAL	99.70

APPENDIX B

Analytical Methodology Used to Obtain Oxide Concentrations of Fractionating Phases

To obtain oxide concentrations of fractionating phases, a CAMECA - CAMEBAX wavelength dispersive electron microprobe of McGill University was used to analyze all major and some minor phases. Specimen currents were between 8 and 10 nanoamps and the counting times between 20 and 30 seconds. Various silicate and sulphide standards were used, depending on the mineral analyzed, and raw data were converted to weight percent oxides. Sample numbers and descriptions are presented in Table A.1. Probe results and stoichiometries are presented in Table A.3.

Plagioclase compositions vary from 12% An to 66% An with an average of 40% An. The widest compositional range for an individual zoned crystal is 32% An. Zoning is oscillatory and the rims are usually more calcic than the cores.

All clinopyroxene analyses were classified on a Ca-Mg-Fe ternary plot (Figure B.1). Structural formulas were calculated based on 24 oxygen. An estimate of the Fe^{3+} content was determined by solving the charge balance equation for pyroxenes of Papike et al. (1974). Fe and Mg were divided between sites M1 and M2 according to their oxide abundance. The compositions cluster around the junction of diopside, augite, and magnesian augite fields. Titanium is present in significant amounts, averaging 0.30 weight percent. In one sample, one concentrically zoned crystal was analyzed in each optically distinct zone from core to rim (analyses 23a-h, Table A.3), revealing oscillations of major components between most zones.

All amphiboles were classified according to the scheme of Leake (1978). All are calcic amphiboles ($Ca + Na \geq 1.34$ and $Na < 0.67$) and are characterised by silica contents between 41 and 55 weight percent. Structural formulas are based on 23 oxygens and were determined by first estimating an Fe^{3+} content using the charge balance equation for amphiboles of Papike et al. (1974). Na was assigned to site M4 until M4 contained 2 cations, then the excess was assigned to site NaA. Magnesio-hornblende, ferro-hornblende, ferro-tschermakitic hornblende, edenite, edenitic-hornblende, pargasite, ferroan pargasitic hornblende, actinolitic hornblende and actinolite were identified.

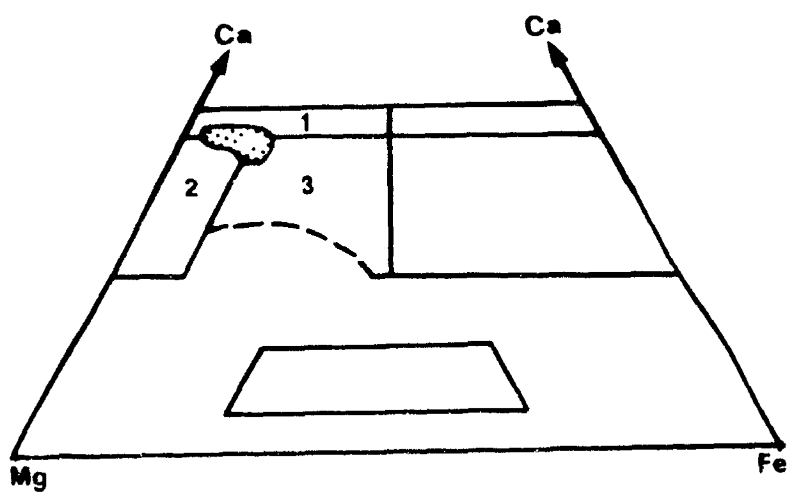

Figure B.1 Subdivisions and nomenclature of the Ca-Mg-Fe clinopyroxenes. After Heinrich (1965). Field 1 is diopside, field 2 magnesian augite, and field 3 augite.

Table B.1 Microprobe Analyses Results

PLAGIOCLASE — * SAMPLE NUMBER - CRYSTAL NUMBER U/C/M/R (unzoned, core, mid, rim)

	13-1U	21-1U	21-2U	34-1U	20-1C	20-1M	20-1R	4-1R	4-1C	4-2C	4-2M	4-2R	4-3C	4-3R	4-4C	4-4R	4-5R	4-5C	5-4C*
SiO2	65.10	63.86	55.09	66.23	60.58	60.38	59.79	54.03	61.74	58.48	59.58	59.22	63.58	56.44	52.29	56.15	57.92	58.38	54.25
TiO2	0.04	0.03	0.02	0.00	0.00	0.03	0.00	0.01	0.01	0.03	0.00	0.03	0.00	0.03	0.01	0.03	0.00	0.01	0.00
Al2O3	21.69	22.68	28.25	21.51	24.99	25.39	24.64	29.16	24.27	26.75	25.88	25.39	23.66	27.70	28.36	28.02	26.28	25.46	28.80
Fe2O3	0.00	0.00	0.00	0.00	0.00	0.00	0.00	0.00	0.00	0.00	0.00	0.00	0.00	0.00	0.00	0.00	0.00	0.00	0.00
Cr2O3	0.00	0.00	0.00	0.00	0.00	0.00	0.00	0.00	0.00	0.00	0.00	0.00	0.00	0.00	0.00	0.00	0.00	0.00	0.00
FeO	0.03	0.08	0.22	0.11	0.10	0.12	0.05	0.24	0.08	0.16	0.27	0.19	0.04	0.29	0.39	0.23	0.25	0.42	0.38
MnO	0.03	0.00	0.00	0.04	0.02	0.04	0.01	0.04	0.06	0.00	0.00	0.01	0.01	0.04	0.03	0.01	0.00	0.01	0.00
MgO	0.00	0.00	0.00	0.01	0.00	0.00	0.01	0.01	0.01	0.00	0.02	0.01	0.01	0.00	0.04	0.00	0.01	0.03	0.03
BaO	0.00	0.00	0.00	0.00	0.00	0.00	0.00	0.00	0.00	0.00	0.00	0.00	0.00	0.00	0.00	0.00	0.00	0.00	0.00
CaO	2.76	4.22	10.75	2.38	7.02	7.17	6.41	12.14	6.20	9.15	8.62	6.94	5.15	10.13	11.96	9.88	8.51	7.91	11.93
Na2O	10.32	9.38	5.50	10.40	7.61	7.50	7.76	4.68	8.54	6.47	6.67	7.86	9.10	5.94	4.76	6.08	6.60	7.15	4.77
K2O	0.07	0.27	0.21	0.09	0.41	0.40	0.47	0.07	0.12	0.09	0.19	0.19	0.09	0.14	0.10	0.13	0.18	0.15	0.11
F	0.00	0.00	0.00	0.00	0.00	0.00	0.00	0.00	0.00	0.00	0.00	0.00	0.00	0.00	0.00	0.00	0.00	0.00	0.00
TOTAL	100.04	100.52	100.04	100.77	100.73	101.03	99.14	100.38	101.03	101.13	101.23	99.84	101.64	100.71	97.94	100.53	99.75	99.52	100.27
NUMBER OF CATIONS BASED ON 32(O)																			
Si	11.467	11.246	9.942	11.561	10.734	10.673	10.755	9.742	10.883	10.364	10.534	10.603	11.091	10.097	9.692	10.058	10.403	10.513	9.794
Ti	0.005	0.004	0.003	0.000	0.000	0.004	0.000	0.001	0.001	0.004	0.000	0.004	0.000	0.004	0.001	0.004	0.000	0.001	0.000
Al	4.499	4.703	6.003	4.421	5.214	5.284	5.219	6.191	5.037	5.582	5.388	5.352	4.860	5.835	6.190	5.910	5.558	5.399	6.122
Fe3+	0.000	0.000	0.000	0.000	0.000	0.000	0.000	0.000	0.000	0.000	0.000	0.000	0.000	0.000	0.000	0.000	0.000	0.000	0.000
Cr	0.000	0.000	0.000	0.000	0.000	0.000	0.000	0.000	0.000	0.000	0.000	0.000	0.000	0.000	0.000	0.000	0.000	0.000	0.000
Fe2+	0.004	0.012	0.033	0.016	0.015	0.018	0.008	0.036	0.012	0.024	0.040	0.028	0.006	0.043	0.060	0.034	0.038	0.063	0.057
Mn	0.004	0.000	0.000	0.006	0.003	0.006	0.002	0.006	0.00[illegible]	0.000	0.000	0.002	0.001	0.006	0.005	0.002	0.000	0.002	0.000
Mg	0.000	0.000	0.000	0.003	0.000	0.000	0.003	0.003	0.003	0.000	0.005	0.003	0.003	0.000	0.011	0.000	0.003	0.008	0.008
Ba	0.000	0.000	0.000	0.000	0.000	0.000	0.000	0.000	0.000	0.000	0.000	0.000	0.000	0.000	0.000	0.000	0.000	0.000	0.000
Ca	0.521	0.796	2.079	0.445	1.333	1.358	1.235	2.345	1.171	1.737	1.633	1.331	0.963	1.942	2.375	1.896	1.638	1.526	2.308
Na	3.525	3.203	1.924	3.520	2.614	2.570	2.706	1.636	2.919	2.223	2.286	2.728	3.078	2.060	1.711	2.112	2.298	2.496	1.670
K	0.016	0.061	0.048	0.020	0.093	0.090	0.108	0.016	0.027	0.020	0.043	0.043	0.020	0.032	0.024	0.030	0.041	0.034	0.025
Xsite	15.971	15.952	15.947	15.982	15.947	15.961	15.974	15.935	15.922	15.950	15.921	15.959	15.951	15.936	15.883	15.972	15.961	15.913	15.916
Ysite	4.070	4.071	4.084	4.010	4.057	4.042	4.061	4.043	4.140	4.005	4.007	4.136	4.070	4.083	4.186	4.073	4.018	4.130	4.068
Xor	0.004	0.015	0.012	0.005	0.023	0.022	0.027	0.004	0.007	0.005	0.011	0.010	0.005	0.008	0.006	0.007	0.010	0.008	0.006
Xab	0.866	0.787	0.47[illegible]	0.878	0.644	0.636	0.666	0.405	0.705	0.555	0.571	0.660	0.756	0.505	0.409	0.518	0.572	0.604	0.410
Xan	0.130	0.198	0.517	0.117	0.333	0.342	0.307	0.591	0.288	0.440	0.419	0.330	0.239	0.488	0.586	0.474	0.418	0.387	0.583

Table B.1 PLAGIOCLASE continued

	5-4M	5-4R	5-5C	5-5M	5-5R	3-1C	3-1M	3-1R	3-2R	3-2C	20-2C	-------- progressively toward rim --------------							20-2R
SiO2	56.22	58.34	53.89	58.71	55.05	55.67	58.09	64.46	62.41	55.00	61.37	60.62	61.67	59.36	59.83	60.75	61.92	60.93	59.56
TiO2	0.00	0.03	0.04	0.01	0.01	0.02	0.00	0.00	0.01	0.04	0.00	0.00	0.02	0.00	0.01	0.02	0.00	0.02	0.00
Al2O3	27.54	26.30	28.87	25.98	28.30	28.17	26.65	22.69	23.90	28.25	24.33	24.61	23.71	24.99	25.02	24.39	23.95	23.98	25.06
Fe2O3	0.00	0.00	0.00	0.00	0.00	0.00	0.00	0.00	0.00	0.00	0.00	0.00	0.00	0.00	0.00	0.00	0.00	0.00	0.00
Cr2O3	0.00	0.00	0.00	0.00	0.00	0.00	0.00	0.00	0.00	0.00	0.00	0.00	0.00	0.00	0.00	0.00	0.00	0.00	0.00
FeO	0.24	0.18	0.38	0.15	0.25	0.40	0.23	0.10	0.15	0.26	0.05	0.02	0.07	0.10	0.09	0.13	0.08	0.09	0.14
MnO	0.00	0.00	0.00	0.06	0.00	0.01	0.00	0.01	0.03	0.00	0.02	0.00	0.00	0.00	0.05	0.01	0.02	0.00	0.00
MgO	0.03	0.02	0.02	0.01	0.02	0.01	0.00	0.00	0.00	0.01	0.00	0.01	0.00	0.00	0.00	0.00	0.00	0.00	0.00
BaO	0.00	0.00	0.00	0.00	0.00	0.00	0.00	0.00	0.00	0.00	0.00	0.00	0.00	0.00	0.00	0.00	0.00	0.00	0.00
CaO	10.36	8.86	11.95	8.37	10.92	10.67	8.98	4.21	5.37	11.11	6.07	6.48	5.96	7.59	7.01	6.44	5.76	6.40	7.57
Na2O	5.97	6.55	4.85	6.80	5.34	5.46	6.59	9.86	8.80	5.17	7.64	7.56	7.70	6.84	7.10	7.53	7.77	7.66	6.86
K2O	0.09	0.15	0.11	0.20	0.10	0.10	0.18	0.08	0.08	0.13	0.44	0.41	0.35	0.37	0.34	0.46	0.56	0.45	0.37
F	0.00	0.00	0.00	0.00	0.00	0.00	0.00	0.00	0.00	0.00	0.00	0.00	0.00	0.00	0.00	0.00	0.00	0.00	0.00
TOTAL	100.45	100.43	100.11	100.29	99.99	100.51	100.72	101.41	100.75	99.97	99.92	99.71	99.48	99.25	99.45	99.73	100.06	99.53	99.56
NUMBER OF CATIONS BASED ON 32(O)																			
Si	10.089	10.410	9.754	10.481	9.934	9.990	10.349	11.257	10.999	9.930	10.910	10.818	10.999	10.672	10.718	10.845	10.988	10.897	10.675
Ti	0.000	0.004	0.005	0.001	0.001	0.003	0.000	0.000	0.001	0.005	0.000	0.000	0.003	0.000	0.001	0.003	0.000	0.003	0.000
Al	5.819	5.525	6.152	5.461	6.013	5.952	5.590	4.665	4.959	6.006	5.093	5.171	4.979	5.290	5.277	5.126	5.004	5.050	5.289
Fe3+	0.000	0.000	0.000	0.000	0.000	0.000	0.000	0.000	0.000	0.000	0.000	0.000	0.000	0.000	0.000	0.000	0.000	0.000	0.000
Cr	0.000	0.000	0.000	0.000	0.000	0.000	0.000	0.000	0.000	0.000	0.000	0.000	0.000	0.000	0.000	0.000	0.000	0.000	0.000
Fe2+	0.036	0.027	0.058	0.022	0.038	0.060	0.034	0.015	0.022	0.039	0.007	0.003	0.010	0.015	0.013	0.019	0.012	0.013	0.021
Mn	0.000	0.000	0.000	0.009	0.000	0.002	0.000	0.001	0.004	0.000	0.003	0.000	0.000	0.000	0.008	0.002	0.003	0.000	0.000
Mg	0.008	0.005	0.005	0.003	0.005	0.003	0.000	0.000	0.000	0.003	0.000	0.003	0.000	0.000	0.000	0.000	0.000	0.000	0.000
Ba	0.000	0.000	0.000	0.000	0.000	0.000	0.000	0.000	0.000	0.000	0.000	0.000	0.000	0.000	0.000	0.000	0.000	0.000	0.000
Ca	1.992	1.694	2.317	1.601	2.111	2.052	1.714	0.788	1.014	2.149	1.156	1.239	1.139	1.462	1.345	1.232	1.095	1.226	1.454
Na	2.077	2.266	1.702	2.354	1.868	1.900	2.276	3.338	3.007	1.810	2.633	2.616	2.663	2.384	2.466	2.606	2.673	2.656	2.384
K	0.021	0.034	0.025	0.046	0.023	0.023	0.041	0.018	0.018	0.030	0.100	0.093	0.080	0.085	0.078	0.105	0.127	0.103	0.085
Xsite	15.908	15.939	15.912	15.944	15.949	15.945	15.940	15.922	15.960	15.941	16.003	15.989	15.981	15.963	15.996	15.974	15.992	15.949	15.964
Ysite	4.134	4.026	4.108	4.034	4.046	4.038	4.066	4.160	4.065	4.031	3.900	3.954	3.892	3.946	3.910	3.964	3.910	3.998	3.943
Xor	0.005	0.008	0.006	0.011	0.006	0.006	0.010	0.004	0.004	0.007	0.026	0.024	0.020	0.022	0.020	0.026	0.032	0.026	0.021
Xab	0.502	0.563	0.414	0.583	0.462	0.470	0.560	0.802	0.740	0.449	0.675	0.662	0.684	0.604	0.631	0.658	0.684	0.664	0.605
Xan	0.493	0.429	0.579	0.405	0.533	0.524	0.430	0.193	0.256	0.544	0.299	0.315	0.295	0.374	0.349	0.316	0.284	0.310	0.374

Table B.1 PLAGIOCLASE continued

	9-1R	9-1C	5-1C	5-1M	5-1R	5-2R	5-2C	5-3R	5-3M	5-3C
SiO2	61.00	56.56	55.91	57.58	56.93	57.86	54.38	56.33	56.01	51.99
TiO2	0.00	0.00	0.03	0.00	0.01	0.02	0.00	0.00	0.00	0.02
Al2O3	24.60	27.22	27.60	25.73	26.73	26.80	28.77	27.43	27.69	30.09
Fe2O3	0.00	0.00	0.00	0.00	0.00	0.00	0.00	0.00	0.00	0.00
Cr2O3	0.00	0.00	0.00	0.00	0.00	0.00	0.00	0.00	0.00	0.00
FeO	0.14	0.19	0.31	0.12	0.17	0.17	0.28	0.20	0.41	0.35
MnO	0.02	0.01	0.02	0.01	0.00	0.00	0.00	0.00	0.00	0.02
MgO	0.02	0.01	0.02	0.02	0.01	0.00	0.09	0.01	0.02	0.07
BaO	0.00	0.00	0.00	0.00	0.00	0.00	0.00	0.00	0.00	0.00
CaO	6.72	9.67	10.47	8.56	9.61	9.44	11.84	10.38	10.60	13.23
Na2O	7.88	6.20	5.63	6.68	6.26	6.25	4.83	5.82	5.61	3.89
K2O	0.09	0.12	0.12	0.19	0.10	0.11	0.09	0.12	0.14	0.10
F	0.00	0.00	0.00	0.00	0.00	0.00	0.00	0.00	0.00	0.00
TOTAL	100.47	99.98	100.11	98.89	99.82	100.65	100.28	100.29	100.48	99.76
NUMBER OF CATIONS BASED ON 32(O)										
Si	10.811	10.175	10.067	10.436	10.251	10.314	9.808	10.117	10.056	9.473
Ti	0.000	0.000	0.004	0.000	0.001	0.003	0.000	0.000	0.000	0.003
Al	5.134	5.766	5.851	5.491	5.667	5.625	6.110	5.800	5.854	6.455
Fe3+	0.000	0.000	0.000	0.000	0.000	0.000	0.000	0.000	0.000	0.000
Cr	0.000	0.000	0.000	0.000	0.000	0.000	0.000	0.000	0.000	0.000
Fe2+	0.021	0.029	0.047	0.018	0.026	0.025	0.042	0.030	0.062	0.053
Mn	0.003	0.002	0.003	0.002	0.000	0.000	0.000	0.000	0.000	0.003
Mg	0.005	0.003	0.005	0.005	0.003	0.000	0.024	0.003	0.005	0.019
Ba	0.000	0.000	0.000	0.000	0.000	0.000	0.000	0.000	0.000	0.000
Ca	1.276	1.864	2.020	1.662	1.854	1.803	2.288	1.997	2.039	2.583
Na	2.708	2.163	1.965	2.347	2.185	2.160	1.689	2.027	1.953	1.374
K	0.020	0.028	0.028	0.044	0.023	0.025	0.021	0.027	0.032	0.023
Xsite	15.945	15.941	15.923	15.927	15.919	15.942	15.918	15.917	15.910	15.931
Ysite	4.033	4.087	4.068	4.079	4.091	4.013	4.064	4.084	4.091	4.056
Xor	0.005	0.007	0.007	0.011	0.006	0.006	0.005	0.007	0.008	0.006
Xab	0.671	0.529	0.483	0.576	0.534	0.538	0.416	0.496	0.477	0.339
Xan	0.324	0.464	0.510	0.414	0.460	0.456	0.579	0.497	0.515	0.655

Table B.1 continued PYROXENE

	38-1	38-2	38-3	38-4	38-5	38-6	41-1	36-1C	----- progressively toward rim ----------						36-1R	36-2	36-3	38-7	38-8
SiO2	51.00	51.03	55.08	53.25	54.35	52.98	52.98	52.00	51.30	51.32	50.81	51.04	52.47	50.28	50.12	53.28	52.50	50.08	51.47
TiO2	0.36	0.38	0.06	0.18	0.07	0.25	0.23	0.39	0.34	0.37	0.46	0.47	0.18	0.44	0.51	0.20	0.28	0.40	0.39
Al2O3	3.34	3.02	0.83	1.59	0.91	2.68	2.02	2.54	2.59	2.69	3.16	3.74	1.50	4.65	4.13	2.30	3.10	4.74	2.90
Fe2O3	0.00	0.00	0.00	0.00	0.00	0.00	0.00	0.00	0.00	0.00	0.00	0.00	0.00	0.00	0.00	0.00	0.00	0.00	0.00
Cr2O3	0.00	0.00	0.00	0.00	0.00	0.00	0.00	0.00	0.00	0.00	0.00	0.00	0.00	0.00	0.00	0.00	0.00	0.00	0.00
FeO	6.74	6.71	2.64	4.08	2.84	6.76	5.19	6.79	7.08	7.03	7.48	6.76	3.60	6.54	6.01	4.40	5.37	6.78	7.12
MnO	0.13	0.24	0.09	0.15	0.13	0.10	0.12	0.16	0.23	0.20	0.19	0.06	0.14	0.13	0.13	0.09	0.16	0.18	0.21
MgO	15.69	15.86	18.14	16.76	17.98	17.05	16.56	16.55	15.76	16.11	15.43	15.54	17.70	15.28	15.31	16.55	16.06	15.42	16.01
BaO	0.00	0.00	0.00	0.00	0.00	0.00	0.00	0.00	0.00	0.00	0.00	0.00	0.00	0.00	0.00	0.00	0.00	0.00	0.00
CaO	21.57	21.48	23.13	22.60	23.30	21.00	21.94	21.53	21.62	21.42	21.32	22.66	22.98	22.20	22.49	22.42	21.84	21.66	21.51
Na2O	0.23	0.17	0.13	0.15	0.08	0.18	0.25	0.21	0.26	0.24	0.28	0.16	0.13	0.25	0.19	0.15	0.21	0.22	0.21
K2O	0.00	0.02	0.00	0.00	0.02	0.02	0.03	0.00	0.00	0.00	0.00	0.00	0.01	0.00	0.00	0.00	0.00	0.03	0.00
F	0.00	0.00	0.00	0.00	0.00	0.00	0.00	0.00	0.00	0.00	0.00	0.00	0.00	0.00	0.00	0.00	0.00	0.00	0.00
TOTAL	99.06	98.96	100.10	98.76	99.68	101.02	99.32	100.17	99.18	99.38	99.13	100.43	98.71	99.77	98.89	99.39	99.52	99.51	99.82

STOICHIOMETRIES BASED ON 24 OXYGENS

Si	7.563	7.587	7.966	7.866	7.913	7.683	7.801	7.616	7.609	7.586	7.550	7.475	7.719	7.400	7.440	7.820	7.725	7.391	7.581
AlZ	0.437	0.413	0.034	0.134	0.087	0.317	0.199	0.384	0.391	0.414	0.450	0.525	0.260	0.600	0.560	0.180	0.275	0.609	0.419
Fe3Z	0.000	0.000	0.000	0.000	0.000	0.000	0.000	0.000	0.000	0.000	0.000	0.000	0.021	0.000	0.000	0.000	0.000	0.000	0.000
AlM1	0.147	0.116	0.107	0.143	0.070	0.141	0.151	0.055	0.062	0.055	0.104	0.121	0.000	0.207	0.163	0.218	0.263	0.215	0.085
Ti	0.040	0.042	0.007	0.020	0.008	0.027	0.025	0.043	0.038	0.041	0.051	0.052	0.020	0.049	0.057	0.022	0.031	0.044	0.043
Cr	0.000	0.000	0.000	0.000	0.002	0.002	0.003	0.000	0.000	0.000	0.000	0.000	0.001	0.000	0.000	0.000	0.000	0.003	0.000
Fe3M1	0.276	0.261	-0.050	-0.007	0.021	0.169	0.063	0.302	0.329	0.345	0.324	0.346	0.276	0.366	0.338	-0.039	0.010	0.363	0.307
FeM1	0.492	0.502	0.294	0.461	0.300	0.549	0.514	0.460	0.487	0.458	0.530	0.433	0.134	0.391	0.370	0.489	0.577	0.414	0.497
MgM1	3.046	3.079	3.604	3.377	3.600	3.112	3.243	3.140	3.086	3.102	2.991	3.049	3.569	2.988	3.073	3.281	3.120	2.961	3.068
M1	4.000	4.000	3.963	3.995	4.000	4.000	4.001	4.001	4.001	4.001	4.001	4.001	4.001	4.001	4.001	3.970	4.000	4.001	4.001
FeM2	0.068	0.070	0.025	0.043	0.025	0.101	0.062	0.069	0.063	0.066	0.076	0.049	0.012	0.048	0.038	0.051	0.074	0.060	0.072
MgM2	0.422	0.432	0.306	0.313	0.302	0.574	0.391	0.473	0.398	0.448	0.426	0.343	0.312	0.365	0.315	0.340	0.403	0.431	0.447
Mn	0.016	0.030	0.011	0.019	0.016	0.012	0.015	0.020	0.029	0.025	0.024	0.007	0.017	0.016	0.016	0.011	0.020	0.023	0.026
Ca	3.427	3.418	3.584	3.577	3.635	3.263	3.461	3.379	3.436	3.393	3.394	3.556	3.622	3.501	3.577	3.526	3.443	3.425	3.395
Na	0.066	0.049	0.036	0.043	0.023	0.051	0.071	0.060	0.075	0.069	0.081	0.045	0.037	0.071	0.055	0.043	0.060	0.063	0.060
M2	4.000	4.000	3.963	3.995	4.000	4.000	4.001	4.001	4.001	4.001	4.001	4.001	4.001	4.001	4.001	3.970	4.000	4.001	4.001
Total	16.001	16.001	15.925	15.990	16.001	16.001	16.001	6.001	16.001	16.001	16.001	16.001	16.001	16.002	16.001	15.941	16.000	16.002	16.001
XMgM1	0.761	0.770	0.910	0.845	0.900	0.778	0.811	0.785	0.771	0.775	0.748	0.762	0.892	0.747	0.768	0.826	0.780	0.740	0.767
XMgM2	0.106	0.108	0.077	0.078	0.075	0.143	0.098	0.118	0.100	0.112	0.107	0.086	0.078	0.091	0.079	0.086	0.101	0.108	0.112
XCaM2	0.857	0.855	0.904	0.895	0.909	0.816	0.865	0.845	0.859	0.848	0.848	0.889	0.905	0.875	0.894	0.888	0.861	0.856	0.849

Table B.1 continued AMPHIBOLE

	25-1	25-2	34-1	34-2	30-1	30-2	30-3	30-4	30-5	37-1	37-2	37-3	37-4	32-1	32-2	32-3	38-1	38-2	39-1	39-2	39-3
SiO2	55.56	55.03	54.00	54.68	42.13	42.08	42.62	41.91	40.54	52.95	52.31	53.33	52.57	53.34	53.71	54.04	43.48	52.16	41.35	42.07	41.64
TiO2	0.06	0.06	0.07	0.03	1.96	2.14	2.06	2.22	2.16	0.05	0.05	0.01	0.07	0.04	0.04	0.05	0.40	0.08	1.76	1.67	2.01
Al2O3	3.29	3.68	3.30	2.30	14.60	14.55	14.26	14.42	14.37	3.36	3.63	3.28	3.96	4.46	3.64	3.80	14.80	4.47	15.39	14.28	13.45
Fe2O3	0.00	0.00	0.00	0.00	0.00	0.00	0.00	0.00	0.00	0.00	0.00	0.00	0.00	0.00	0.00	0.00	0.00	0.00	0.00	0.00	0.00
Cr2O3	0.00	0.00	0.00	0.00	0.00	0.00	0.00	0.00	0.00	0.00	0.00	0.00	0.00	0.00	0.00	0.00	0.00	0.00	0.00	0.00	0.00
FeO	9.95	9.69	11.68	11.39	10.43	10.26	10.54	10.98	11.06	11.46	11.50	11.30	11.58	11.23	10.30	10.21	13.60	15.15	9.74	10.53	11.35
MnO	0.22	0.24	0.23	0.21	0.06	0.14	0.12	0.06	0.12	0.42	0.44	0.45	0.47	0.32	0.32	0.33	0.32	0.27	0.08	0.12	0.11
MgO	17.12	16.93	16.11	16.40	14.51	14.65	14.20	14.13	14.36	16.11	16.03	16.12	15.95	16.48	16.64	16.70	11.23	13.88	14.97	15.21	14.78
BaO	0.00	0.00	0.00	0.00	0.00	0.00	0.00	0.00	0.00	0.00	0.00	0.00	0.00	0.00	0.00	0.00	0.00	0.00	0.00	0.00	0.00
CaO	12.96	12.87	12.91	12.84	12.05	12.18	12.17	12.17	12.07	12.61	12.82	12.79	12.84	12.84	12.81	12.92	12.15	12.34	12.32	11.87	11.87
Na2O	0.18	0.18	0.27	0.19	2.50	2.47	2.51	2.24	2.45	0.16	0.25	0.16	0.26	0.24	0.19	0.20	1.56	0.39	2.22	2.17	2.36
K2O	0.09	0.13	0.13	0.08	0.19	0.24	0.27	0.23	0.23	0.10	0.11	0.10	0.13	0.16	0.08	0.10	0.40	0.12	0.34	0.33	0.19
F	0.00	0.00	0.00	0.00	0.00	0.00	0.00	0.00	0.00	0.00	0.00	0.00	0.00	0.00	0.00	0.00	0.00	0.00	0.00	0.00	0.00
TOTAL	99.43	98.81	98.70	98.12	98.43	98.71	98.75	98.36	97.36	97.22	97.14	97.54	97.83	99.11	97.73	98.35	97.94	98.86	98.17	98.25	97.76
NUMBER OF CATIONS BASED ON 23 OXYGENS (PAPIKE)																					
Si	7.737	7.706	7.660	7.782	6.070	6.045	6.142	6.050	5.917	7.607	7.527	7.636	7.517	7.505	7.641	7.639	6.355	7.502	5.934	6.042	6.045
AlZ	0.263	0.294	0.340	0.218	1.930	1.955	1.858	1.950	2.083	0.393	0.473	0.364	0.483	0.495	0.359	0.361	1.645	0.498	2.066	1.958	1.955
Fe3+Z	0.000	0.000	0.000	0.000	0.000	0.000	0.000	0.000	0.000	0.000	0.000	0.000	0.000	0.000	0.000	0.000	0.000	0.000	0.000	0.000	0.000
AlY	0.277	0.314	0.211	0.168	0.549	0.508	0.564	0.504	0.389	0.176	0.143	0.189	0.185	0.245	0.251	0.273	0.905	0.260	0.537	0.460	0.346
Ti	0.006	0.006	0.007	0.003	0.212	0.231	0.223	0.241	0.237	0.005	0.005	0.001	0.008	0.004	0.004	0.005	0.044	0.009	0.190	0.180	0.219
Fe2+	1.159	1.135	1.369	1.356	1.033	0.980	1.173	1.032	0.866	1.234	1.155	1.243	1.197	1.174	1.193	1.202	1.527	1.732	0.700	0.792	0.908
Fe3+Y	-0.000	-0.007	0.016	0.000	0.224	0.252	0.098	0.294	0.484	0.143	0.229	0.110	0.187	0.148	0.032	0.005	0.135	0.090	0.469	0.473	0.470
Mn	0.026	0.028	0.028	0.025	0.007	0.017	0.015	0.007	0.015	0.051	0.054	0.055	0.057	0.038	0.039	0.040	0.040	0.033	0.010	0.015	0.014
Mg	3.553	3.534	3.406	3.479	3.116	3.137	3.050	3.041	3.124	3.450	3.438	3.440	3.400	3.456	3.528	3.519	2.447	2.976	3.202	3.256	3.198
Xoct	0.021	0.017	0.038	0.031	0.141	0.126	0.122	0.119	0.115	0.059	0.024	0.038	0.033	0.065	0.048	0.043	0.098	0.099	0.108	0.175	0.156
Ca	1.934	1.931	1.962	1.958	1.860	1.875	1.879	1.882	1.887	1.941	1.977	1.962	1.967	1.936	1.953	1.957	1.903	1.902	1.894	1.827	1.846
NaM4	0.045	0.049	-0.000	0.011	-0.001	-0.001	-0.001	-0.001	-0.002	-0.000	-0.001	-0.000	-0.001	-0.000	-0.000	-0.000	-0.000	-0.000	-0.002	-0.002	-0.002
NaA	0.003	-0.003	0.074	0.041	0.698	0.688	0.701	0.627	0.693	0.045	0.070	0.044	0.072	0.065	0.052	0.055	0.442	0.109	0.618	0.604	0.664
K	0.016	0.023	0.024	0.015	0.035	0.044	0.050	0.042	0.043	0.018	0.020	0.018	0.024	0.029	0.015	0.018	0.075	0.022	0.062	0.060	0.035
F	0.000	0.000	0.000	0.000	0.000	0.000	0.000	0.000	0.000	0.000	0.000	0.000	0.000	0.000	0.000	0.000	0.000	0.000	0.000	0.000	0.000
CATION	15.019	15.020	15.098	15.056	15.734	15.733	15.751	15.670	15.738	15.063	15.091	15.063	15.096	15.095	15.067	15.073	15.517	15.131	15.682	15.667	15.701
OXYGEN	23.010	23.010	23.049	23.028	23.367	23.367	23.376	23.336	23.370	23.032	23.046	23.032	23.048	23.048	23.034	23.037	23.259	23.066	23.342	23.334	23.352
Alprop	6.524	7.306	6.719	4.723	29.000	28.954	28.282	28.852	29.467	6.959	7.561	6.759	8.154	8.971	7.397	7.654	28.632	9.174	30.491	28.575	27.573
Naprop	2.452	2.468	3.647	2.608	27.295	26.845	27.178	24.985	26.864	2.244	3.409	2.214	3.535	3.272	2.614	2.725	18.853	5.410	24.589	24.858	26.459
NaA+K	0.019	0.020	0.098	0.056	0.733	0.732	0.751	0.669	0.736	0.063	0.090	0.063	0.096	0.094	0.067	0.073	0.517	0.131	0.680	0.665	0.699
Fe+Ti	0.283	0.320	0.235	0.171	0.985	0.992	0.884	1.039	1.110	0.325	0.377	0.300	0.379	0.396	0.288	0.282	1.084	0.359	1.196	1.113	1.036
Mg/Fe	3.067	3.114	2.458	2.566	2.479	2.545	2.401	2.294	2.314	2.505	2.484	2.542	2.455	2.615	2.879	2.915	1.472	1.633	2.739	2.574	2.321

Table B.1 continued AMPHIBOLE

	4-1	9-1	9-2	9-3	5-1	5-2	2-1	2-2	13-1	13-2	21-1	23-1	23-2	23-3	23-4	23-5	23-6	26-1	26-2	24-1	18-1
SiO2	46.00	48.53	48.10	49.92	45.19	45.46	52.80	50.30	42.53	42.33	49.67	51.97	47.14	45.18	53.44	54.67	45.17	42.76	42.72	53.79	52.83
TiO2	2.08	0.93	1.35	1.18	1.84	1.80	0.19	0.21	1.62	1.82	0.71	0.12	0.25	0.35	0.23	0.10	0.54	2.70	0.54	0.24	0.12
Al2O3	10.67	8.21	8.48	6.76	11.60	11.06	4.76	6.40	13.45	14.56	5.82	5.36	9.99	12.32	3.98	3.52	13.23	14.23	14.75	4.27	4.11
Fe2O3	0.00	0.00	0.00	0.00	0.00	0.00	0.00	0.00	0.00	0.00	0.00	0.00	0.00	0.00	0.00	0.00	0.00	0.00	0.00	0.00	0.00
Cr2O3	0.00	0.00	0.00	0.00	0.00	0.00	0.00	0.00	0.00	0.00	0.00	0.00	0.00	0.00	0.00	0.00	0.00	0.00	0.00	0.00	0.00
FeO	11.10	13.32	13.08	12.27	11.50	11.30	12.94	14.16	10.35	10.09	14.82	15.69	18.44	18.78	14.81	14.55	18.02	19.13	20.27	12.55	11.08
MnO	0.14	0.26	0.30	0.29	0.11	0.15	0.47	0.54	0.16	0.14	0.73	0.40	0.46	0.36	0.36	0.31	0.31	0.43	0.62	0.28	0.46
MgO	14.69	15.30	14.97	15.85	14.50	15.14	15.12	14.12	14.60	15.01	13.44	13.07	9.69	8.36	14.16	14.32	8.42	6.57	6.96	14.88	15.93
BaO	0.00	0.00	0.00	0.00	0.00	0.00	0.00	0.00	0.00	0.00	0.00	0.00	0.00	0.00	0.00	0.00	0.00	0.00	0.00	0.00	0.00
CaO	11.31	10.24	10.50	10.57	11.01	11.07	11.99	12.03	11.92	11.84	11.21	11.94	11.60	11.82	12.07	12.11	11.59	12.56	11.37	12.37	12.55
Na2O	2.23	1.51	1.69	1.41	2.26	2.23	0.72	0.84	2.46	2.43	1.20	0.32	0.74	0.76	0.49	0.29	1.02	1.14	1.23	0.39	0.41
K2O	0.26	0.22	0.24	0.19	0.29	0.24	0.24	0.30	0.24	0.25	0.42	0.19	0.23	0.37	0.10	0.12	0.34	0.38	0.36	0.15	0.14
F	0.00	0.00	0.00	0.00	0.00	0.00	0.00	0.00	0.00	0.00	0.00	0.00	0.00	0.00	0.00	0.00	0.00	0.00	0.00	0.00	0.00
TOTAL	98.48	98.57	98.71	98.44	98.30	98.45	99.23	98.90	97.33	98.47	98.02	99.06	98.54	98.30	99.64	99.99	98.64	99.90	98.82	98.92	97.63
NUMBER OF CATIONS BASED ON 23 OXYGENS (PAPIKE)																					
Si	6.623	6.985	6.924	7.153	6.531	6.555	7.508	7.239	6.198	6.078	7.268	7.482	6.947	6.703	7.609	7.723	6.658	6.317	6.373	7.631	7.573
AlZ	1.377	1.015	1.076	0.847	1.469	1.445	0.492	0.761	1.802	1.922	0.732	0.518	1.053	1.297	0.391	0.277	1.342	1.683	1.627	0.369	0.427
Fe3+Z	0.000	0.000	0.000	0.000	0.000	0.000	0.000	0.000	0.000	0.000	0.000	0.000	0.000	0.000	0.000	0.000	0.000	0.000	0.000	0.000	0.000
AlY	0.434	0.378	0.363	0.295	0.507	0.435	0.305	0.324	0.509	0.542	0.272	0.391	0.682	0.858	0.277	0.309	0.956	0.794	0.967	0.345	0.268
Ti	0.225	0.106	0.146	0.127	0.200	0.195	0.020	0.023	0.178	0.197	0.078	0.013	0.028	0.039	0.025	0.011	0.060	0.300	0.061	0.026	0.013
Fe2+	1.337	1.603	1.575	1.470	1.390	1.363	1.539	1.602	1.064	0.947	1.814	1.889	2.212	2.258	1.764	1.719	2.221	2.363	2.415	1.489	1.328
Fe3+Y	-0.000	0.000	-0.000	-0.000	0.000	0.000	-0.000	0.102	0.198	0.265	0.000	0.000	0.060	0.072	0.000	-0.000	-0.000	-0.084	0.114	-0.000	-0.000
Mn	0.017	0.032	0.037	0.035	0.013	0.018	0.057	0.066	0.020	0.017	0.090	0.049	0.057	0.045	0.043	0.037	0.039	0.054	0.078	0.034	0.056
Mg	3.153	3.283	3.212	3.385	3.123	3.254	3.204	3.029	3.172	3.212	2.931	2.805	2.129	1.849	3.005	3.015	1.850	1.447	1.548	3.146	3.404
Xoct	0.166	0.402	0.333	0.313	0.233	0.265	0.126	0.146	0.139	0.179	0.185	0.147	0.169	0.121	0.114	0.090	0.125	-0.042	0.183	0.039	0.069
Ca	1.745	1.579	1.620	1.623	1.705	1.710	1.827	1.855	1.861	1.821	1.757	1.842	1.832	1.879	1.841	1.833	1.830	1.988	1.817	1.880	1.928
NaM4	0.089	0.019	0.048	0.064	0.062	0.024	0.048	-0.001	-0.001	-0.001	0.057	0.012	-0.000	-0.000	0.045	0.077	0.044	0.012	-0.000	0.081	0.003
NaA	0.533	0.403	0.424	0.327	0.571	0.599	0.151	0.234	0.695	0.676	0.283	0.078	0.211	0.219	0.091	0.003	0.247	0.314	0.356	0.027	0.111
K	0.048	0.040	0.044	0.035	0.053	0.044	0.044	0.055	0.045	0.046	0.078	0.035	0.043	0.070	0.018	0.022	0.064	0.072	0.069	0.027	0.026
F	0.000	0.000	0.000	0.000	0.000	0.000	0.000	0.000	0.000	0.000	0.000	0.000	0.000	0.000	0.000	0.000	0.000	0.000	0.000	0.000	0.000
CATION	15.581	15.443	15.468	15.362	15.625	15.643	15.194	15.290	15.740	15.723	15.361	15.113	15.255	15.289	15.109	15.024	15.311	15.344	15.425	15.054	15.136
OXYGEN	23.291	23.222	23.234	23.181	23.312	23.322	23.097	23.145	23.370	23.362	23.181	23.056	23.128	23.145	23.054	23.012	23.156	23.193	23.212	23.027	23.068
Alprop	21.469	16.624	17.204	13.764	23.227	22.285	9.605	13.041	27.153	28.846	12.134	10.838	19.986	24.322	8.070	7.053	25.662	28.173	28.924	8.556	8.399
Naprop	26.297	21.063	22.556	19.445	27.084	26.715	9.801	11.218	27.191	27.081	16.227	4.625	10.349	10.422	6.843	4.153	13.738	14.107	16.371	5.397	5.582
NaA+K	0.581	0.443	0.468	0.362	0.625	0.643	0.194	0.289	0.740	0.722	0.361	0.113	0.255	0.289	0.109	0.024	0.311	0.386	0.424	0.054	0.136
Fe+Ti	0.659	0.484	0.509	0.422	0.707	0.630	0.326	0.449	0.884	1.003	0.350	0.404	0.770	0.969	0.302	0.319	1.016	1.094	1.142	0.370	0.281
Mg/Fe	2.359	2.047	2.040	2.302	2.247	2.388	2.083	1.777	2.514	2.651	1.616	1.485	0.937	0.793	1.704	1.754	0.833	0.612	0.612	2.113	2.562

Table B.1 continued BIOTITE

	1	2	3
SiO2	36.25	36.18	36.53
TiO2	3.32	2.00	2.22
Al2O3	15.10	18.62	17.65
Fe2O3	3.83	3.69	3.64
Cr2O3	0.00	0.00	0.00
FeO	15.32	14.77	14.54
MnO	0.28	0.19	0.17
MgO	10.26	10.36	10.50
BaO	0.00	0.00	0.00
CaO	0.01	0.07	0.14
Na2O	0.12	0.10	0.01
K2O	9.57	10.09	9.65
F	0.00	0.00	0.00
TOTAL	94.06	96.07	95.05

STOICHIOMETRYS BASED ON 22 OXYGENS
20.0% OF FeO CONVERTED TO Fe2O3

Si	5.574	5.414	5.505	5.498
AlZ	2.426	2.586	2.495	2.502
Fe3+Z	0.000	0.000	0.000	0.000
Z	8.000	8.000	8.000	8.000
AlY	0.310	0.698	0.640	0.550
TiY	0.384	0.225	0.252	0.287
Fe3+Y	0.443	0.416	0.412	0.424
Y	1.137	1.339	1.304	1.260
MgX	2.351	2.311	2.359	2.340
Fe2+Y	1.970	1.848	1.833	1.884
MnX	0.036	0.024	0.022	0.027
NaX	0.036	0.029	0.003	0.023
X	4.394	4.212	4.216	4.274
K	1.877	1.926	1.855	1.886
NaA	0.000	0.000	0.000	0.000
CaA	0.002	0.011	0.023	0.012
A	1.879	1.937	1.878	1.898
F	0.000	0.000	0.000	0.000
OXYGEN	22.000	22.000	22.000	22.000
CATION	15.409	15.488	15.398	15.432
Fe/Mg	102.625	97.972	95.200	98.599
Fe2/Mg	83.779	79.981	77.718	80.493
Aphlog	0.054	0.051	0.053	0.053

REFERENCES

Ahmedali, T. (1983): XRF Procedures, Circular #1, Department of Geological Sciences, McGill University, 132 pages.

Allegre, C.J. and Minster, J.F. (1987): Quantitative Models of Trace Element Behavior in Magmatic Processes, Earth and Planetary Science Letters, Volume 38, pages 1-25.

Barker, D.S. (1983): Igneous Rocks, New Jersey: Prentice-Hall Inc., 417 pages.

Cas, R.A.F. & Wright, J.V. (1987): Volcanic Successions Modern and Ancient. London: Allen & Unwin, 528 pages.

Clarke, M.C.G. and Beddoe-Stephens, B. (1987): Geochemistry, Mineralogy and Plate Tectonic Setting of a Late Cretaceous Sn-W Granite from Sumatra, Indonesia, Mineralogical Magazine, Volume 51, pages 371-387.

Cox,K.G., Bell, J.D., and Pankhurst, R.J. (1979): The Interpretation of Igneous Rocks. George Allen and Unwin, London.

Foden, J.D. (1983): The Petrology of the Calc-alkaline Lavas of Rindjani Volcano, East Sunda Arc; a Model for Island Arc Petrogenesis, **in** Wilson, M. and Davidson, J.P. (1984): The Relative Roles of Crust and Upper Mantle in the Generation of Oceanic Island Arc Magmas, Philisophical Transactions Royal Society London, Volume 310, pages 661-674.

Francis, D.M., Hynes, A.J., Ludden, J.N., and Bedard, J. (1981): Crystal Fractionation and Partial Melting in the Petrogenesis of a Proterozoic High-MgO Volcanic Suite, Ungave, Quebec, Contributions to Mineralogy and Petrology, Volume 78, pages 27-36.

Gabrielse, H. (1985): Major Dextral Transcurrent Displacements along the Northern Rocky Mountain Trench and Related Lineaments in North-central British Columbia, Geological Society of America Bulletin, Volume 96, pages 1-14.

Green, T.H. (1980): Island Arc and Continent-Building Magmatism - A Review of Petrogenetic Models Based on Experimental Petrology and Geochemistry, Tectonophysics, Volume 63, pages 367-385.

Grove, T.L., Gerlach, D.C., and Sando, T.W. (1982): Origin of Calc-alkaline Series Lavas at Medicine Lake Volcano by Fractionation, Assimilation and Mixing, Contributions to Mineralogy and Petrology, Volume 80, pages 160-182.

Heinrich, E.Wm. (1965): Microscopic Identification of Minerals, New York: McGraw-Hill Book Company, 414 pages.

Irvine, T.N. (1976): Studies of Cordilleran Gabbroic and Ultramafic Intrusives, British Columbia; in Report of Activities, Geological Survey of Canada, Paper 76-1A, pages 75-81.

Irvine, T.N. and Baragar, W.R.A. (1971): A Guide to the Chemical Classification of the Common Volcanic Rocks, Canadian Journal of EarthSciences, Volume 8, pages 523 -548.

Leake, B.E. (1978): Nomenclature of Amphiboles, Canadian Mineralogist, Volume 16, pages 501-520.

Le Bas, M.J., Le Maitre, R.W., Streckeisen, A., and Zanettin,

B. (1986): A Chemical Classification of Volcanic Rocks Based on the Total Alkali-Silica Diagram, Journal of Petrology, Volume 27, Part 3, pages 745-750.

LeMaitre, R.W. (1979): A New Generalised Petrological Mixing Model, Contributions to Mineralogy and Petrology, Volume 71, pages 133-137.

Lord, C.S. (1948): McConnell Creek Map-area, Cassiar District, British columbia, Geological Survey of Canada, Memoir 251, 72 pages.

Miyashiro, A. (1974): Volcanic Rock Series in Island Arcs and Active Continental Margins, American Journal of Science, Volume 274, pages 321-355.

Monger, J.W.H. (1976): Lower Mesozoic Rocks in McConnell Creek Map-Area (94E),British Columbia; in Report of Activities, Geological Survey of Canada, Paper 76-1A, pages 51-55.

______________ (1977): The Triassic Takla Group in McConnell Creek Map-area, North-central British Columbia, Geological Survey of Canada, Paper 76-29, 45 pages.

______________ (1984): Cordilleran Tectonics: A Canadian Perspective, Societe Geologique de France Bulletin, Volume 7, no. 2, pages 255-278.

Monger, J.W.H. and Church, B.N. (1977): Revised Stratigraphy of the Takla Group, North-central British Columbia, Canadian Journal of Earth Sciences, Volume 14, pages 318 -326.

Monger, J.W.H., Price, R.A., and Tempelman-Kluit, D.J. (1982): Tectonic Accretion and the Origin of the Two Major

Metamorphic and Plutonic Welts in the Canadian Cordillera, Geology, Volume 10, pages 70-75.

Mortimer, N. (1986): Late Triassic Arc-Related Potassic Igneous Rocks in the North American Cordillera, Geology, Volume 14, pages 1035-1038.

Nisbet, E.G. and Pearce, J.A. (1977): Clinopyroxene Compositions in Mafic Lavas from Different Tectonic Settings, Contibutions to Mineralogy and Petrology, Volume 63, pages 149-160.

Papike, J.J., Cameron, K.J. and Baldwin, K. (1974): Amphiboles and Pyroxenes: Characterization of Other than Quadrilateral Components and Estimates of Ferric Iron from Micropprope Data, Abstracts with Programs, The Geological Society of America, Volume 6, Number 7, pages 1053-1054.

Pearce, J.A. (1982): Trace Element Characteristics of Lavas from Destructive Plate Boundaries: in Andesites. Edited by R.S. Thorpe. New York: Wiley, pages 525-548.

Pearce, J.A. and Cann, J.R. (1973): Tectonic Setting of Basic Volcanic Rocks Determined Using Trace Element Analyses, Earth and Planetary Science Letters, Volume 19, pages 290-300.

Pearce, J.A. and Norry, M.J. (1979): Petrogenetic Implications of Ti, Zr, Y, and Nb Variations in Volcanic Rocks, Contributions to Mineralogy and Petrology, Volume 69, pages 33-47.

Pearce, J.A., Harris, N.B.W., and Tindle, A.G. (1984):Trace Element Discrimination Diagrams for the Tectonic

Interpretation of Granitic Rocks, Journal of Petrology, Volume 25, Part 4, pages 956-983.

Pearce, T.H., Gorman, B.E., and Birkett, T.C. (1977): The Relationship Between Major Element Chemistry and Teconic Environment of Basic and Intermediate Volcanic Rocks, Earth and Planetary Science Letters, Volume 36, pages 121-132.

Pitcher, W.S. (1982):Granite Type and Tectonic Environment in Mountain Building Processses. Edited by K.J. Hsu. London: Academic Press, pages 19-40.

Plank, T. amd Langmuir, C.H. (1988): An Evaluation of the Global Variations in the Major Element Chemistry of Arc Basalts, Earth and Planetary Science Letters, Volume 90, pages 349-370.

Richards, T.A. (1976): Takla Project (Reports 10-16): McConnell Creek Map area (94D, East Half) British Columbia; in Report of Activities, Geological Survey of Canada, Paper 76-1A, pages 43-50.

Skulski, T, Hynes, A., and Francis, D. (1988): Basic Lavas of the Archean La Grande Greenstone Belt: Products of Polybaric Fractionation and Crustal Contamination, Contributions to Mineralogy and Petrology, Volume 100, pages 236-245.

Souther, J.G. (1977): Volcanism and Tectonic environments in the Canadian Cordillera - A Second Look. In Volcanic Regimes in Canada. Edited by W.R.A. Barager, L.C. Coleman, and J.M. Hall. Geological Association of Canada, Special Paper 16, pages 2-24.

Wilson, M. and Davidson, J.P. (1984): The Relative Roles of Crust and Upper Mantle in the Generation of Oceanic Island Arc Magmas, Philisophical Transactions Royal Society London, Volume 310, pages 661-674.

Woodsworth,G.J. (1976): Plutonic Rocks of McConnell Creek (94D West Half) and Aiken Lake (94C East Half) Map-Areas, British Columbia; in Report of Activities, Geological Survey of Canada, Paper 76-1A, pages 69-73.

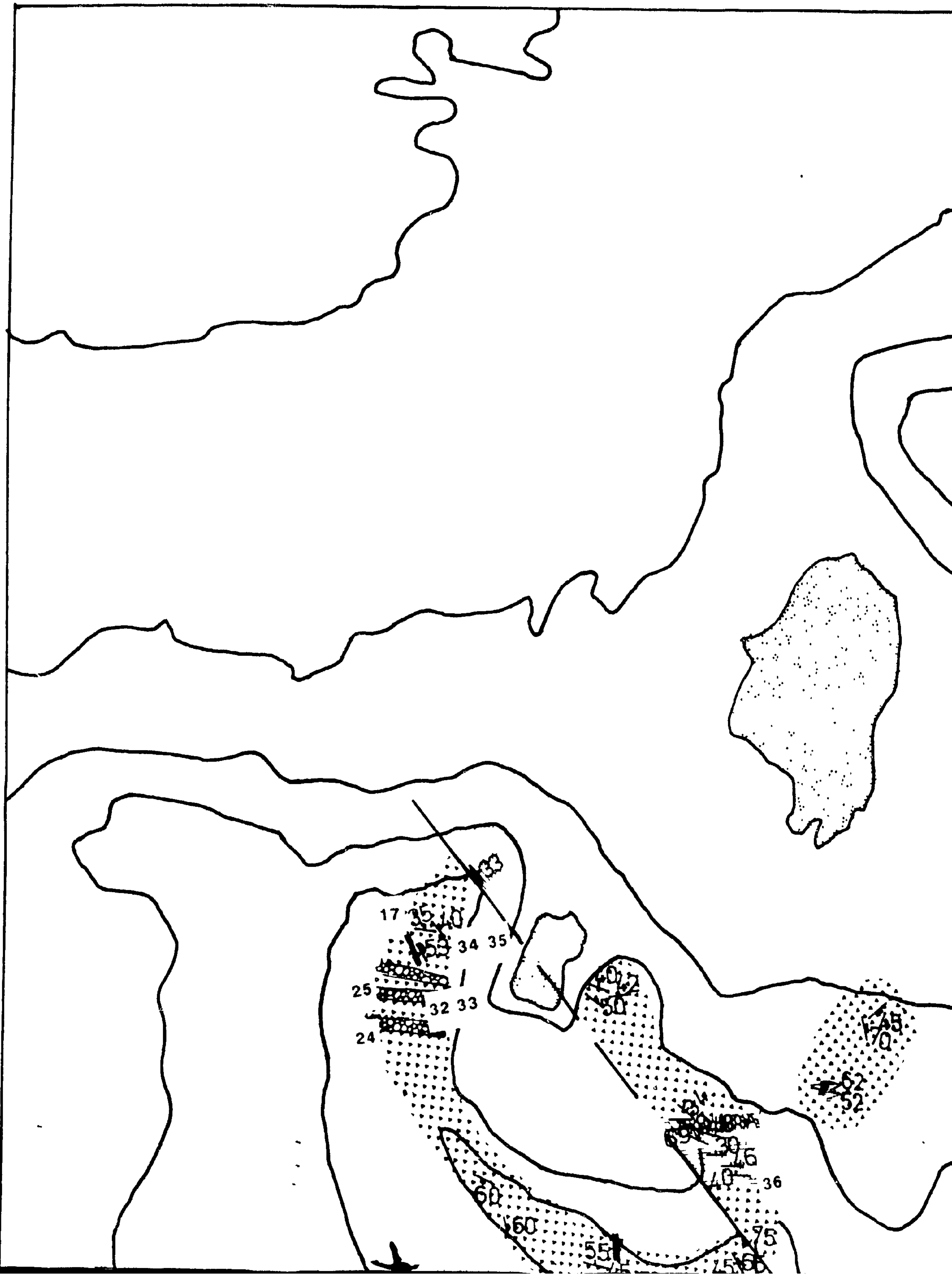

17
34
35
25
32
33
24
36

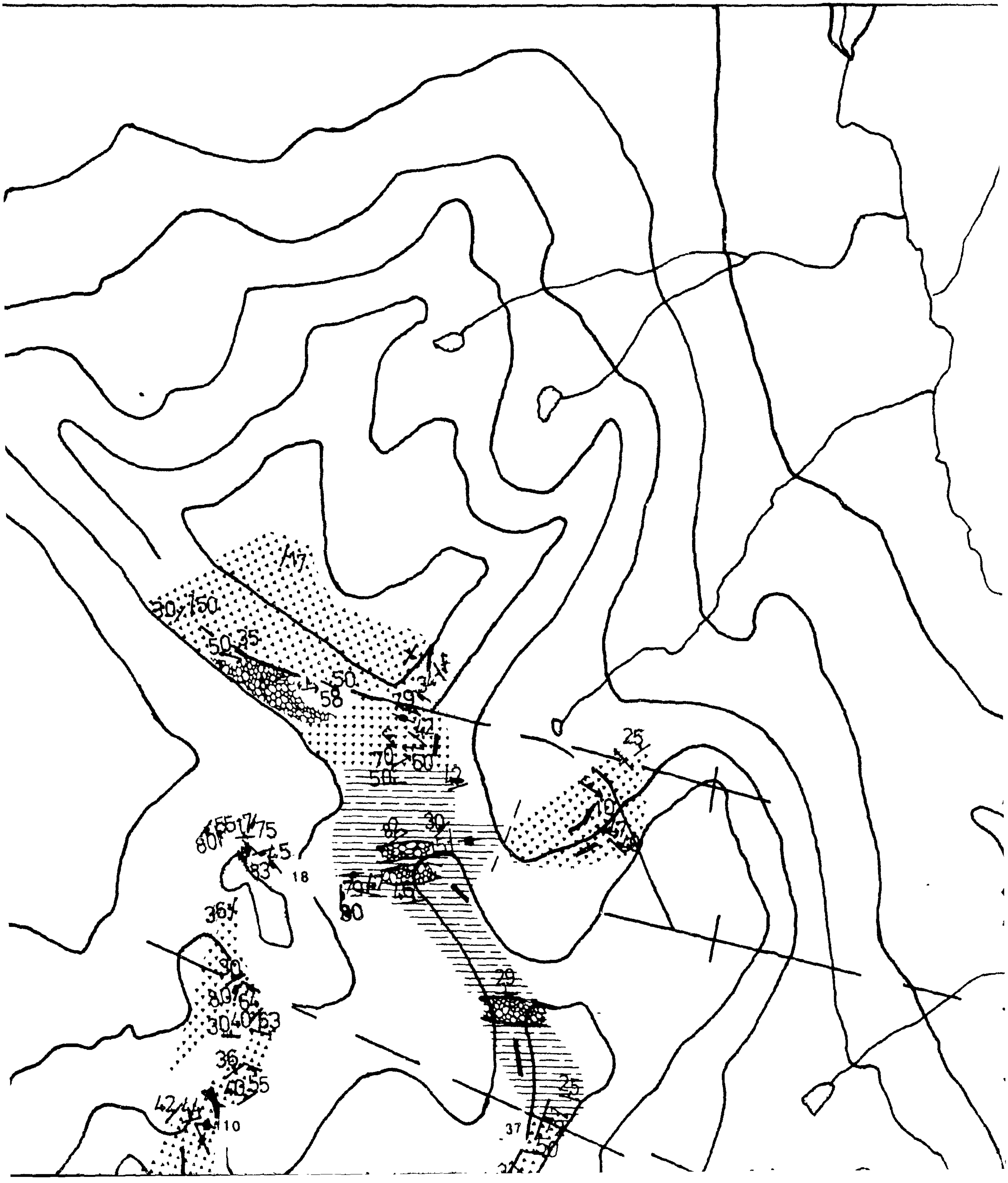
58
18
29
25
37
10

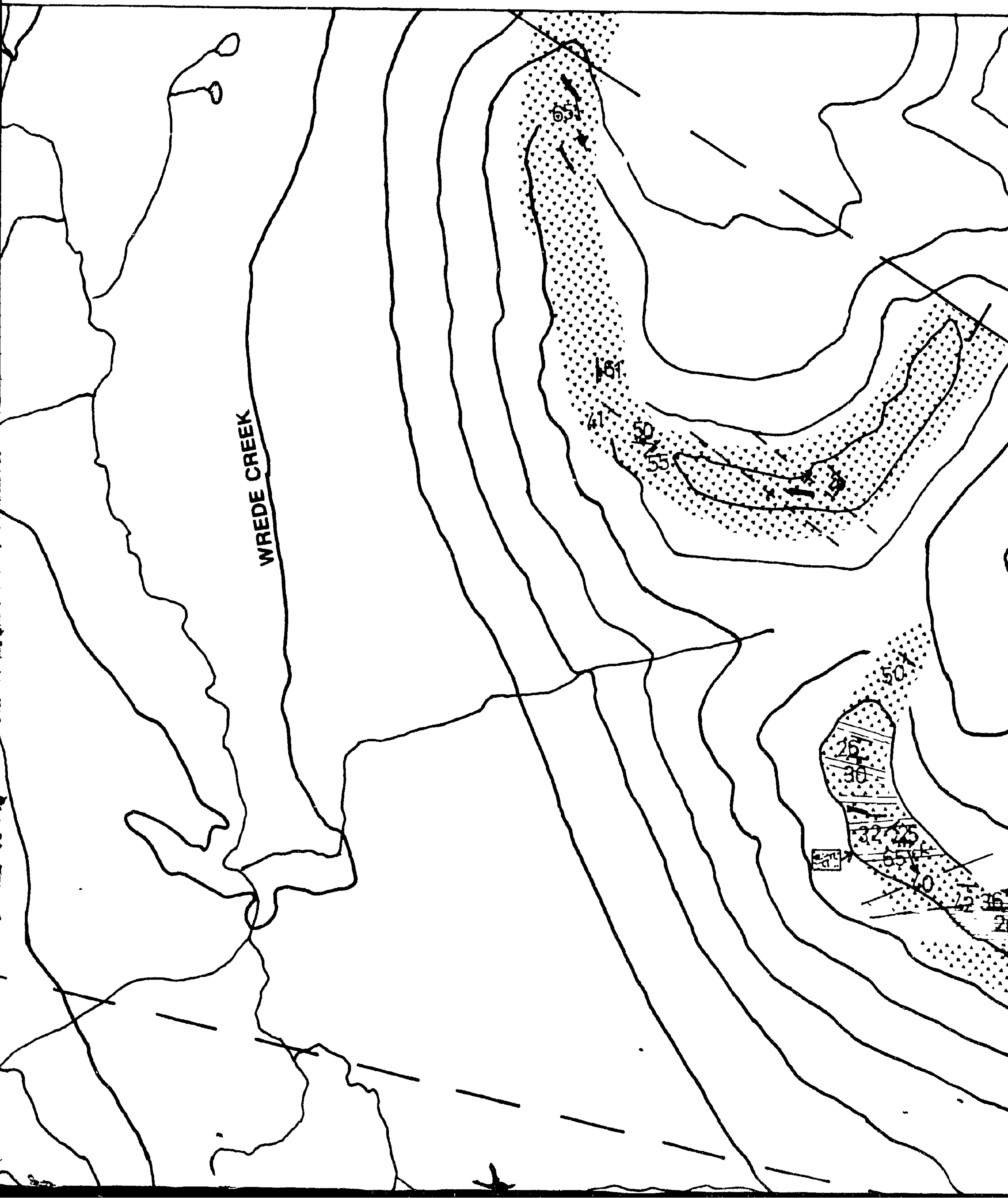
WREDE CREEK
65
61
41
50
55
50
26
30

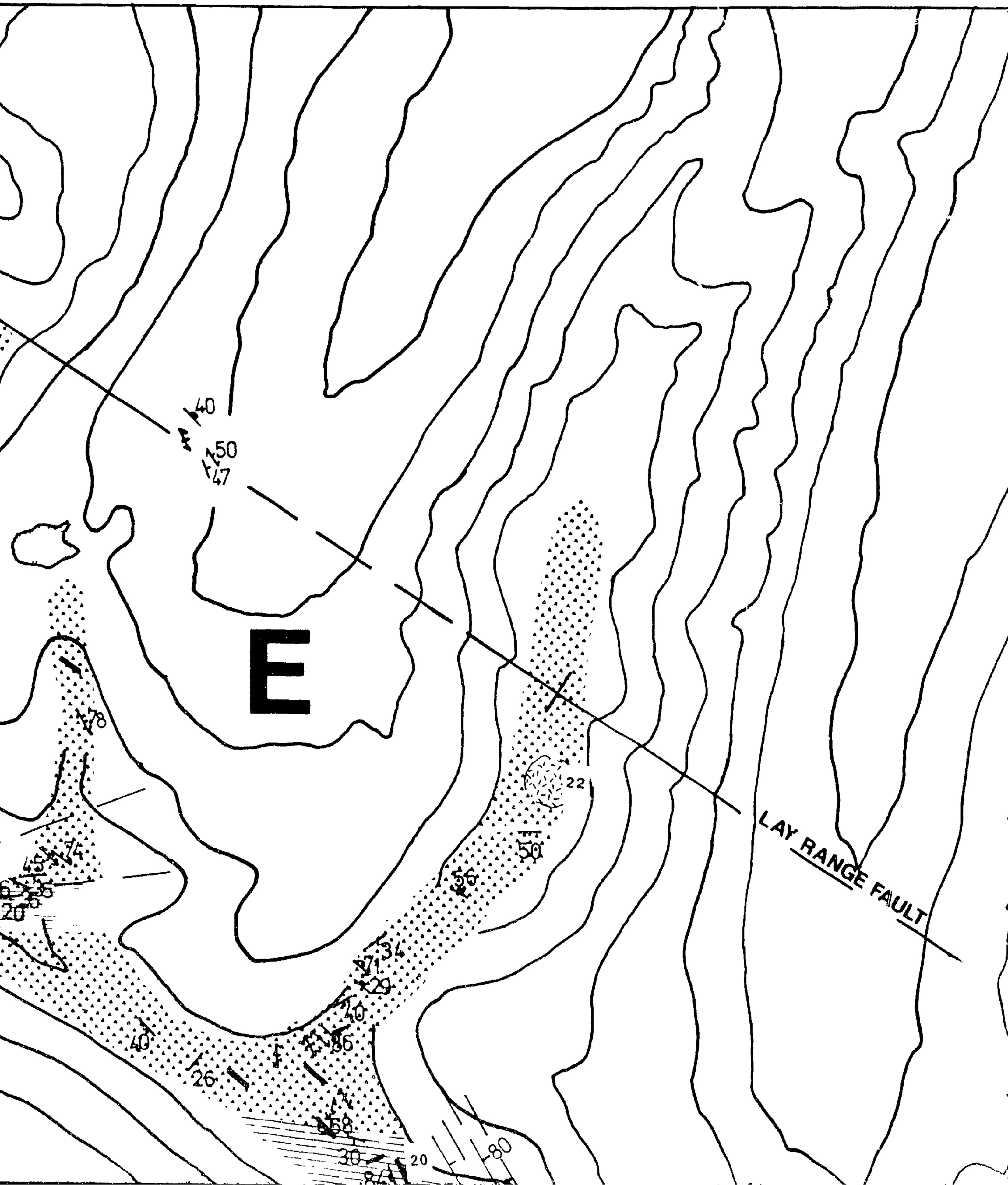
E
LAY RANGE FAULT

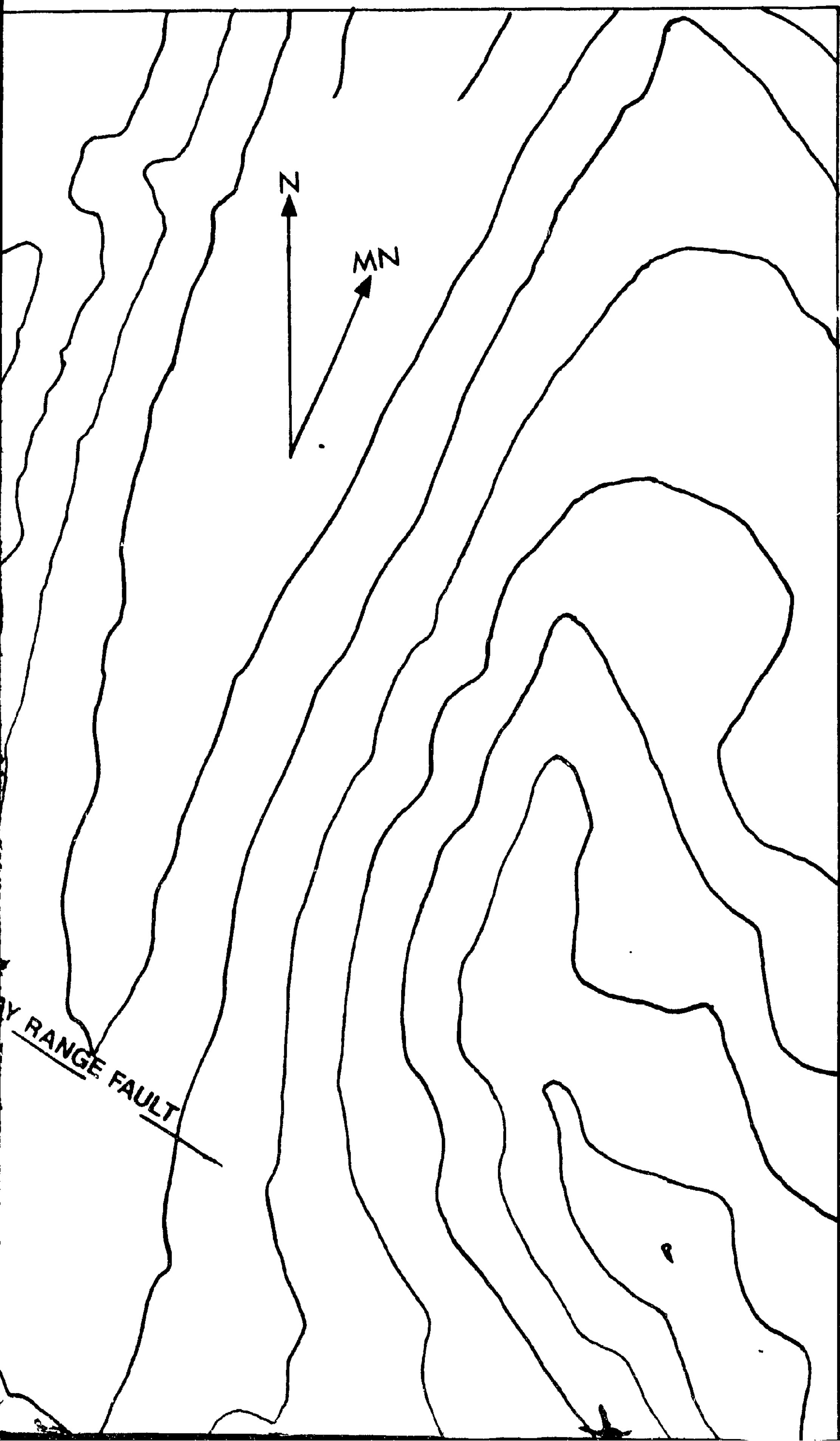
N
MN
RANGE FAULT

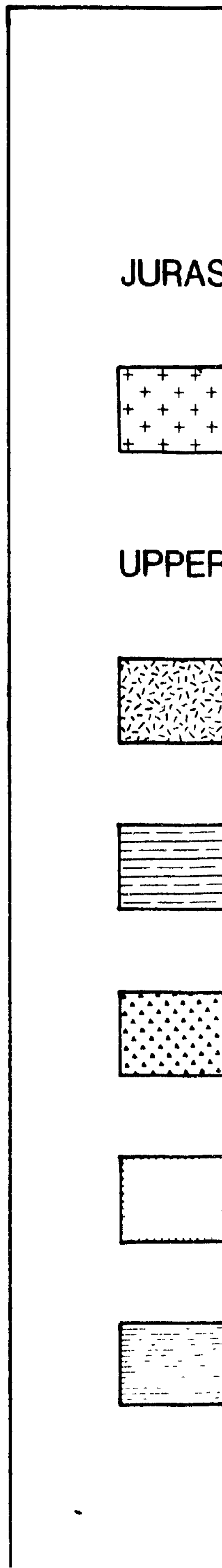
JURAS
UPPER

LEGEND

SSIC (?)

Tonalite, Jensen Peak Pluton

R TRIASSIC

Gabbro/diorite

Black epiclastic siltstone

Volcanogenic breccia

Volcanogenic sandstone

Volcanogenic siltstone

Lava flow

Dykes and sills

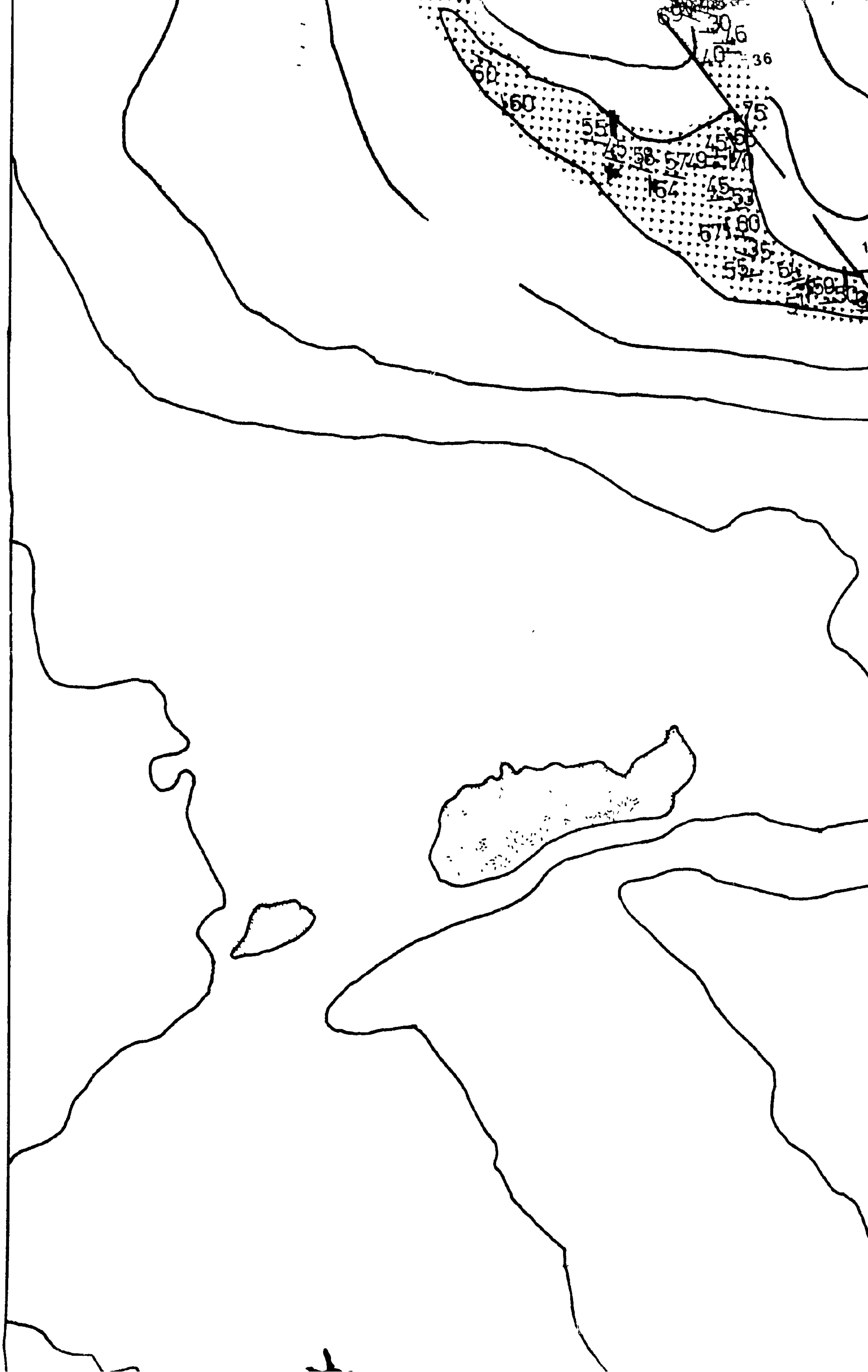

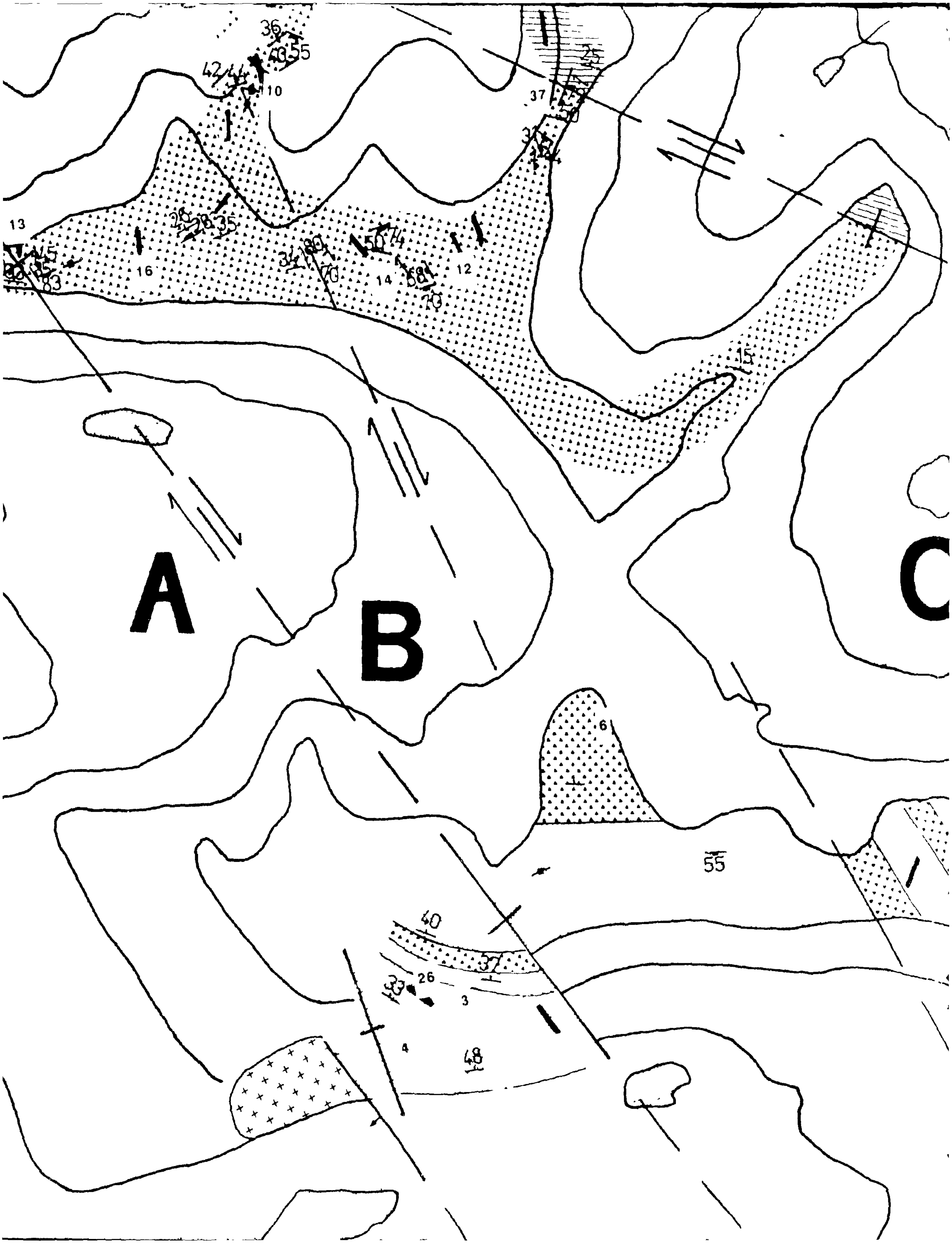

A
B
C
36
40
55
42
44
10
37
25
13
16
28
35
34
80
70
50
74
12
14
68
70
83
45
15
6
55
40
37
26
3
4
48

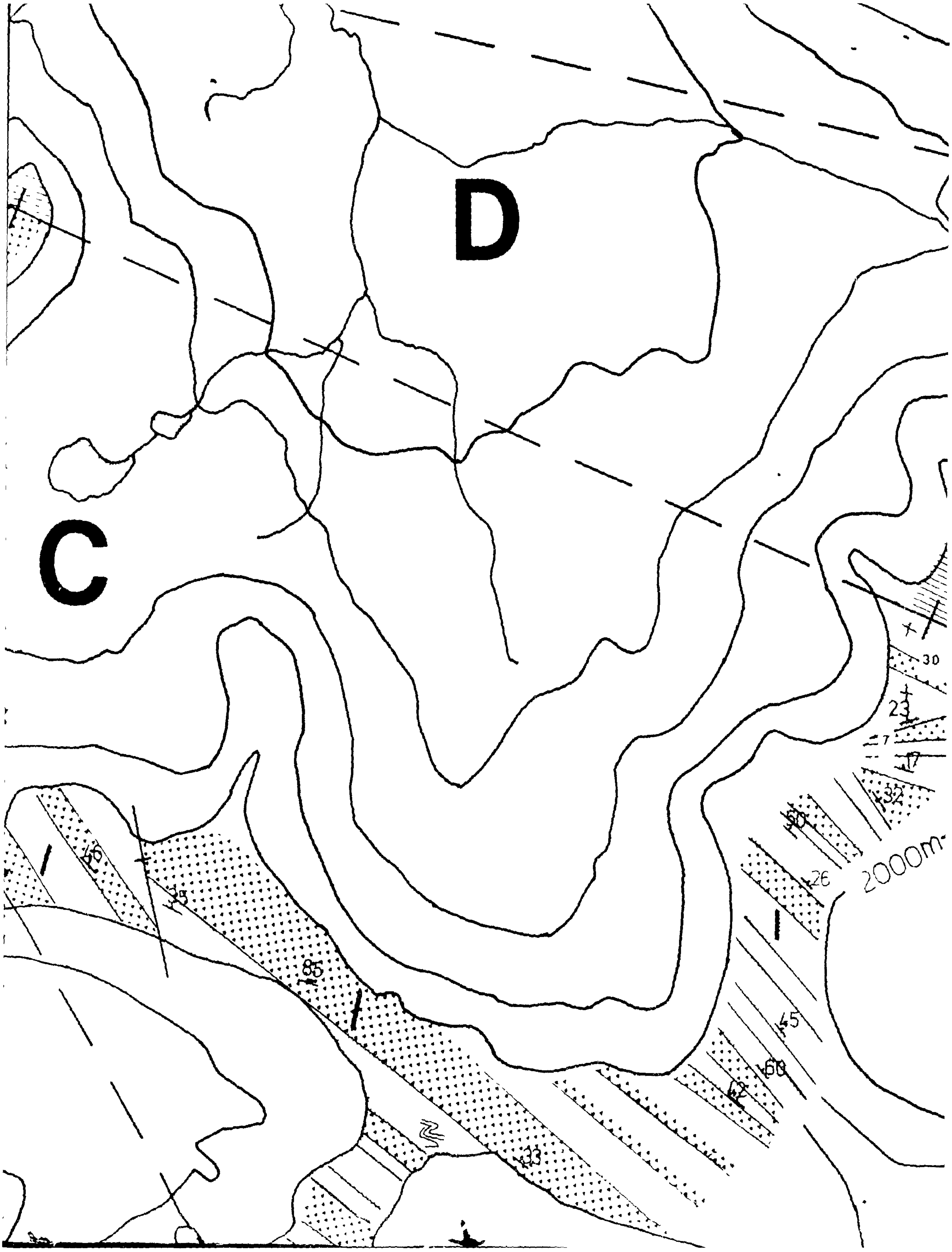

D
C
30
23
7
17
32
60
26
2000m
85
45
60


26
68
30
20
80
84
30
11
90
19
15
30
56
50
31

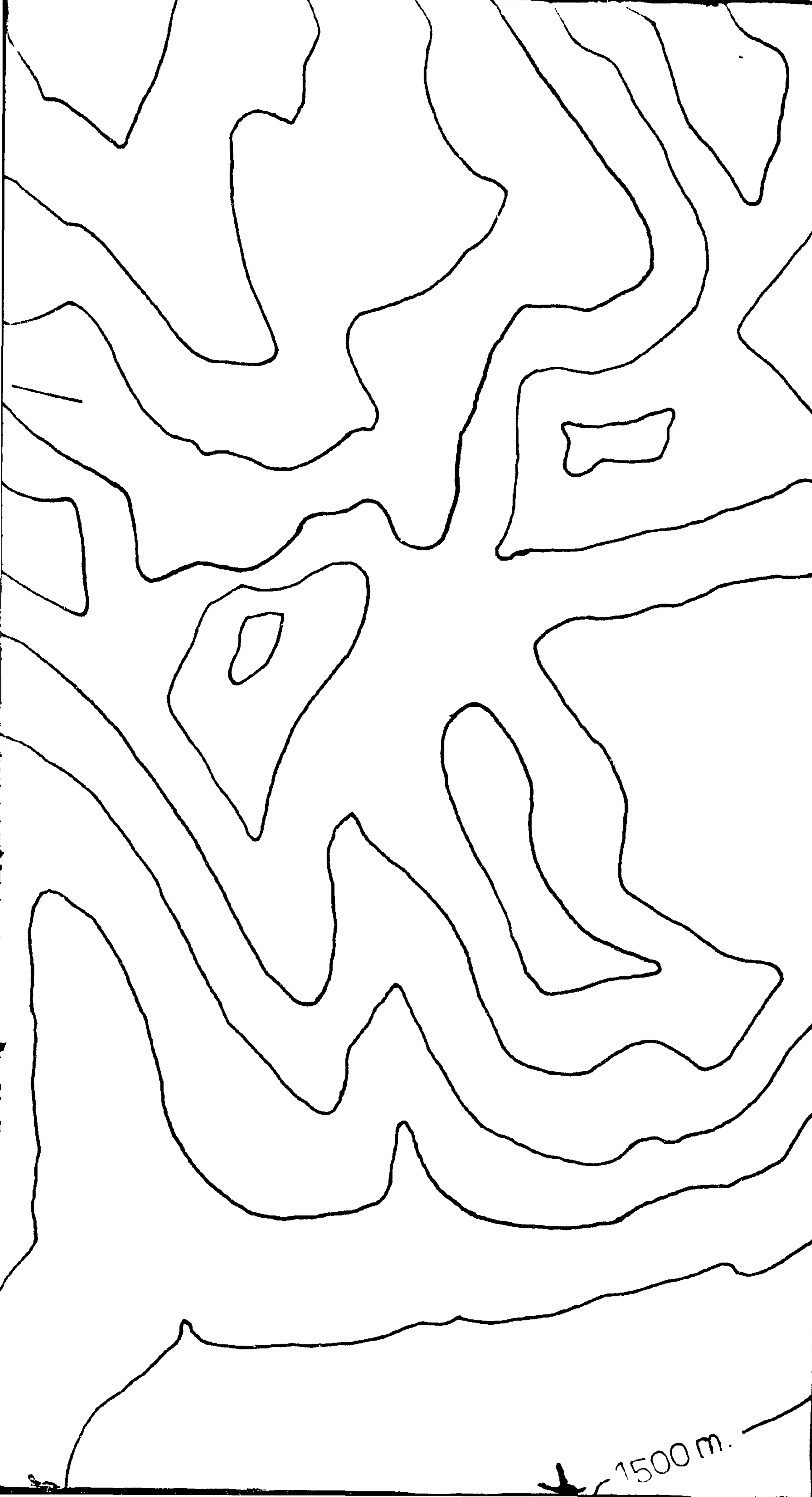

Beddi

Joint

Cleava

Faultin
positio
vertica
arrows

Fold a
plunge
plunge
plunge

Large-

Ripple

Intrusi

Area

Conto

Fault

Grid r

Lake

Appr

ding tops known (inclined, horizontal)

(inclined, vertical)

vage (inclined, vertical)

ting

tion accurate, approximate, assumed

cal, inclined, dumbell on downthrown side

ws show relative movement

axes

ge of fold axis with vergence not known

ge of fold axis showing "z" vergence

ge of fold axis showing "s" vergence

e-scale folding with varied sense of vergence

e marks

sive contact indicating younger unit

of outcrop

tour lines at 100 metre intervals

t block reference

reference

e

proximate sample location

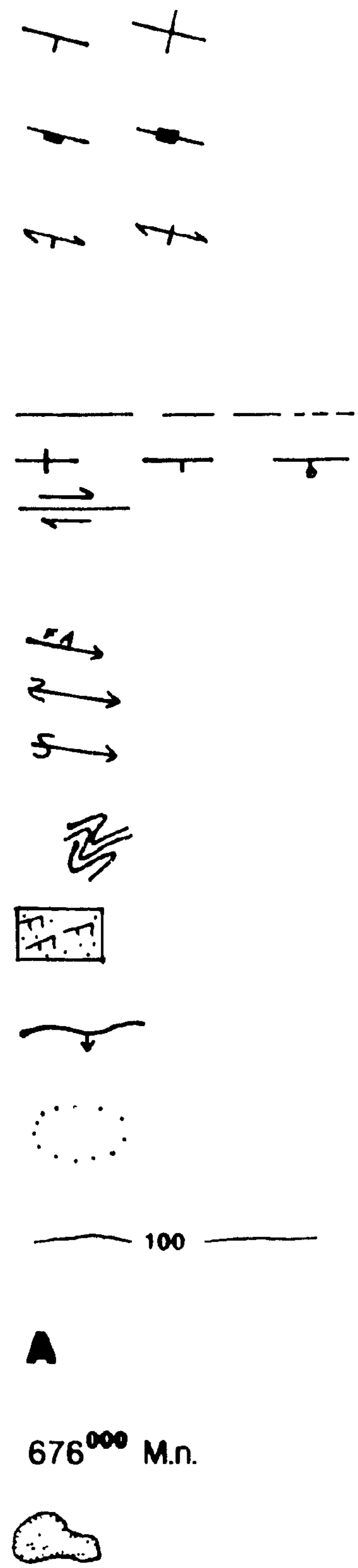

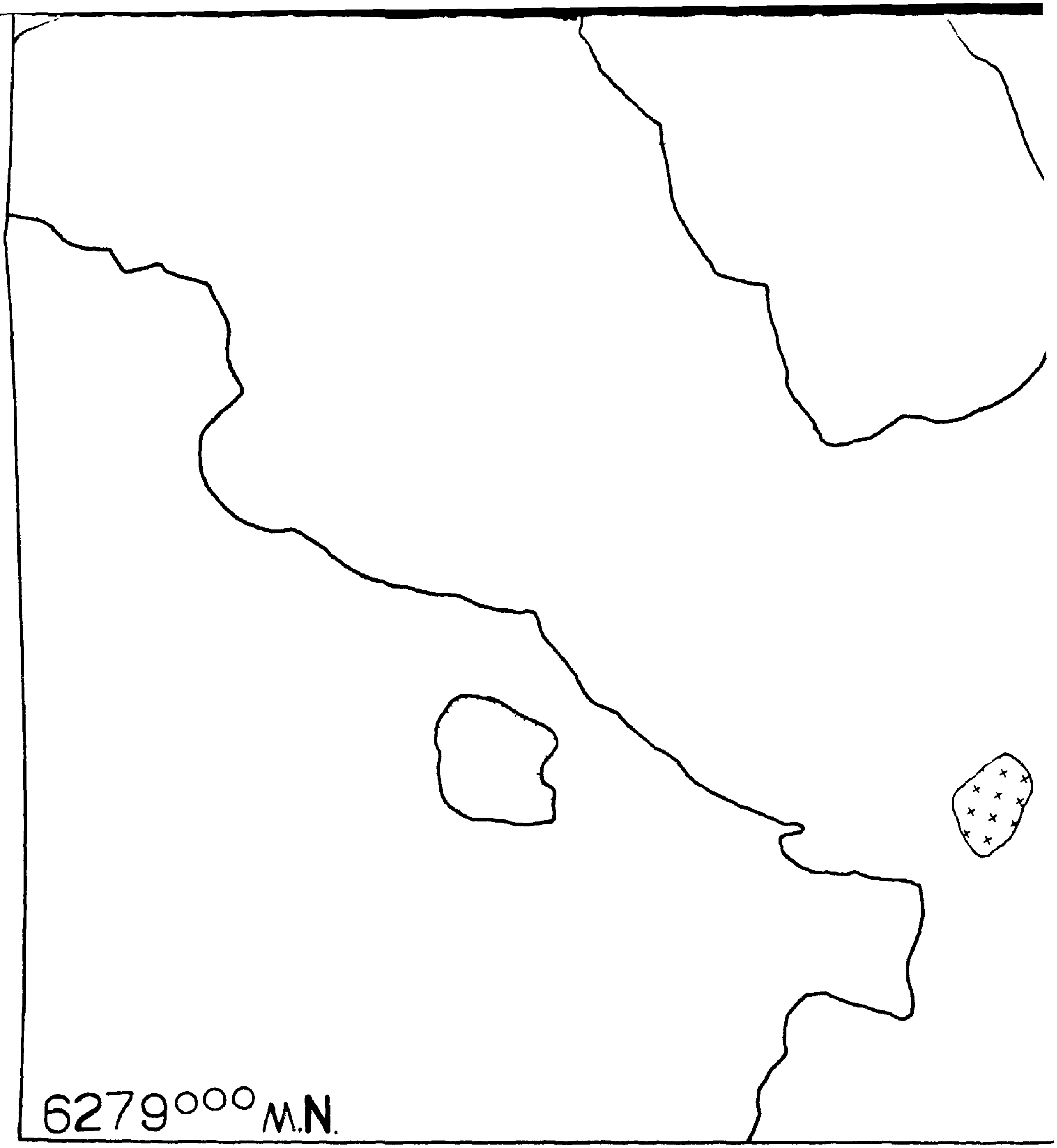
6279000 M.N.

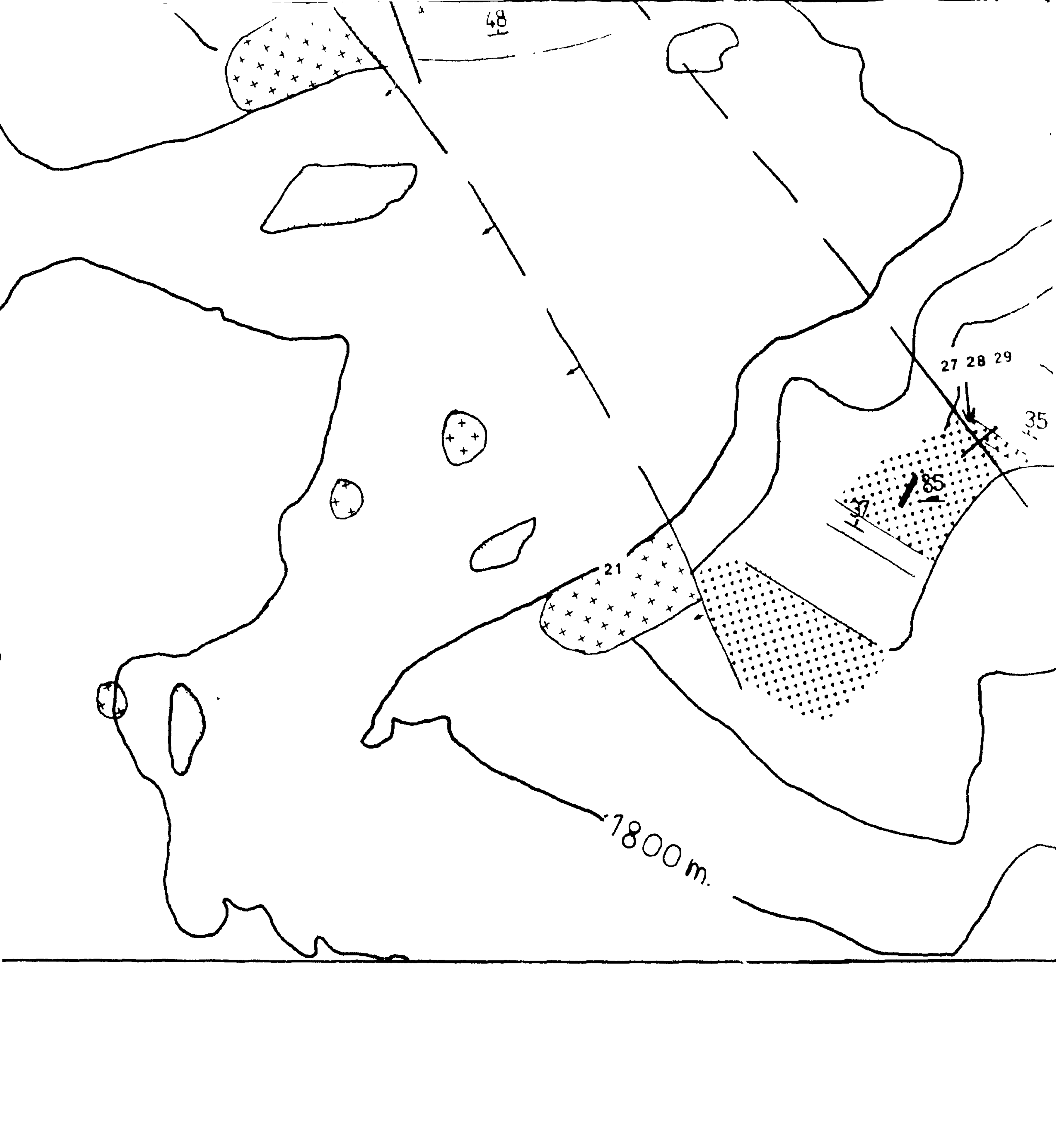

48
27 28 29
35
85
37
21
1800 m.

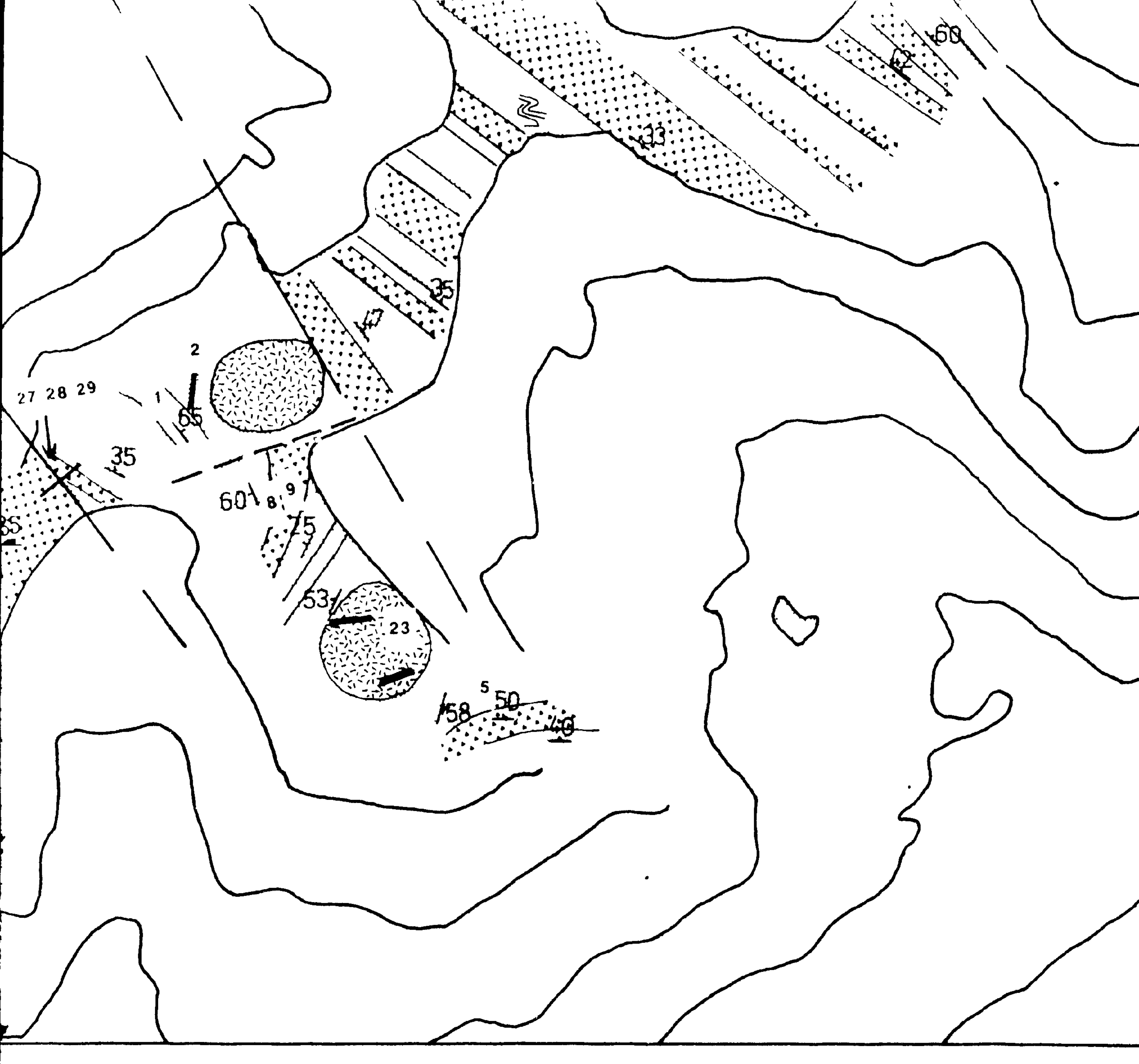

60
33
35
2
27 28 29
1
65
35
60
8
9
75
53
23
58
5
50
40

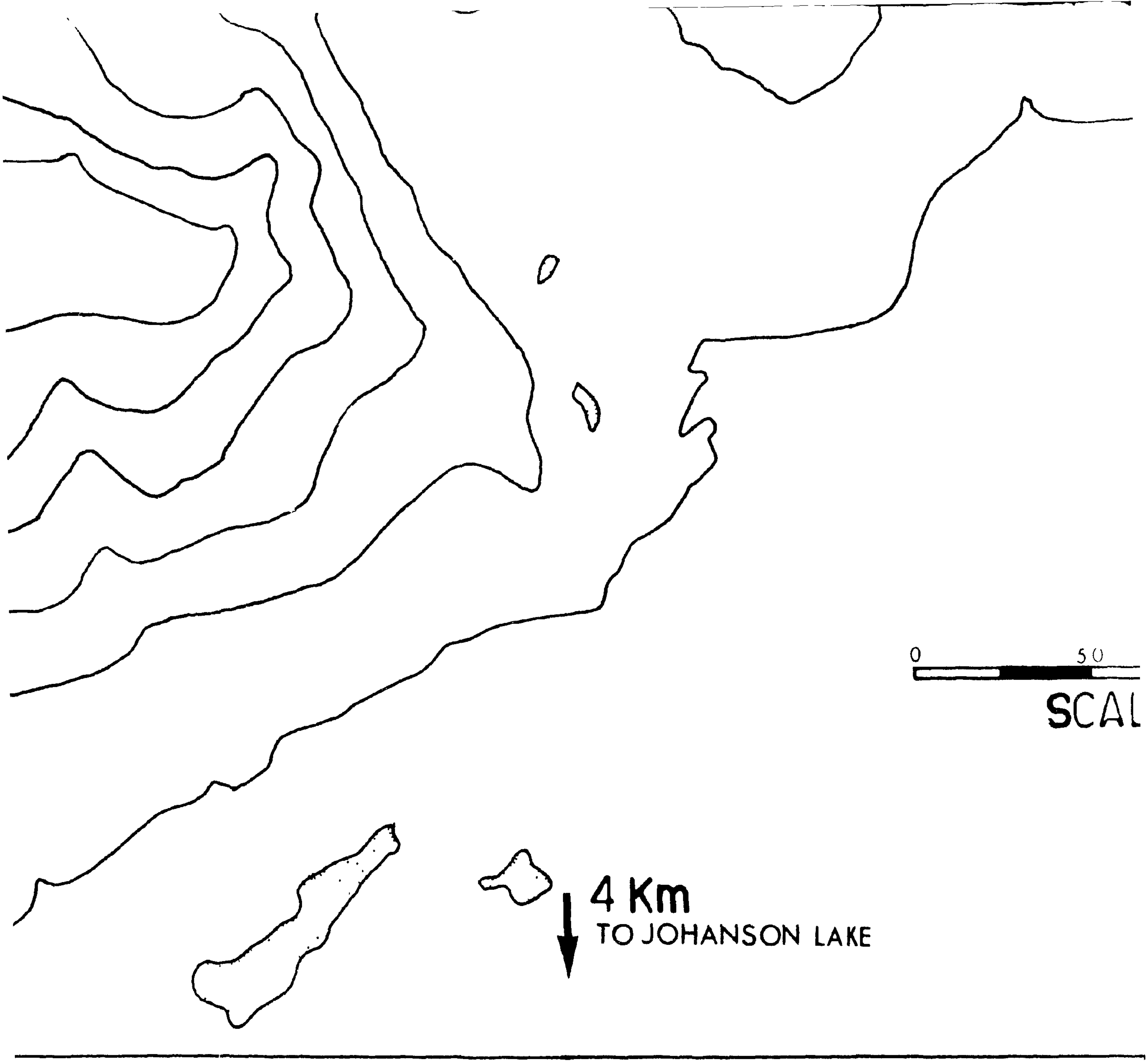

0
50
SCAL
4 Km
TO JOHANSON LAKE

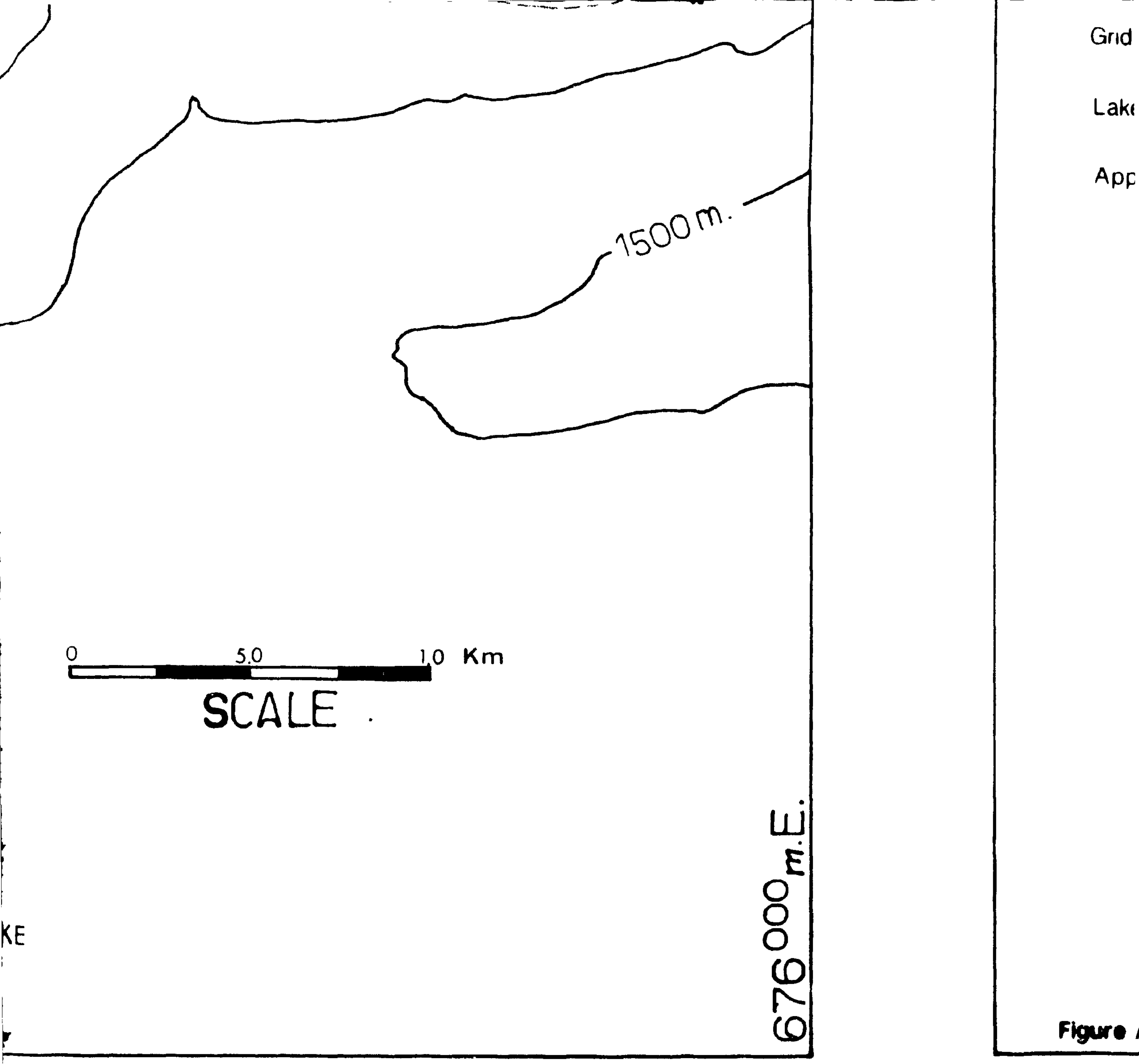
1500 m.
0
5.0
10 Km
SCALE
676000 m.E.
KE
Grid
Lake
App
Figure

d reference	676^{000} M.n
ke	
proximate sample location	1

Takla Group, Quesnellia, McConnell Creek Map Area, North Central British Columbia

by K. Minehan

A.1

McGill University

August, 1989